

Modeling, Design, Analysis, and Control of a Spot Market for Hydrogen

An Application of Economic Circuit Theory

P.E. van den Berkmortel

Master of Science Thesis

Modeling, Design, Analysis, and Control of a Spot Market for Hydrogen

An Application of Economic Circuit Theory

MASTER OF SCIENCE THESIS

For the degree of Master of Science in Systems and Control at Delft
University of Technology

P.E. van den Berkmortel

June 24, 2024

Faculty of Mechanical Engineering (ME) · Delft University of Technology



Copyright © Delft Center for Systems and Control (DCSC)
All rights reserved.

DELFT UNIVERSITY OF TECHNOLOGY
DEPARTMENT OF
DELFT CENTER FOR SYSTEMS AND CONTROL (DCSC)

The undersigned hereby certify that they have read and recommend to the
Faculty of Mechanical Engineering (ME) for acceptance a thesis entitled
MODELING, DESIGN, ANALYSIS, AND CONTROL OF A SPOT MARKET FOR
HYDROGEN

by

P.E. VAN DEN BERKMORTEL

in partial fulfillment of the requirements for the degree of
MASTER OF SCIENCE SYSTEMS AND CONTROL

Dated: June 24, 2024

Supervisor(s):

dr.ir. M.B. Mendel

Reader(s):

dr.ir. S.P. Mulders

ir. C. Hutters

ir. J. Gutknecht

Abstract

In this thesis, we demonstrate the potential of economic circuit theory for the modeling, design, analysis, and control of a spot market for hydrogen. Spot prices are expected to be significantly more volatile than the current marginal-cost-plus pricing schemes and new methods are required to model the dynamics of price as it reacts to fluctuations in supply and demand.

To model such dynamic pricing, we use recently developed economic circuit theory, a subfield of economic engineering where markets are modeled as electrical circuits. We model market agents, including production operators, storage facilities, market makers, and industry clusters, as analogous electrical components. We structure their interactions in an economic network that reflects the flow of hydrogen through the backbone and the balancing of price-driving incentives among the market agents.

We design three economic networks: a core network and two extensions. The core network incorporates a renewable wind-hydrogen supply chain, a low-carbon hydrogen supply chain, and imports of gaseous and liquid hydrogen. One extension divides the hydrogen spot market into renewable and low-carbon segments, and the other integrates an ammonia market. We implement and simulate the networks in MATLAB Simulink.

We analyze the networks' dynamics using dynamic scenario analyses, a technique within economic circuit theory. This permits us to quantify the dynamic resilience of the market under supply disruptions and demand extensions; in particular, we use overshoot and settling time as metrics for the volatility and recovery of stocks, prices, and hydrogen supply. In addition, we establish how wind variability generates a ripple effect that impacts the dynamics across the coupled commodity markets.

In conclusion, we model and analyze a market design that includes intervention by a regulatory agency. Specifically, we design a PID controller to implement a subsidized price-settlement system. We demonstrate that such a controller effectively mitigates excessive spot price levels, reduces price volatility, and secures the supply of hydrogen.

Table of Contents

Preface	vii
1 Introduction	1
2 Economic Circuit Theory and a Spot Market for Hydrogen	5
2-1 Introduction	5
2-2 From Cost-Plus to Supply-and-Demand-Driven Pricing	6
2-3 The Backbone as a Blueprint for Economic Networks	7
2-3-1 The Node Structure of the Hydrogen Backbone	7
2-3-2 The Mesh Structure of the Hydrogen Backbone	8
3 Design Methodology of Economic Circuit Theory	11
3-1 Introduction	11
3-2 The Stock and Flow Variables in Energy Systems	12
3-3 Market Agents as Electrical Components	13
3-4 Energy Systems as Economic Networks	15
3-5 Energy Market Clearing and Kirchhoff's Laws	18
4 Modeling and Design of Economic Networks of a Hydrogen Spot Market	21
4-1 Introduction	21
4-2 Design of the Core Network	22
4-2-1 The Hydrogen Backbone as the Network Topology	22
4-2-2 Central Hydrogen Storage as a Capacitor	25
4-2-3 A Market Operator as a Resistor	26

4-2-4	The Hydrogen Spot Market Dynamics	26
4-3	Design of the Hydrogen Supply Chains	27
4-3-1	Gaseous Hydrogen Import by Pipeline	27
4-3-2	The Wind-Hydrogen Supply Chain for Renewable Hydrogen Production	28
4-3-3	Low-Carbon Hydrogen Production	31
4-3-4	Import of Liquid Hydrogen	35
4-4	Industry Clusters as Active Demanders	37
4-5	The Core Network as a Dynamical System	39
4-5-1	The Dynamics of Storage Levels	39
4-5-2	The Dynamics of Spot Prices	42
4-5-3	State-Space Representation	44
4-6	Design of Core Network Extensions	46
4-6-1	Renewable and Low-Carbon Hydrogen as Separate Commodities	46
4-6-2	Integration of the Ammonia Market	46
4-7	System Identification	49
5	Dynamic Scenario Analyses and Control of the Networks	51
5-1	Introduction	51
5-2	Dynamic Scenario Analyses	52
5-2-1	Market Stabilization	52
5-2-2	Dynamic Resilience	54
5-2-3	Wind Variability	60
5-3	Control	65
5-3-1	Closed-Loop Imbalance Settlement Design	65
6	Conclusions	71
A	Analysis of the Hydrogen Market	73
A-1	Hydrogen Supply Chains	73
A-1-1	Domestic Hydrogen Production	73
A-1-2	Hydrogen Import	74
A-2	Industrial Demand for Hydrogen	75
A-3	The Hydrogen Backbone Connecting Supply and Demand	76
A-4	Storage of Hydrogen	77
A-5	A Supply-and-Demand-Driven Spot Market for Hydrogen	78
A-5-1	Spot Price Volatility	78
A-5-2	Market Design and Regulatory Intervention	79
A-6	Model Assumptions	80

B	Modeling a Marginal-Cost-Plus-Pricing Market for Hydrogen	83
B-1	Existing Hydrogen Market Models	83
B-2	Overview of General Energy Systems Modeling Approaches	84
B-2-1	An Overarching Classification Based on Discipline	84
C	Spot Market Clearing Conditions	89
C-1	Core Network Simplification	89
C-1-1	Graphical Network Representation	89
C-2	Node, Mesh, and Market Matrices	91
C-3	Clearing Conditions for Spot Prices and Energy Flows	94
D	Modeling Offshore Wind Distribution	97
D-1	Average Yearly and Daily Wind Distributions	97
D-2	Measured Wind Distribution	97
E	System Identification	99
E-1	Identification Method	99
E-2	Core Network	100
E-2-1	Hydrogen Supply Chains	101
E-2-2	Industry Clusters	104
E-2-3	Market Operators	106
E-2-4	Storage in Salt Caverns	107
E-3	Two-Sort Hydrogen Model	107
E-4	Integrated Ammonia Model	107
E-5	Model Calibration	110
F	Matlab and Simulink	113
F-1	Overview of Matlab Scripts and Simulink Files	113
	Bibliography	115
	Glossary	119
	List of Acronyms	119

Preface

Economic engineering has sparked my interest since my bachelor's in mechanical engineering, motivating me to pursue a master's in systems and control. The potential to apply abstract engineering principles to real-world economic problems fascinated me, offering a perspective I had never considered before.

My thesis topic stems from my keen interest in energy systems, energy technology, and particularly hydrogen. The Dutch plans for a hydrogen economy, coupled with the current mix of skepticism and optimism, inspired me to model the potential dynamics of hydrogen spot trade.

Initially, I was uncertain about how to model this hydrogen spot market. However, the development of economic circuit theory during my thesis provided an intuitive link with energy systems. Working with this newly developed theory has been both challenging and very exciting.

The past few years have been a valuable learning experience for which I am very thankful. I have deepened my understanding of systems and control theory, mechanics, economics, and energy systems. More importantly, I have learned how to navigate challenges, take steps back to make progress, and effectively present and write about my work. I am confident that the skills and knowledge gained will benefit me in my professional career.

I am grateful for the support of many people during my thesis. In particular, I would like to thank my supervisors, Dr. Ir. M.B. Mendel and Ir. C. Hutters, for their invaluable guidance. I also appreciate the challenging discussions within the economic engineering group during our weekly meetings.

I am excited to see how economic engineering, and specifically economic circuit theory, will evolve in the coming years, as I believe there is much more potential to be realized.

Delft, University of Technology
June 24, 2024

P.E. van den Berkmortel

Master of Science Thesis

P.E. van den Berkmortel

Chapter 1

Introduction

The energy landscape is undergoing a transformative shift towards a zero-emission future. In the Netherlands, hydrogen is envisioned as a crucial component of this energy transition, particularly for decarbonizing industrial operations. Recognizing its potential, the Dutch government is actively developing a hydrogen economy [1].

The current hydrogen market is dominated by locally produced hydrogen with minimal time variation and a limited number of suppliers and demanders. Hydrogen is primarily produced from fossil fuels through steam methane reforming and transported via privately owned pipelines. Hydrogen trade typically occurs through long-term contracts to ensure predictable revenue streams for hydrogen projects, with prices determined by marginal-cost-plus pricing.

The future hydrogen market is expected to integrate large quantities of intermittent renewable hydrogen, with production fluctuating throughout the day and across seasons. The planned establishment of the hydrogen backbone will physically connect the five largest industry clusters in the Netherlands, allowing for hydrogen to be traded for immediate physical delivery.

To balance supply and demand in real-time, market experts envision a spot market for hydrogen, similar to the existing natural gas spot market [2, 3].

In such a spot market, prices become dynamic as they react to fluctuations in supply, demand, and storage levels. These dynamic prices lead to considerable uncertainty for hydrogen projects, as revenue streams are no longer predictable.

The problem is that currently there are no models of a hydrogen spot market that employs a supply-and-demand-driven pricing mechanism; instead, they rely on marginal-cost-plus-pricing. Hence, we need models that can accurately predict how hydrogen spot prices evolve over time.

In this thesis, we demonstrate that economic circuit theory can be used to design such models. Economic circuit theory is a recently developed subfield of economic engineering based on electrical circuit theory. For those interested in the theoretical foundation of economic engineering, the paper "*The Newtonian Mechanics of Demand*" by M.B. Mendel [4] is highly recommended. This thesis builds on the preprint "*Economic Circuit Theory: Electrical Network Theory for Dynamical Economic Systems*" by C. Hutter and M.B. Mendel [5]. Readers seeking a deeper theoretical understanding should refer to this preprint.

In Chapter 2, we lay down the main concepts of economic circuit theory that allow us to design a spot market as an economic network. While we recognize the node structure as accurately describing the flow of hydrogen through the backbone, we argue that it is the mesh structure that takes care of the price dynamics of the spot market.

In Chapter 3, we detail the design methodology of economic circuit theory to design energy systems as economic networks. We adapt the generalized theory to the terminology used in energy systems. First, we match the stock and flow variables in energy systems to those in electrical circuits and the energy market agents to basic electrical components. Then, we interconnect these market agents using topological concepts from graph theory to form the node and mesh structures of the market. By applying the node and mesh laws inherent to economic circuit theory, we derive the energy market clearing conditions from which we derive the dynamics of storage levels and energy prices. Readers new to economic circuit theory are recommended to read this chapter.

In Chapter 4, we design a core network of a hydrogen spot market and two networks that form extensions. First, we present the core network in Section 4-2-1, and in subsequent sections, we detail the design of four hydrogen supply chains and the coupled energy markets, as well as the design of industry clusters that act as active demanders. Then in Section 4-5, we exploit the node and mesh structures of the core network to analytically derive the differential equations describing the dynamics of the energy prices and storage levels. In Section 4-6, we present two extensions of the core network: one that treats renewable and low-carbon hydrogen as distinct commodities, and another that integrates an ammonia market. Readers can jump to the sections they are interested in, but we particularly recommend reading the design of the supply chains in Section 4-3, which are the most complex parts of the network.

The three economic network models are built as electrical circuits in MATLAB Simulink, a graphical programming environment for modeling, simulating, and analyzing dynamical systems. During simulations, we track the energy flows and changes in market incentives across the networks using current and voltage sensors. From these real-time measurements, we derive the time evolution of storage levels and energy prices within the economic networks.

In chapter 5, we show the quantitative results of our simulations, where we exactly determine the price dynamics in our networks. This chapter is divided into analysis and control parts. In Section 5-2, we analyze the price dynamics of the economic networks

using dynamic scenario analysis, a technique within economic circuit theory. We leverage established engineering tools for transient analysis to analyze the volatility and recovery of energy prices, storage levels, and hydrogen supply chains after supply disruptions and a demand extension. We explicitly quantify the dynamic resilience using metrics such as overshoot and settling time. Additionally, we analyze the impact of wind variability using real-world wind data. In Section 5-3, we model and analyze a market design that includes intervention by a regulatory agent, such as the government. We design a Proportional-Integral-Derivative (PID) controller to emulate this intervention and demonstrate that such a controller effectively and intuitively regulates hydrogen spot prices and improves the market's dynamic resilience.

In Chapter 6, we draw conclusions on the potential of economic circuit theory for accurately addressing price dynamics in the modeling, design, analyses, and control of a spot market for hydrogen.

Economic Circuit Theory and a Spot Market for Hydrogen

2-1 Introduction

In this chapter, we lay down the concepts of economic circuit theory for the modeling of a supply-and-demand-driven spot market for hydrogen. We build on the recent publication by Mendel on economic engineering (2023) [4] and on the preprint on economic circuit theory by Hutter and Mendel (2024) [5].

In Section 2-2, we treat the shift from marginal-cost-plus-pricing to supply-and-demand-driven pricing, highlighting its impact on the predictability of revenue streams for hydrogen projects. We explain how this shift presents an opportunity for applying economic circuit theory to model these new pricing dynamics.

In Section 2-3, we demonstrate how the hydrogen backbone functions as a blueprint for modeling the spot market for hydrogen as an economic network. We distinguish two structures within the backbone: the node structure, which manages hydrogen distribution, and the mesh structure, which manages the distribution of incentives. Whereas the node structure is familiar, the mesh structure is new.

2-2 From Cost-Plus to Supply-and-Demand-Driven Pricing

Currently, the Dutch hydrogen market operates through specialized contracts between suppliers and demanders, known as Hydrogen Purchase Agreements (HPAs), as illustrated in Figure 2-1a. These contracts ensure predictable revenue streams for hydrogen projects, with prices typically set using marginal-cost-plus pricing, incorporating fixed and variable costs along with additional margins.

A key development in the hydrogen market is the future establishment of the hydrogen backbone¹, a pipeline infrastructure connecting suppliers and demanders across the country. This backbone fosters the growth and diversification of hydrogen supply and demand.

The introduction of new hydrogen supply chains, especially those relying on renewable energy sources, is expected to lead to greater fluctuations in supply. This increases the need for a spot market for hydrogen, where prices react in real time to balance supply and demand under the regulation of a central market operator. Figure 2-1b illustrates this new supply-and-demand-driven pricing mechanism.

The transition from current marginal-cost-plus pricing to a supply-and-demand-driven spot market aligns with the Netherlands' goal of developing a robust hydrogen economy [6]. Initiatives like HyXchange are currently working on the development of a spot market for hydrogen [3], aiming to create a market similar to the Title Transfer Facility (TTF) for natural gas [2, 7, 8, 9, 10].

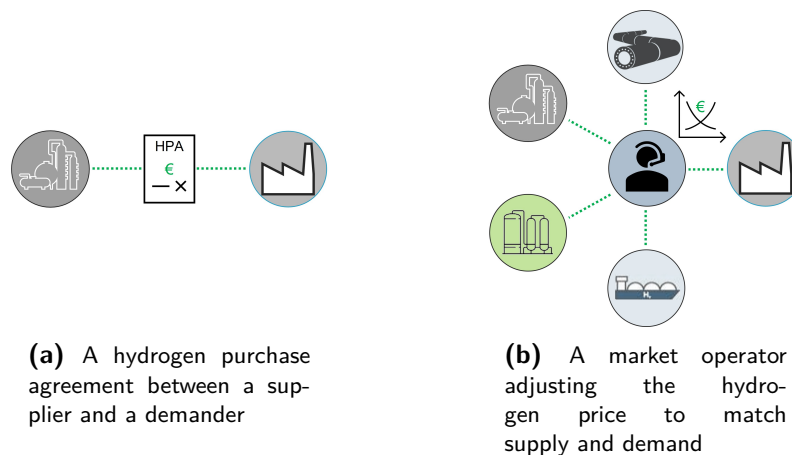


Figure 2-1: From marginal-cost-plus pricing (a) to supply-and-demand-driven pricing (b)

In a spot market, hydrogen prices become volatile as they change in response to fluctuations in supply, demand, and storage levels, making revenue streams unpredictable. This uncertainty poses challenges for hydrogen investments. A representative hydrogen

¹For more details on the hydrogen backbone, see Section A-3.

spot market model is necessary to better understand this volatile spot market behavior and provide indications of hydrogen prices.

Currently, no model exists that accurately reflects the supply-and-demand-driven aspect of hydrogen spot prices. Existing hydrogen price indices, such as HYCLICX from HyXchange, and spot market models, like the Integrated Electricity, Hydrogen and Gas (I-ELGAS) model of TNO [11] (see Section B-1), still rely on a pricing mechanism driven by marginal costs. Other existing energy systems modeling approaches either depend on marginal cost pricing or apply static pricing based on static supply and demand profiles, see Section B-2.

The transition to supply-and-demand-driven pricing presents an opportunity for economic circuit theory, which this thesis aims to exploit. By introducing a mesh structure and a well-defined elementary demander, this technique allows us to explicitly model the price dynamics in a spot market for hydrogen.

2-3 The Backbone as a Blueprint for Economic Networks

2-3-1 The Node Structure of the Hydrogen Backbone

The node structure is a familiar concept in energy networks. Existing hydrogen market models, such as HyWay27 [12] and I-ELGAS [11] (see Section B-1), represent the hydrogen backbone as a system of nodes and edges. In these models, nodes represent the locations of supply, demand, and storage, while edges represent the pipeline infrastructure. These models determine local imbalances and resulting hydrogen flows between nodes to balance supply and demand throughout the market.

Economic circuit theory also views the hydrogen backbone and market agents as a system of nodes and edges, but with a different interpretation. Here, nodes are exchange loci for hydrogen, and edges represent the behavioral laws of hydrogen market agents. We treat the market agents in Section 3-3.

In Figure 2-2a, we illustrate the node structure of the envisioned hydrogen backbone with blue dots. Each branch is identified as a node. In Section 3-4, we treat the node structure in more detail and show that the number of nodes reduces in an analogous economic network.

The hydrogen backbone in Figure 2-2a shows how the market agents (listed in Figure 2-2c) are connected and thus how hydrogen is transported from one location to another and where it can be stored. Hydrogen can be thought of as a flow moving through this backbone, entering and exiting nodes and storage locations. This interpretation of hydrogen as a flow variable is further detailed in Section 3-2.

At storage locations, hydrogen flows accumulate into storage levels. Economic circuit theory treats these storage levels as state variables, allowing us to track their evolution over time. We treat the behavior of the storage element in more detail in Section 3-3.

To maintain constant pressure in the backbone, supply and demand must balance in real time. Economic circuit theory ensures this balance with a node law that functions as a physical clearing mechanism for the hydrogen spot market. This means that any hydrogen surplus must be stored, and any deficit must be extracted from storage, highlighting the importance of the storage element. The node law is further explained and demonstrated in Section 3-5.

The node structure captures the distribution of hydrogen flows and their accumulation into storage, following the node law inherent to economic circuit theory. The node structure represents what is thought of as the kinematics of the hydrogen spot market.

2-3-2 The Mesh Structure of the Hydrogen Backbone

The identification of a mesh structure in the hydrogen backbone is one of our main contributions, as this structure captures the pricing mechanism of a spot market for hydrogen. A mesh indicates a circular flow of hydrogen, necessary for market agents to communicate incentives and exchange hydrogen. As shown in Figure 2-2b, this mesh structure is less apparent than the node structure. This explains why this structure has not been recognized and exploited before.

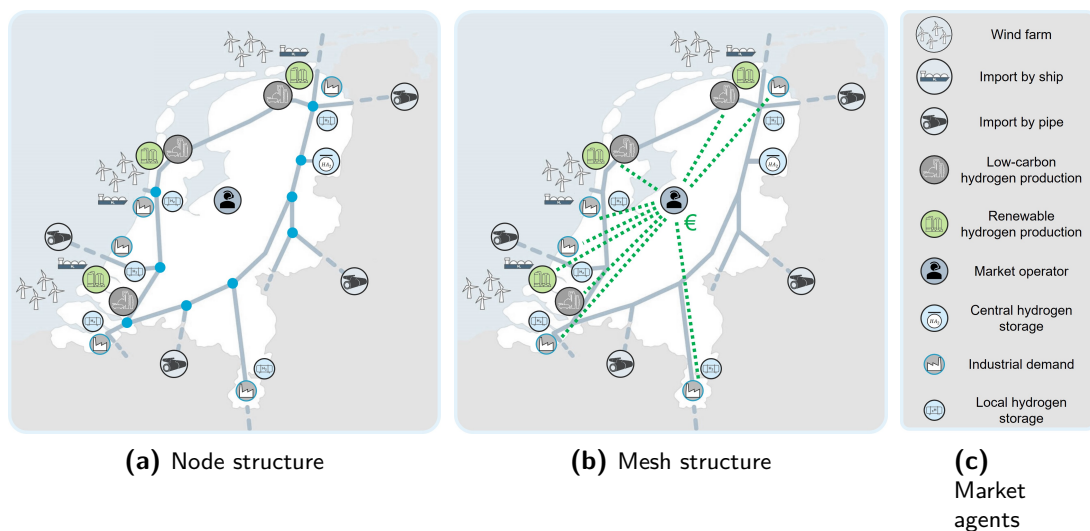


Figure 2-2: The structures within the hydrogen backbone. The hydrogen backbone is indicated in gray-blue and the market agents are listed in the legend on the right. The node structure is indicated by the blue dots. The mesh structure is not directly visible but instead, it is indicated by the communication of incentives via the market operator with the dashed green lines. The market operator balances the incentives to obtain a hydrogen spot price where supply and demand balance.

Although the mesh structure cannot be directly visualized as closed loops in the figure, it is intuitively represented by the green dashed lines indicating the communication of

incentives via the market operator. The market operator balances these incentives to achieve a hydrogen spot price where supply and demand balance. In Section 3-4, when we draw the circuit theory analog of the hydrogen backbone, the mesh structure will become apparent.

The incentives are the driving forces behind hydrogen price changes (see Section 3-2). The introduction of incentives allows us to model the influences of storage levels and market friction on hydrogen spot prices. The incentives provided by the corresponding market agents are determined by their behavioral law, see Section 3-3.

The mesh structure is made possible through the introduction of an elementary demander, which is treated in more detail in Section 3-3. This elementary demander maintains a hydrogen price. Based on this price, the demander adjusts its quantity demanded according to the economic law of demand. The introduction of this elementary demander allows us to treat hydrogen prices as state variables, such that we can precisely track their time evolution.

To determine the hydrogen spot price, the incentives in each mesh must balance. This is ensured by the mesh law within economic circuit theory. In case of an imbalance, this law prescribes that this leads to a price adjustment that exactly equals the imbalance, to retain the balance of incentives. We think of this law as the price-clearing mechanism of the hydrogen spot market.

The mesh structure captures the price-driving incentives and their accumulation into hydrogen spot prices by the elementary demanders, following the node law. This structure captures the causes behind the distribution of the hydrogen flows and changes in storage levels, which can be thought of as the dynamics of the spot market. By identifying the mesh structure of the hydrogen backbone and employing the node law, we precisely determine the hydrogen spot price dynamics.

Design Methodology of Economic Circuit Theory

3-1 Introduction

In this chapter, we present a detailed design methodology for modeling energy systems as economic networks, building upon the concepts introduced in the previous chapter. We extend the general framework of economic circuit theory, as presented in the preprint by Hutters and Mendel (2024), to make it applicable to energy systems modeling.

We start by aligning the stock and flow variables in energy systems with their analogs in electrical circuits, as detailed in Section 3-2. Here, we explain how flow variables accumulate into stock variables, forming pairs of conjugate variables.

Next, in Section 3-3, we identify market agents and model them as electrical components by matching their behavioral laws with the constitutive laws of electrical components.

In Section 3-4, we look at the interactions of market agents. We describe the topological concepts of economic circuit theory and illustrate how to match the interactions between agents within a network topology. We also demonstrate how to aggregate market agents into circuit modules and model energy markets as closed economic circuits.

Finally, in Section 3-5, we explain and demonstrate how Kirchhoff's laws, interpreted as the node and mesh laws, provide inherent stock-flow and price-incentive consistencies for energy market clearing, allowing us to model a supply-and-demand-driven pricing mechanism.

We illustrate the design methodology with the same hydrogen backbone as presented in the previous chapter. All the design steps come together in Figure 3-2, where we model the hydrogen market operating on the backbone as an economic network.

3-2 The Stock and Flow Variables in Energy Systems

To design energy systems as economic networks, we adjust the general electrical analogy of economic circuit theory to the specifics of energy systems. This involves matching the stock and flow variables in an energy system to their analogs in an electrical circuit. An overview of this matching is shown in Table 3-1. As energy is generally traded in MWh, the units of the stock and flow variables are chosen accordingly.

As introduced in the previous chapter, energy systems feature two separate flows: the flow of energy and the flow of incentives. The match with their electrical analogs is very intuitive when considering the flow of energy passing from one agent to another as the electric current (the rate of electron flow), and the incentives exerted by an agent as the voltage (the driving force behind electron flow). In an analogous electrical circuit, the energy flows are represented by the electrical wiring connecting two agents, and the incentives are represented by the potential difference across an agent.

	Energy system	Electrical circuit	Symbol	Units
<i>Stock</i>	Energy storage level	Charge	$q = \int f dt$	MWh
	Energy price	Flux linkage	$p = \int v dt$	$\frac{\text{€}}{\text{MWh}}$
<i>Flow</i>	Energy flow	Current	$f = \frac{dq}{dt}$	$\frac{\text{MWh}}{\text{h}}$
	Incentive	Voltage	$v = \frac{dp}{dt}$	$\frac{\text{€}}{\text{MWh}\cdot\text{h}}$

Table 3-1: The stock and flow variables for energy systems modeling and their stock-flow relationships. Adjusted from Hutter and Mendel (2024) [5]

The stock-flow relations, included in the fourth column of table Table 3-1, are determined by the accumulation of energy flows (f) into energy storage levels (q) and the accumulation of incentives (v) into energy prices (p). These energy storage levels and prices together make up the state variables of the energy system.

The energy storage level, maintained by a storage agent, is analogous to the electrical charge in a capacitor, while the energy price, maintained by a demander, is analogous to the flux linkage in an inductor. These electrical components are detailed in Section 3-3.

In Figure 3-2b we draw the circuit theory analog of the hydrogen market operating on the backbone. The flow of hydrogen and the storage levels are indicated in **blue**, while the flow of incentives and energy prices are indicated in **green**.

Conjugacy

Energy storage levels and energy prices form pairs of conjugate state variables, and energy flows and incentives form pairs of conjugate flow variables [5]. This conjugacy indicates the mutual influence between these variables: the energy prices drive the flows

of energy and the conjugate storage levels drive the incentives. It stems from the behavioral laws of the market agents, which link the stock and flow variables with each other. The behavioral laws of the market agents are treated in the next section.

3-3 Market Agents as Electrical Components

The next step is to identify the market agents and model them as analogous dynamical electrical components. We do this by matching their behavior laws with the constitutive laws of basic electrical components.

We model market agents using three passive components, whose dynamics are endogenous, and one active element, whose influence is exogenous. These basic electrical components allow us to design market agents as economic network agents ranging from simple representations of a single component to complex combinations of multiple components. The components and their analogs are listed in Table 3-2, with the basic market agents represented by the symbols in the last column. In Figure 3-2b, these symbols indicate the market agents in the hydrogen market. The following paragraphs treat each basic market agent individually.

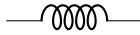



	Market agent	Electrical component	Behavioral law	Symbol
	Energy demand	Inductor	$f = \varepsilon p$	
<i>Passive</i>	Energy storage	Capacitor	$v = kq$	
	Market friction	Resistor	$v = bf$	
<i>Active</i>	Energy flow	Current Source	$f = f(t)$	

Table 3-2: Market agents as electrical components. With the price elasticity ε being the inverse of the inductance parameter ($\varepsilon = 1/L$), the storage inelasticity k being the inverse of the capacitance parameter ($k = 1/C$), and the market friction parameter b being equal to the resistance parameter R . Adjusted from Hutter and Mendel (2024) [5].

Demand for Energy as an Inductor

We model energy demand (or supply) as an inductor. This elementary demander is the crucial element for incorporating price dynamics in our economic networks.

The causal behavioral law of the demander follows the law of demand, which states that the price level p maintained by the demander determines the quantity demanded f , proportional to the price elasticity of demand ε which indicates how sensitive the agent's demand is to changes in energy price. In economic engineering, this relation is referred

to as the unified demand schedule¹, given by:

$$f = \varepsilon p. \quad (3-1)$$

A price acceleration or movement \dot{p} is interpreted as the force of demand that causes a movement along the demand schedule \dot{f} , dictating exactly how a change in the price level causes a change in the quantity demanded. These dynamics along the demand schedule are visualized in Figure 3-1.

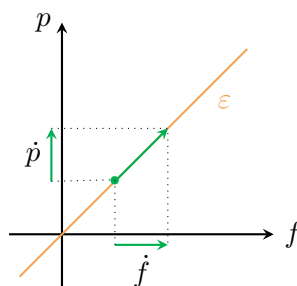


Figure 3-1: The dynamics of the demander (or supplier) as movements (green) along the unified demand schedule $f = \varepsilon p$ (orange)

We know that such a price movement \dot{p} has to be an incentive v , according to the stock-flow relation in Table 3-1. These incentives, also known as price drivers, may follow from factors such as scarcity and trade friction. These price drivers exerted by the storing element and friction element, respectively, are treated in the following paragraphs.

In Figure 3-2, we model industrial demand as an inductor that maintains a hydrogen price. On the supply side, hydrogen import by pipeline and low-carbon hydrogen production are also modeled as inductors, as they depend on the hydrogen price. The price storing aspect of the inductor is visualized by the inductor filling up with the flow of incentives, both indicated in green.

Energy Storage as a Capacitor

We model energy storage as a capacitor that maintains a storage level. The causal behavioral law of this storage relates the energy storage level q to an incentive v , which measures the convenience of holding more or less energy in storage, proportional to the storage inelasticity k :

$$v = kq. \quad (3-2)$$

This incentive drives changes in the energy price, affecting the quantities demanded and supplied. We interpret this as the law of scarcity. When energy is scarce, a positive

¹The concept of a unified demand schedule is presented by Mendel (2023) in [4].

incentive drives the energy price up; when energy is abundant, a negative incentive drives the price down.

In our economic circuit analog of the hydrogen market, central hydrogen storage in salt caverns and local storage at industry clusters are modeled as capacitors, each maintaining a hydrogen storage level. The capacitor is visualized as a storage element filling up with the flow of hydrogen, both indicated in [blue](#).

Market Friction as a Resistor

We model market friction imposed by a market operator as a resistor. Market friction acts as a damper to the energy system. Its behavioral law states that the market operator needs to be incentivized with a motive v to broker an energy flow f with a friction coefficient b :

$$v = bf. \quad (3-3)$$

This law indicates how an energy flow results in a price-driving incentive. The friction law is bi-causal and can also be used for other purposes, such as modeling consumption [5].

In Figure 3-2b, the market operator connects the central hydrogen storage to the rest of the market by brokering the imbalance between supply and demand. Since the resistor does not accumulate any flow, it is visualized with a gray friction element.

Energy Flow as a Current Source

We model time-dependent, exogenously imposed energy flows as a current source. These energy flows do not change in response to market prices but are only a function of time $f(t)$. This component is used to model constant or seasonal energy flows or to model an active demander when combined with an inductor.

In our example, renewable hydrogen production and import by ship are modeled as current sources that continuously inject a flow of hydrogen into the hydrogen backbone. Since renewable hydrogen production depends on intermittent offshore wind generation and import by ship is based on shipment schedules, these flows do not change in response to market prices.

3-4 Energy Systems as Economic Networks

Edges, Nodes, and Meshes

We design economic networks analogously to electrical networks by wiring the market agents together in a topological structure that represents the energy market where these agents trade. This structure determines how energy flows through the economic network



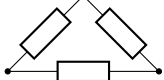
Graph theory	Energy systems	Graph	Symbol
Edge	Market agent		\mathcal{E}
Node	Energy exchange locus		\mathcal{N}
Mesh	Circular flow of energy		\mathcal{M}

Table 3-3: Topological concepts within energy systems. Adjusted from Hutter and Mendel (2024) [5].

and how incentives are balanced among the market agents. We use the topological concepts of graph theory listed in Table 3-3.

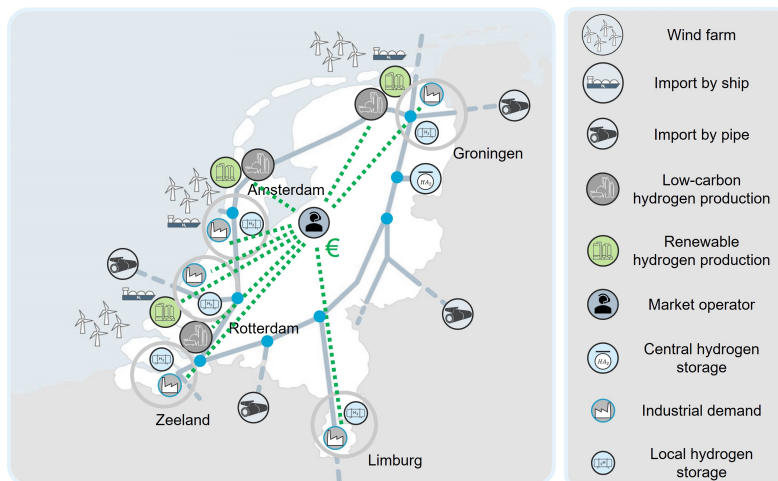
The identified market agents, treated in Section 3-3, make up the edges in the economic network. Each edge is associated with a unique drop in desirability, representing the incentive required by the market agent to process the flow of energy.

Market agents can interact in different network topologies. Cooperative interactions are modeled in series interconnection within an economic circuit, while competitive interactions are modeled in parallel interconnection. In the hydrogen market shown in Figure 3-2, suppliers and demanders compete for the flow of hydrogen, thus forming a parallel interconnection. The market operator, connecting the central storage to the rest of the market, brokers hydrogen surpluses and deficits to balance supply and demand. Consequently, the central storage and market operator cooperate (series interconnection) and together compete with suppliers and demanders (parallel interconnection).

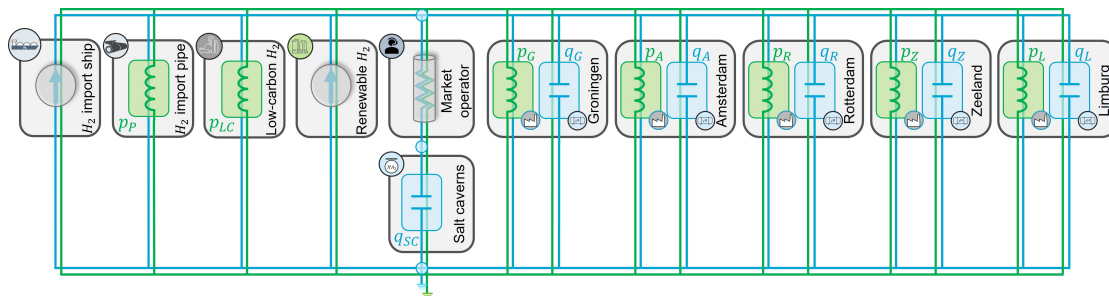
By identifying the interactions of the market agents, we can make up the node and mesh structures of the economic network. The concepts of these structures have been introduced in Section 2-3.

The nodes represent the loci where energy flows are exchanged. At each node, connected market agents share a common level of desirability. For example, between two cooperative agents, we find a node (see the middle node in Figure 3-2b). The nodes in Figure 3-2b are indicated by the thick blue dots. We can reduce the node structure to three key nodes: one for hydrogen exchange between suppliers, demanders, and storage; one for the exchange between the market operator and storage; and one reference node. Each economic circuit includes a reference node, or ground node, to calibrate desirability levels at the other nodes (see the bottom node in Figure 3-2b).

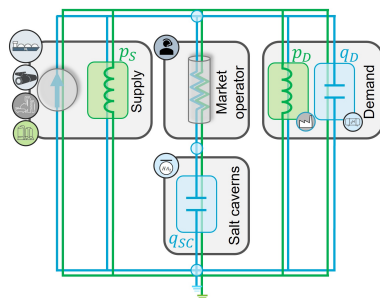
A mesh is a loop that contains no other loops, sustaining a single circular energy flow. Competitive market agents modeled in parallel naturally form meshes. Agents within a mesh can exchange energy flows while maintaining a mutual reference for desirability levels, ensuring consistent perceived value across the mesh. While the mesh structure may not be directly recognizable in the hydrogen backbone in Figure 3-2a, it becomes apparent in its analogous circuit in Figure 3-2b.



(a) The hydrogen market with the node structure indicated by the blue dots, the mesh structure indicated by the dashed green lines, and the market agents included in the legend on the right.



(b) The hydrogen market as an analogous electrical circuit. The suppliers are on the left and the industry clusters are on the right. The market operator, who connects the salt caverns with the rest of the market, is positioned in the middle. The accumulation of the hydrogen flow (blue) into hydrogen storage (q) is indicated by the blue capacitor. The accumulation of the flow of incentives (green) by the industrial demanders (indicated by the industry symbol) and suppliers (the three supply chains on the left) into a hydrogen transfer price (p) is indicated by the green inductor. The market operator is indicated by the gray resistor. The node structure reduces to three nodes indicated in blue, and the meshes have now become apparent as closed loops.



(c) Aggregated version of the analogous electrical circuit. With the suppliers modeled with one representative supplier and the demanders with one representative demander.

Figure 3-2: The circuit theory analog of the hydrogen market operating on the hydrogen backbone. This figure comprises all the design steps treated in this chapter.

An Energy Market as a Closed Economic Circuit

An energy market is modeled as a closed economic circuit, where only one commodity is traded.

If an energy system includes multiple energy markets, it is modeled as an economic network of topologically disconnected economic circuits. These circuits are magnetically coupled through mutual inductance, emulating the influence of prices across interconnected energy markets.

In Figure 3-2, we model only the hydrogen market, representing it with a single electrical circuit. In Chapter 4, we will design more complex networks for the hydrogen spot market as part of a larger energy system. Besides a hydrogen market, these networks incorporate different hydrogen supply chains and their related energy markets coupled through mutual inductance.

Representative Agents as Circuit Modules

Economic circuit theory allows us to simplify our economic network by representing multiple components by a single equivalent component, which we refer to as a circuit module. This significantly reduces the complexity of the network. In Figure 3-2c, we illustrate the aggregated version of the network in Figure 3-2b. We reduce the four suppliers to a single representative supplier and the five industry clusters into a single representative demander. For a more detailed explanation of this procedure, see Hutter and Mendel (2024) [5].

3-5 Energy Market Clearing and Kirchhoff's Laws

For an energy market to clear, both physical energy flows and energy prices must be balanced. In economic circuit theory, market clearing is enforced by Kirchhoff's current and voltage laws, which we interpret as the node and mesh laws for economic circuits. These laws allow us to formulate the physical and price-clearing conditions of the energy market, from which we derive a consistent description of the network dynamics [5].

We demonstrate energy market clearing based on the circuit² in Figure 3-3. The directions of the hydrogen flows and incentives follow the sign convention presented by Hutter and Mendel. In this simple network, the dynamics are easily derived. More complex networks, as you will see in the next chapter, require a more robust accounting approach to track the flows and incentives in the network.

²We have chosen to further simplify the network in Figure 3-2c by omitting the current source on the supply side and the capacitor on the demand side.

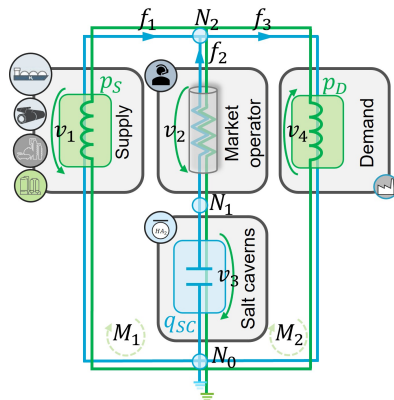


Figure 3-3: Hydrogen market clearing in an even further simplified version of the circuit shown in Figure 3-2c. The hydrogen flows and nodes are indicated in blue and the incentives and meshes are indicated in green.

The Node Law

First, we demonstrate the physical clearing of the node structure through the node law. This clearing involves the energy flows, storage levels, and nodes, all indicated in blue in the electrical circuit in Figure 3-3.

The node law states that the net energy flow at each node equals zero ($\sum f = 0$), where flows entering a node are positive and flows leaving a node are negative. By applying this law to the entire node structure, we achieve stock-flow consistency within the network.

The circuit in Figure 3-3 contains three nodes, indicated by \mathcal{N}_0 , \mathcal{N}_1 , and \mathcal{N}_2 . At node \mathcal{N}_2 , supply and demand converge. From this node, we derive that $f_1 + f_2 - f_3 = 0$, and thus $f_1 + f_2 = f_3$. If there is an imbalance between supply (f_1) and demand (f_3), the node law tells us that exactly this imbalance must be stored or extracted from the storage (f_2). Node \mathcal{N}_1 shows that the flow brokered by the market operator equals the flow in/out of the storage, equal to the imbalance. Node \mathcal{N}_0 serves as the reference node.

The dynamics of the storage level in the salt caverns can thus be expressed in terms of the imbalance between supply and demand, according to:

$$\frac{dq_{sc}}{dt} = f_3 - f_1. \quad (3-4)$$

The Mesh law

More pivotal is the price-clearing of the mesh structure through the mesh law. This clearing involves the incentives, energy prices, and meshes, all indicated in green in the electrical circuit in Figure 3-3. The mesh law ensures the conservation of total economic value through price-incentive consistency. Such consistency is not present in existing energy systems models, as argued in Chapter 2.

The mesh law ensures the balancing of incentives within a mesh. It states that the net incentive within a mesh equals zero ($\sum v = 0$). If the direction of the incentives agrees with the direction of the mesh, it is positive, and when the direction of the incentive disagrees with the direction of the mesh, it is negative. By applying this law to the entire mesh structure, we achieve price-incentive consistency within the economic network.

In Figure 3-3, we have two meshes, indicated by \mathcal{M}_1 and \mathcal{M}_2 . We analyze these meshes in a clockwise direction. For \mathcal{M}_1 , we derive that $-v_1 + v_2 + v_3 = 0$, and for \mathcal{M}_2 , we derive that $-v_2 - v_3 - v_4 = 0$. Substituting the equations provides the equality: $v_1 = v_2 + v_3 = -v_4$. If there is an imbalance in incentives, the hydrogen price adjusts based on the incentives within the meshes to ultimately reach a balance of incentives.

From our derivation, it follows that suppliers and demanders adjust their prices at the same rate, and subsequently, they adjust their quantities supplied and demand. This supply-and-demand-driven pricing mechanism of the hydrogen market is visualized in Figure 3-4. The negative incentive on the demand side follows from the downward-sloping demand schedule, as shown in the same figure.

The dynamics of the hydrogen price can thus be expressed in terms of the incentives exerted by the market operator and storage, according to:

$$\frac{dp^{H_2}}{dt} = v_1 = v_2 + v_3 = -v_4 \quad (3-5)$$

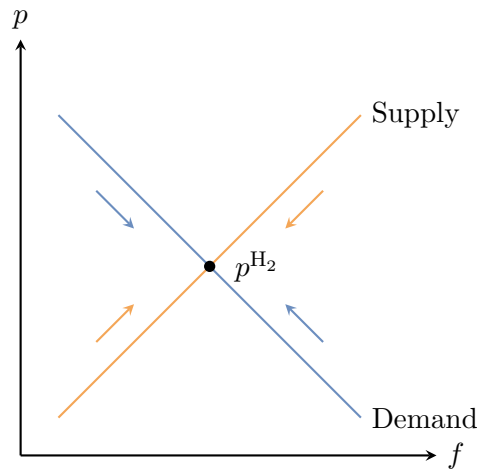


Figure 3-4: Supply-and-demand-driven pricing. The incentives, indicated by the arrows, as movements along the supply and demand curves such that they balance and we obtain a market clearing price p^{H_2}

Modeling and Design of Economic Networks of a Hydrogen Spot Market

4-1 Introduction

In this chapter, we design three economic networks of a hydrogen spot market: a core network and two extensions. We design the networks based on our model assumptions that follow from our analysis of the hydrogen market, which can be found in Section A-6.

We start with the design of the core network in Section 4-2, where we address the network topology, central hydrogen storage, the market operator, and spot market clearing. Section 4-3 details the design of four hydrogen supply chains, and Section 4-4 details the design of industry clusters.

In Section 4-5, we use the clearing conditions for stock-flow and price-incentive consistencies to derive the dynamics of spot prices and storage levels within the core network and construct a state-space representation. This derivation is supported by Appendix C, where we use a matrix-based accounting approach to consistently apply the node and mesh laws.

In Section 4-6, we present two alternative economic networks that form extensions of the core network. One design treats renewable and low-carbon hydrogen as separate commodities, and the other integrates an ammonia market.

Finally, in Section 4-7, we briefly describe the identification process for the networks.

4-2 Design of the Core Network

4-2-1 The Hydrogen Backbone as the Network Topology

Following the design methodology as introduced in the previous section, we design a core network for the hydrogen spot market. The design of the core network is in line with the analysis of the hydrogen spot market in Appendix A. The core network is a base model for which we design two extensions in Section 4-6.

The hydrogen backbone forms the foundation of the topology of the core network. The hydrogen backbone, see Section A-3, prescribes the trade network in which market agents interact and distribute hydrogen. The hydrogen traded on this backbone is treated as a homogeneous commodity in the core network.

The core network is a multi-carrier energy network that integrates various energy markets through different hydrogen supply chains. This integration allows the hydrogen (H_2) spot market to interact with related commodity markets, including liquid hydrogen (LH_2), offshore wind energy (OWE), and natural gas (NG).

The core network is presented in Figure 4-1. The main energy flows are indicated in the network and listed in Table 4-1. The colored boxes indicate the different building blocks, including supply chains, industry clusters, and storage. In remaining part of this chapter, we treat the design of these building blocks in more detail.

The locations of the prices are indicated in the network by (p) and the stocks by (q). The voltages or incentives are indicated by the curved arrows over the electrical components. The direction of currents or energy flows is indicated by small arrowheads on the network lines. The ground (indicated by the two decreasing-length lines), located at the bottom of the network, corresponds to the zero desirability level, while the + sign at the top indicates a positive desirability level.

A Competitive Market as a Parallel Configuration

On a spot market for hydrogen, prices are determined by supply and demand. This market mechanism ensures that the prices reflect the current market conditions. We further assume a standardized product, transparent pricing, and sufficient suppliers and demanders. Based on these assumptions, we posit that a spot market for hydrogen functions as a competitive market where suppliers and demanders compete to sell and buy hydrogen.

To model this competitive behavior, we represent the economic network agents in a parallel configuration [5]. The agents compete for the total flow of hydrogen within the market while being subjected to the same market incentives.

The total hydrogen flow supplied through the four competitive supply chains $n \in \{1, \dots, 4\}$ sums up to:

$$f_s^{\text{H}_2}(t) = \sum_{n=1}^4 s_n^{\text{H}_2}(t). \quad (4-1)$$

For the five competitive demanders, representing the five industry cluster $m \in \{1, \dots, 5\}$, it follows that the total flow of hydrogen demanded is given by

$$f_d^{\text{H}_2}(t) = \sum_{m=1}^5 d_m^{\text{H}_2}(t). \quad (4-2)$$

LH₂, OWE, and NG market		Hydrogen market	
w^{LH_2}	LH ₂ import	$f_s^{\text{H}_2}$	Total H ₂ supply
$f_e^{\text{LH}_2}$	LH ₂ excess demand flow	$s_1^{\text{H}_2}$	Regasified LH ₂
$f_d^{\text{LH}_2}$	Total demand of LH ₂	$s_2^{\text{H}_2}$	Gaseous H ₂ import
$d_2^{\text{LH}_2}$	LH ₂ demand for regasification	$s_3^{\text{H}_2}$	Renewable H ₂ through electrolysis
$d_3^{\text{LH}_2}$	General LH ₂ demand	$s_4^{\text{H}_2}$	Low-carbon H ₂ through
w^{OWE}	Generated OWE		steam methane reforming (SMR)
d_1^{OWE}	OWE demand for electrolysis	$f_e^{\text{H}_2}$	H ₂ excess demand flow
d_1^{OWE}	OWE demand for electricity	$f_d^{\text{H}_2}$	Total H ₂ demand
f_s^{NG}	Total supply of NG	$d_m^{\text{H}_2}$	H ₂ demand industry cluster (ic) m
$f_{i,s}^{\text{NG}}$	Elastic NG supply	$f_{i,m}^{\text{H}_2}$	Elastic H ₂ demand ic m
w^{NG}	Inelastic NG supply	$u_m^{\text{H}_2}$	Inelastic H ₂ demand ic m
f_e^{NG}	NG excess demand flow	$f_{c,m}^{\text{H}_2}$	Excess H ₂ demand ic m
f_d^{NG}	Total demand of NG		
d_2^{NG}	NG demand for SMR		
d_3^{NG}	General NG demand		

Table 4-1: Overview of the main energy flows in the core network

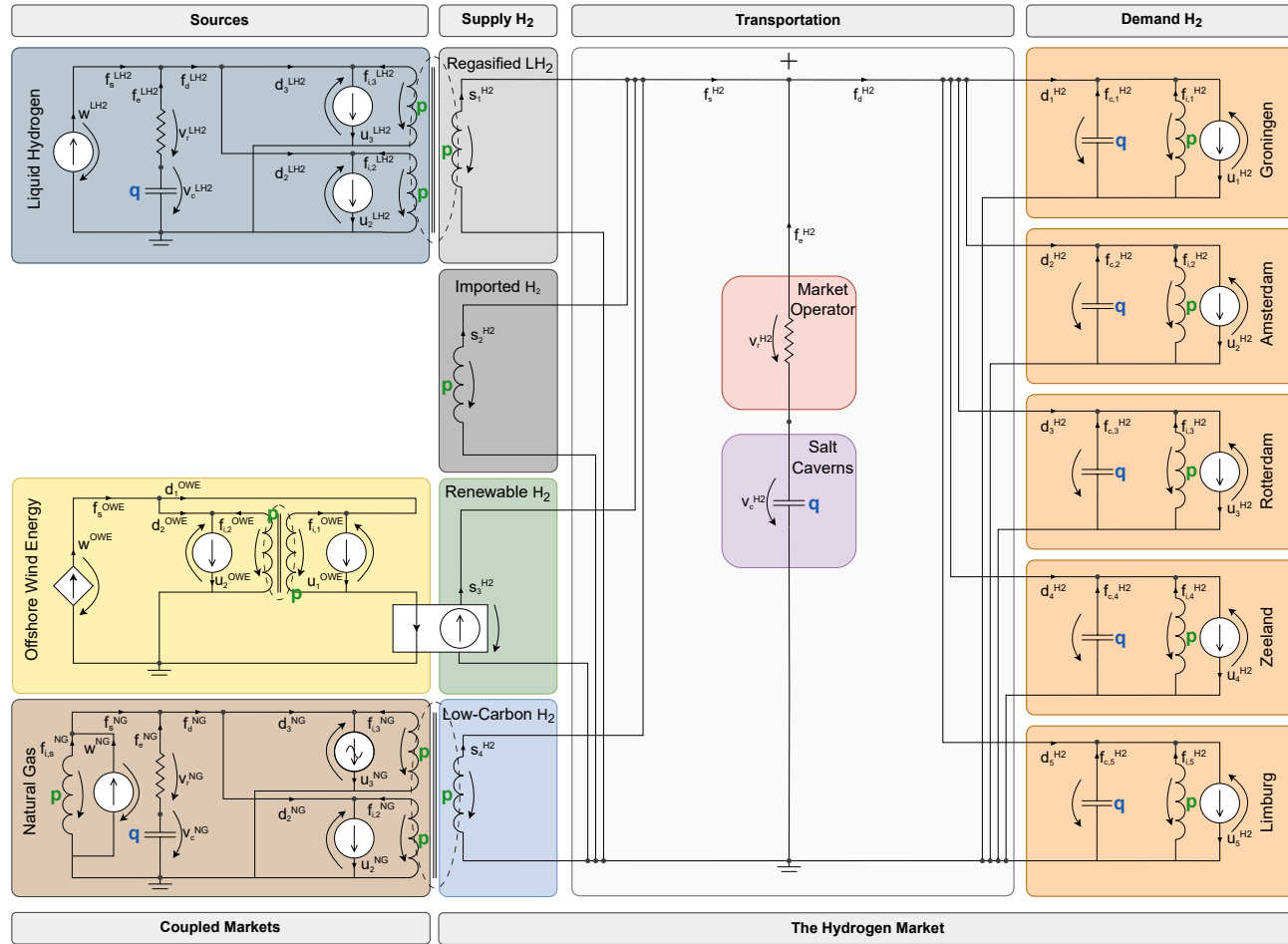


Figure 4-1: Topological structure of the core network. Hydrogen storage in salt caverns (purple) is treated in Section 4-2-2; market friction induced by a market operator (pink) is treated in Section 4-2-3; gaseous hydrogen import by pipeline (dark-gray) is treated in Section 4-3-1; renewable hydrogen production by a wind-hydrogen operator (yellow/green) is treated in Section 4-3-2; low-carbon hydrogen production by a SMR agent (brown/blue) is treated in Section 4-3-3; LH₂ import and regasification (gray-blue/light-gray) is treated in Section 4-3-4; the industry clusters as active demanders (orange) are treated in Section 4-4.

4-2-2 Central Hydrogen Storage as a Capacitor

In a future hydrogen spot market, hydrogen is stored in central salt caverns to cope with fluctuations in supply and demand (see Section A-4). This central hydrogen storage is modeled as a capacitor, indicated by the purple colored boxes in Figures 4-1 and 4-2.

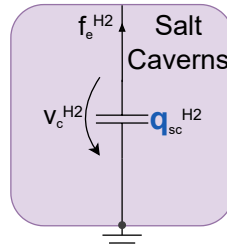


Figure 4-2: Central storage in salt caverns as a capacitor connected to the ground. With the hydrogen flow extracted from the storage indicated by $f_e^{H_2}$ and the incentive exerted by the storage indicated by $v_c^{H_2}$.

The desired hydrogen storage level is modeled as the zero level at which no incentive is exerted on the hydrogen spot market. When the storage is not at its desired level, an incentive is exerted by the storage $v_c^{H_2}$ proportional to the quantity of hydrogen stored $q_{sc}^{H_2}$, according to:

$$v_c^{H_2} = k_{sc}^{H_2} q_{sc}^{H_2}, \quad (4-3)$$

with $k_{sc}^{H_2}$ the agent's convenience yield for holding hydrogen in storage. As the storage in salt caverns is primarily for long-term use, this convenience yield is high.

When the storage is understocked, the storage operator imposes a positive incentive on the market to drive up the hydrogen spot price. Higher prices incentivize suppliers to provide more hydrogen and demanders to demand less. As a result, more hydrogen will be injected into storage. Conversely, when the storage is overstocked, a negative incentive is exerted on the market, lowering spot prices. Lower prices discourage further storage and lead to the extraction of hydrogen to meet the increased hydrogen demand.

The stock-flow relation, as described in Table 3-1, dictates that the rate of change in the hydrogen storage levels is determined by the flow into or out of the storage. This flow equals the imbalance between supply and demand, referred to as the excess hydrogen flow $f_e^{H_2}$, in which the positive direction is chosen in line with the quantity demanded:

$$f_c^{H_2} = f_e^{H_2} = f_d^{H_2} - f_s^{H_2}. \quad (4-4)$$

When $f_e^{H_2} > 0$, hydrogen is extracted from the storage, and when $f_e^{H_2} < 0$, hydrogen is injected into the storage.

4-2-3 A Market Operator as a Resistor

In a hydrogen spot market, a market operator manages the trade activity in real-time by imposing market friction. This operator is modeled as a resistor, represented by the pink boxes in Figures 4-1 and 4-3.

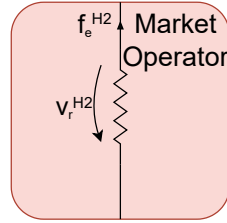


Figure 4-3: A market operator brokering the hydrogen flow between central storage and the rest of the market as a resistor. With the brokered hydrogen flow indicated by $f_e^{H_2}$ and the needed incentive indicated by $v_r^{H_2}$.

The market operator connects the central hydrogen storage to the rest of the market. The two market agents collaborate to manage supply and demand and are thus modeled in series interconnection. The agents share the same hydrogen flow $f_e^{H_2}$ while their incentives collectively influence the network dynamics. The market operator needs to be incentivized with a motive $v_r^{H_2}$ to broker the flow of hydrogen $f_e^{H_2}$ according to:

$$v_r^{H_2} = b^{H_2} f_e^{H_2}, \quad (4-5)$$

with friction parameter b^{H_2} . Depending on the market imbalance, this leads to price-increasing or -lowering incentives. An excess hydrogen demand ($f_e^{H_2} > 0$) results in a price premium, whereas an excess supply ($f_e^{H_2} < 0$) leads to a discount. This incentivizes suppliers and demanders to adjust their supply and demand in order to balance supply and demand.

4-2-4 The Hydrogen Spot Market Dynamics

To derive the hydrogen spot market dynamics in the core network, we apply the node and mesh laws to formulate the network-wide clearing of both energy flows and spot prices, following the procedure in [5]. The physical clearing conditions prescribe that the excess flow in each energy market is determined by the imbalance between supply and demand, and the price-clearing conditions prescribe that the imbalance in incentives equals the rate of change in energy prices (see Section 3-5).

We derive one physical and one price clearing condition per energy market. The full derivation of the clearing conditions can be found in Appendix C.

The price clearing conditions prescribe that all suppliers and demanders of a certain energy commodity experience the same market incentives and thus adjust their reservation price at the same rate. For the hydrogen, LH₂, and natural gas market, the market incentive equals the sum of the incentives exerted by the market operator and the incentive exerted by the storage operator.

To demonstrate, we follow this procedure for the hydrogen market clearing. For the physical clearing, we find that the rate of change in the hydrogen storage level is given by stock-flow relation:

$$\frac{dq_{cs}^{\text{H}_2}(t)}{dt} = f_e^{\text{H}_2}(t). \quad (4-6)$$

For the hydrogen spot price clearing, we find that the rate of change in the hydrogen spot price is given by:

$$\frac{dp^{\text{H}_2}(t)}{dt} = v^{\text{H}_2}(t) = v_r^{\text{H}_2}(t) + v_c^{\text{H}_2}(t) = b^{\text{H}_2} f_e^{\text{H}_2}(t) + k_{sc}^{\text{H}_2} q_{cs}^{\text{H}_2}(t). \quad (4-7)$$

The expressions for $v_r^{\text{H}_2}(t)$ and $v_c^{\text{H}_2}(t)$ follow from Equations 4-5 and 4-3.

The derivation of the dynamics of natural gas and LH₂ spot prices and storage levels follow the same procedure. For the offshore wind energy market, no storage exists and the price dynamics are fully determined by the supply and therefore the wind variability. The analytically derived price dynamics for the different energy commodities can be found in Section 4-5-2.

The Hydrogen Spot Price

The hydrogen spot price is derived by accumulating the price-driving incentives. If we assume the integration constant is zero ($p^{\text{H}_2}(0) = 0$), we obtain that under our conditions all transactions occur at the same contemporary spot price.

$$p^{\text{H}_2}(t) = \int v^{\text{H}_2}(t) dt + p^{\text{H}_2}(0) \quad (4-8)$$

For natural gas, liquid hydrogen, and offshore wind energy, we also derive a single contemporary spot price.

4-3 Design of the Hydrogen Supply Chains

4-3-1 Gaseous Hydrogen Import by Pipeline

The import of gaseous hydrogen through international pipelines (see the European Hydrogen Backbone (EHB) in Section A-3), is regulated by an import agent. The import

agent is indicated by the dark-gray box in the Figures 4-1 and 4-4. We model the gaseous hydrogen importer as a single inductor¹.

The gaseous hydrogen importer is a flexible supplier. The amount it supplies depends directly on the hydrogen spot price, according to the law of supply. Its importer's supply schedule follows the law of supply and demand and is prescribed by the constitutive law of the inductor.

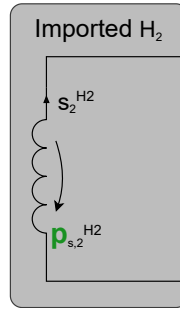


Figure 4-4: Gaseous hydrogen importer as a single inductor. With $p_{s,2}^{\text{H}_2} = p^{\text{H}_2}$ the hydrogen spot price, and the imported hydrogen indicated by $s_2^{\text{H}_2}$.

The quantity supplied by the gaseous hydrogen importer $s_2^{\text{H}_2}$ is given by

$$s_2^{\text{H}_2}(t) = \varepsilon_{s,2}^{\text{H}_2} p_{s,2}^{\text{H}_2}(t), \quad (4-9)$$

where $p_{s,2}^{\text{H}_2}(t) = p^{\text{H}_2}(t)$ (see Section 4-2-4).

The first derivative of the slope of the supply schedule represents the price elasticity of supply $\varepsilon_{s,2}^{\text{H}_2}$.

4-3-2 The Wind-Hydrogen Supply Chain for Renewable H₂ Production

The Wind-Hydrogen Operator

The wind-hydrogen supply chain is managed by a wind-hydrogen operator, as illustrated in Figure 4-5 with the main energy flows listed in Table 4-2. This agent operates in two

¹This design choice assumes that the international hydrogen trade occurs at a larger scale compared to the national trade. This allows the importer to modify its hydrogen supply freely. Moreover, due to the broader sectoral coverage and higher trade volumes in the international hydrogen market, it is further assumed that prices within this market are lower than those in the national market. With this assumption, we ensure that there is always an incentive to import gaseous hydrogen when there is a national shortage.

markets: the offshore wind energy (OWE) market² and the hydrogen market. The supply of renewable hydrogen depends on weather conditions and the production strategy of the wind-hydrogen operators.

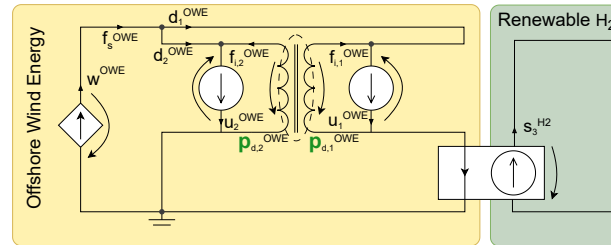


Figure 4-5: The wind-hydrogen operator

Wind-hydrogen supply chain	
w^{OWE}	Generated OWE
f_s^{OWE}	Total OWE supply
d_1^{OWE}	OWE demand for renewable H ₂ production
d_2^{OWE}	OWE demand for direct selling
$f_{i,1}^{\text{OWE}}$	Price-elastic OWE demand for H ₂ production
$f_{i,2}^{\text{OWE}}$	Price-elastic OWE demand
u_1^{OWE}	Inelastic OWE demand for H ₂ production
u_2^{OWE}	Inelastic OWE demand
$s_3^{\text{H}_2}$	Total renewable H ₂ supply

Table 4-2: Overview of energy flows within the wind-hydrogen supply chain

Offshore Wind Energy Generation

We use a controlled current source to model offshore wind energy generation. This component uses a wind distribution as its input, which modeling is detailed in Appendix D.

We determine the total generated OWE using an offshore wind capacity³ of 12 GW. To calculate the generated OWE, we make use of the power curve of a wind turbine⁴ as

²Please note this OWE market is not a representation of the whole offshore wind energy market. However, it is a fictitious market that is needed to determine the production strategy.

³This is the aggregate capacity of wind parks coupled to electrolyzers. This is a rough estimate if we assume an electrolyzer capacity of 3-4 GW.

⁴Data is used from the Vestas V164-9.5 turbine. This turbine is used for the Blauwwind and Borssele 3 & 4 wind farms and has a rated power of 9.5 MW at a rated speed of 14 m/s. It has a cut-in wind speed of 3 m/s and a cut-off wind speed of 25 m/s. Note that the power output of the turbine at an average wind speed of 10 m/s is just 5 MW.

shown in Figure 4-6. This power curve is used to determine the output power of a single turbine at each point in time.

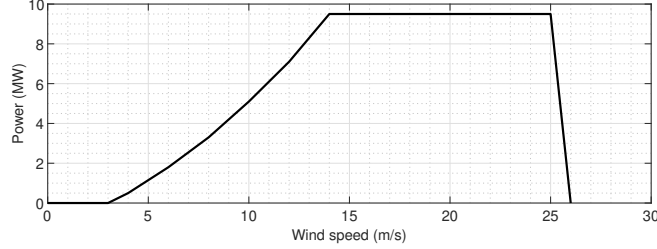


Figure 4-6: Power curve of Vestas V164-9.5 turbine

We scale this generated OWE such that it is compatible with the model. The current exerted by the controlled current source, representing the generated OWE, is given by $w^{\text{OWE}}(t) = f_s^{\text{OWE}}(t)$.

The Renewable Hydrogen Production Strategy

The wind-hydrogen supply chain operator has the choice to sell the generated OWE directly or utilize it to produce and sell hydrogen. The production strategy depends on the fictitious price the operator ascribes to their generated OWE. This price reflects the scarcity and abundance of OWE.

As a production/selling strategy, the operator adjusts its demand according to the best combination of selling OWE and producing and selling hydrogen. We see this strategy as the operator maximizing its running utility, which we model with a mutual inductor⁵.

To include the price effects on the strategy of the operator, its demand is split into demand for OWE to sell it directly d_2^{OWE} , and the demand for OWE for hydrogen production through electrolysis d_1^{OWE} . As there is no storage, the OWE supply equals the demand:

$$f_s^{\text{OWE}}(t) = f_d^{\text{OWE}}(t) = d_1^{\text{OWE}}(t) + d_2^{\text{OWE}}(t). \quad (4-10)$$

Each quantity demanded d_j^{OWE} is determined by three factors: the inelastic demand, the elastic demand, and the cross-elasticity between the two kinds of demand.

⁵See Hutter (2023) where he links the link between mutual inductance and utility maximization. [13]

The quantity demanded d_j^{OWE} is determined by:

$$\begin{aligned} d_j^{\text{OWE}}(t) &= u_j^{\text{OWE}} - f_{i,j}^{\text{OWE}} \\ &= u_j^{\text{OWE}} - \sum_{k \in j} \varepsilon_{jk}^{\text{OWE}} p_{d,j}^{\text{OWE}} \quad \forall j \in \{1, 2\}, \end{aligned} \quad (4-11)$$

where $p_{d,j}^{\text{OWE}}$ is the operator's reservation price for the generated OWE, $\varepsilon_{jk}^{\text{OWE}}$ its cross-elasticity of demand if $j \neq k$, and u_j^{OWE} the inelastic demand. When $j = k$, $\varepsilon_{jk}^{\text{OWE}}$ returns the regular price elasticity denoted by $\varepsilon_j^{\text{OWE}}$.

In matrix form, the demand can be written as follows.

$$\begin{aligned} \begin{pmatrix} d_1^{\text{OWE}} \\ d_2^{\text{OWE}} \end{pmatrix} &= \begin{pmatrix} u_1^{\text{OWE}} \\ u_2^{\text{OWE}} \end{pmatrix} - \begin{pmatrix} \varepsilon_1^{\text{OWE}} & \varepsilon_{12}^{\text{OWE}} \\ \varepsilon_{12}^{\text{OWE}} & \varepsilon_2^{\text{OWE}} \end{pmatrix} \begin{pmatrix} p_{d,1}^{\text{OWE}} \\ p_{d,2}^{\text{OWE}} \end{pmatrix} \\ &= \begin{pmatrix} u_1^{\text{OWE}} \\ u_2^{\text{OWE}} \end{pmatrix} - \begin{pmatrix} \varepsilon_1^{\text{OWE}} + \varepsilon_{12}^{\text{OWE}} \\ \varepsilon_{12}^{\text{OWE}} + \varepsilon_2^{\text{OWE}} \end{pmatrix} p^{\text{OWE}} \end{aligned} \quad (4-12)$$

The second equation follows from the price clearing condition for OWE, see Section 4-2-4.

Electrolysis Efficiency

To incorporate the losses associated with electrolysis, we use a current-controlled current source that relates the electrolyzer input to the electrolyzer output, the flow of produced hydrogen. The coupling c^{OWE} reflects the electrolyzer efficiency.

The renewable hydrogen flow into the hydrogen backbone is thus given by

$$\begin{aligned} s_3^{\text{H}_2}(t) &= c^{\text{OWE}} d_1^{\text{OWE}}(t) \\ &= c^{\text{OWE}} \left(u_1^{\text{OWE}} - (\varepsilon_{11}^{\text{OWE}} + \varepsilon_{12}^{\text{OWE}}) p^{\text{OWE}} \right). \end{aligned} \quad (4-13)$$

4-3-3 Low-Carbon Hydrogen Production

The Low-Carbon Hydrogen Supply Chain

The low-carbon hydrogen supply chain is particularly important for absorbing fluctuations in supply as SMR plants already exist and can be turned on and off easily. The hydrogen production through SMR will therefore highly depend on the hydrogen spot price, reflecting the fluctuations in renewable hydrogen supply.

The low-carbon hydrogen supply chain is modeled as visualized in Figure 4-7. The energy flows in this supply chain model are listed on the next page in Table 4-3. The SMR operator, indicated by the dashed box, is modeled with a three-winding mutual

inductance. The agent operates in two markets: in the natural gas market⁶ and the hydrogen market.

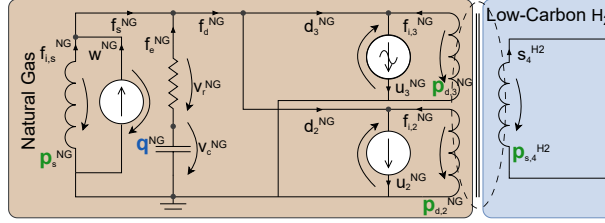


Figure 4-7: The low-carbon hydrogen supply chain with the SMR operator indicated by the dashed box

Low-carbon hydrogen supply chain	
$f_{i,s}^{NG}$	Elastic NG supply
w^{NG}	Inelastic NG supply
f_s^{NG}	Total NG supply
f_e^{NG}	Excess NG flow
f_d^{NG}	Total NG demand
d_2^{NG}	NG demand for low-carbon H ₂ production
d_3^{NG}	General NG demand
$f_{i,2}^{NG}$	Price-elastic NG demand for H ₂ production
$f_{i,3}^{NG}$	Price-elastic NG demand
u_2^{NG}	Inelastic NG demand for H ₂ production
u_3^{NG}	Seasonal inelastic NG demand
$s_4^{H_2}$	Total low-carbon H ₂ supply

Table 4-3: Overview of energy flows within the low-carbon hydrogen supply chain

The Natural Gas Market

The supply of natural gas in the Netherlands, which comes predominantly from import, is modeled as a supplier which consists of a current source and an inductor, representing the inelastic w^{NG} and elastic natural gas supply $f_{i,s}^{NG}$ respectively. The total supply is therefore given by:

$$f_s^{NG} = w^{NG} + f_{i,s}^{NG} = w^{NG} + \varepsilon_s^{NG} p_s^{NG}, \quad (4-14)$$

with $p_s^{NG} = p^{NG}$ the natural gas price, see Section 4-2-4.

⁶The natural gas market in the network represents the industrial natural gas market. This is an extremely simplified version of this market.

To capture the price effects between natural gas and hydrogen, natural gas demand is split into two types of demanders: demanders who specifically demand natural gas for hydrogen production (SMR facilities) and demanders who demand it for other purposes.

$$f_d^{\text{NG}} = d_2^{\text{NG}} + d_3^{\text{NG}} \quad (4-15)$$

Natural gas can be stored in the case of an excess supply, which is modeled as a capacitor (see Section 4-2-2). A market operator intervenes by providing price-increasing or -lowering incentives. The market operator is modeled with the resistor (see Section 4-2-3). The excess flow f_e^{NG} equals to flow through the resistor f_r^{NG} and in the capacitor f_c^{NG} :

$$f_e^{\text{NG}} = f_s^{\text{NG}} - f_d^{\text{NG}}. \quad (4-16)$$

The Low-Carbon Hydrogen Production Strategy

The SMR operator is a demander of natural gas in the natural gas market and a supplier of low-carbon hydrogen in the hydrogen market. Its production strategy, and thus its buying and selling strategy, depends on both the prices of gas and hydrogen. In economics, these price effects between a demanded good and a supplied good, from a producer's perspective, are often overlooked.

To model the desired price effects, this section details the design process of the SMR operator and motivates why a three-winding mutual inductor is used. The most important characteristics that should be included in modeling the price effects between the demanded natural gas and the supplied hydrogen, from the perspective of the SMR agent, are listed below.

- The price-dependent production of hydrogen ($s_4^{\text{H}_2}$), influenced by both the natural gas price and the hydrogen price: $s_4^{\text{H}_2} = f(p^{\text{H}_2}, p^{\text{NG}})$.
- The proportionality between the output and input flow of the SMR to include the conversion losses ($s_4^{\text{H}_2} \approx 0.9d_2^{\text{NG}}$).
- The negative correlation between the two different flows of natural gas demand.
- The natural gas demand d_3^{NG} should follow the industrial demand pattern (higher demand in winter months and lower in summer months).
- The share of low-carbon hydrogen matches the supply distribution as shown in Figure A-3 in Section A-6.

In economic engineering, we distinguish two kinds of price effects: a change in price elasticity, akin to a rotation of the demand curve⁷, and the substitution effect, which is modeled as mutual inductance. The price effect associated with the production strategy of the SMR agent fits somewhat between those two.

We focus on price coupling through mutual inductance such that the economic network model remains LTI. Due to the cross-relations, a mutual inductor indirectly influences the price elasticities of supply and demand. This sufficiently resembles the desired price effects. From a mutual inductor, as seen in Section 4-3-2, we can derive a utility function representing the strategy of the agent. This utility function can be described both analytically and geometrically, making parameter tuning more intuitive.

We use a three-winding⁸ mutual inductor to model the price coupling as a two-winding mutual inductor does not lead to the desired characteristics. This three-winding mutual inductor couples the SMR production agent with the general natural gas demander. The upper two inductors together belong to the SMR agent, as indicated by the dashed box in Figure 4-7, while the remaining inductor belongs to the natural gas demander. The current-voltage relationships of the three-winding mutual inductor are prescribed by the mutual inductance blocks embedded in Simscape. These equations capture the relations between the flows and prices in the natural gas and hydrogen market.

We can write the low-carbon hydrogen supply $s_4^{\text{H}_2}$ and the demand for natural gas, split in d_2^{NG} and d_3^{NG} , in terms of the elasticity matrix as described in Equation (4-17). Following the price clearing conditions in Section 4-2-4, we know that $p_{s,4}^{\text{H}_2} = p^{\text{H}_2}$ and $p_{d,2}^{\text{NG}} = p_{d,3}^{\text{NG}} = p^{\text{NG}}$.

$$\begin{aligned} \begin{pmatrix} s_4^{\text{H}_2} \\ d_2^{\text{NG}} \\ d_3^{\text{NG}} \end{pmatrix} &= \begin{pmatrix} 0 \\ u_2^{\text{NG}} \\ u_3^{\text{NG}} \end{pmatrix} - \begin{pmatrix} \varepsilon_{11}^{\text{NG}} & \varepsilon_{12}^{\text{NG}} & \varepsilon_{13}^{\text{NG}} \\ \varepsilon_{12}^{\text{NG}} & \varepsilon_{22}^{\text{NG}} & \varepsilon_{23}^{\text{NG}} \\ \varepsilon_{13}^{\text{NG}} & \varepsilon_{23}^{\text{NG}} & \varepsilon_{33}^{\text{NG}} \end{pmatrix} \begin{pmatrix} p_{s,4}^{\text{H}_2} \\ p_{d,2}^{\text{NG}} \\ p_{d,3}^{\text{NG}} \end{pmatrix} \\ &= \begin{pmatrix} 0 \\ u_2^{\text{NG}} \\ u_3^{\text{NG}} \end{pmatrix} - \begin{pmatrix} \varepsilon_{11}^{\text{NG}} & \varepsilon_{12}^{\text{NG}} + \varepsilon_{13}^{\text{NG}} \\ \varepsilon_{12}^{\text{NG}} & \varepsilon_{22}^{\text{NG}} + \varepsilon_{23}^{\text{NG}} \\ \varepsilon_{13}^{\text{NG}} & \varepsilon_{23}^{\text{NG}} + \varepsilon_{33}^{\text{NG}} \end{pmatrix} \begin{pmatrix} p^{\text{H}_2} \\ p^{\text{NG}} \end{pmatrix} \end{aligned} \quad (4-17)$$

As the behavior depends heavily on the chosen elasticities, the parameter identification requires precise tuning to create a resemblance of the desired effect. The identification process is described in detail in Section E-2-1.

⁷A rotation of the hydrogen supply curve could depend on the prices in both markets such that $\varepsilon_{s,4}^{\text{H}_2} = f(p^{\text{H}_2}, p^{\text{NG}})$. To include the proportionality between $s_4^{\text{H}_2}$ and d_2^{NG} , the price elasticity of natural gas demand should then also depend on the spot prices $\varepsilon_{d,2}^{\text{NG}} = f(p^{\text{H}_2}, p^{\text{NG}})$. However, the greatest disadvantage of this approach is that we create a time-varying ε , which means we do not obtain a linear time-invariant (LTI) economic network model.

⁸The SMR agent could be described with a two-winding mutual inductor, as seen in Section 4-3-2, coupling natural gas demand for hydrogen production and the supplied hydrogen. However, with this inductor, it is not possible to adequately include the proportionality between the two flows. A three-winding mutual inductor, that incorporates the general demand for natural gas, provides an extra dimension to fit the listed characteristics.

The low-carbon hydrogen supply, depending on both the hydrogen and natural gas price, is thus determined by the following relation:

$$s_4^{\text{H}_2}(t) = \varepsilon_{11}^{\text{NG}} p^{\text{H}_2}(t) + (\varepsilon_{12}^{\text{NG}} + \varepsilon_{13}^{\text{NG}}) p^{\text{NG}}(t). \quad (4-18)$$

4-3-4 Import of Liquid Hydrogen

The LH₂-H₂ Supply Chain

Liquid hydrogen (LH₂) import predominantly serves as a strategic measure to ensure sufficient hydrogen supply. The hydrogen supply through this supply chain is therefore much lower compared to the low-carbon hydrogen supply chain.

The LH₂-H₂ supply chain, visualized in Figure 4-8, looks almost identical to the low-carbon hydrogen supply chain. The only exception is the supply of LH₂, which is here modeled with only a current source. Due to these similarities, this section presents more concise derivations.

The production (or gasification) agent is modeled through mutual inductance, indicated by the dashed box, and operates in both the LH₂ market and the hydrogen market.

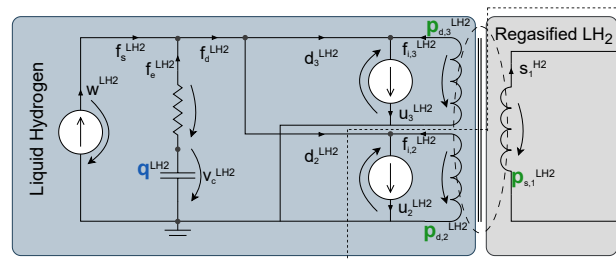


Figure 4-8: The LH₂-H₂ supply chain with the LH₂ gasification agent indicated by the dashed box.

The Liquid Hydrogen Market

LH₂ import by ship is modeled as a current source, representing a fixed and inelastic supply⁹. This representation is based on the expectation that LH₂ import will primarily occur through long-term contractual agreements, ensuring a consistent and predictable

⁹Despite LH₂ arriving in batches, its supply is assumed to remain constant for two main reasons. At the import locations, LH₂ is unloaded and stored in large tanks. From these storage units, the LH₂ is gradually gasified and fed into the hydrogen backbone, maintaining a steady supply of both LH₂ and hydrogen. This process is repeated when a new shipment arrives.

LH₂-H₂ supply chain	
w^{LH_2}	Inelastic LH ₂ supply
$f_s^{\text{LH}_2}$	Total LH ₂ supply
$f_e^{\text{LH}_2}$	Excess LH ₂ flow
$f_d^{\text{LH}_2}$	Total LH ₂ demand
$d_2^{\text{LH}_2}$	LH ₂ demand for regasification
$d_3^{\text{LH}_2}$	General LH ₂ demand
$f_{i,2}^{\text{LH}_2}$	Price-elastic LH ₂ demand for regasification
$f_{i,3}^{\text{LH}_2}$	Price-elastic LH ₂ demand
$u_2^{\text{LH}_2}$	Inelastic LH ₂ demand for regasification
$u_3^{\text{LH}_2}$	Inelastic LH ₂ demand
$s_4^{\text{H}_2}$	Total regasified LH ₂

Table 4-4: Overview of the energy flows within the LH₂-H₂ supply chain

flow of LH₂. Also, this ensures that the price of LH₂ remains relatively stable and is influenced only by fluctuations in demand¹⁰.

The demand for LH₂ is split into the demand for LH₂ for regasification ($d_2^{\text{LH}_2}$) and the general demand for LH₂ ($d_3^{\text{LH}_2}$), given by:

$$f_d^{\text{LH}_2} = d_2^{\text{LH}_2} + d_3^{\text{LH}_2}. \quad (4-19)$$

The LH₂ market does include storage and a market operator who adjusts the LH₂ price according to the excess flow $f_e^{\text{LH}_2}$ to match supply and demand.

The LH₂ Gasification Strategy

The regasification strategy of the production agent relies on the spot prices of both LH₂ and hydrogen. A three-winding mutual inductor is used and tuned such that it matches the listed characteristics.

- The price-dependent gasification¹¹ of LH₂, given by $s_1^{\text{H}_2}$, is influenced by both the LH₂ and hydrogen prices¹²: $s_1^{\text{H}_2} = f(p^{\text{LH}_2}, p^{\text{H}_2})$.

¹⁰The price of LH₂ is predetermined by long-term contracts. Fluctuations in demand result in changes in the LH₂ spot price.

¹¹The losses of this process are minimal and therefore neglected in its modeling.

¹²The hydrogen price will have more influence as the LH₂ is relatively constant.

- The proportionality between the output and input flow of the gasifier¹³ ($s_1^{\text{H}_2} \approx d_2^{\text{LH}_2}$).
- The negative correlation between the two different flows of LH₂ demand.
- The share of gasified LH₂ needs to be in line with the supply distribution as shown in Figure A-3 in Section A-6.

Following the same derivation as in Section 4-3-3, we derive that the regasified LH₂ flow is determined by the following relation, depending on both the hydrogen and LH₂ prices:

$$s_1^{\text{H}_2}(t) = \varepsilon_{11}^{\text{LH}_2} p^{\text{H}_2}(t) + (\varepsilon_{12}^{\text{LH}_2} + \varepsilon_{13}^{\text{LH}_2}) p^{\text{LH}_2}(t). \quad (4-20)$$

4-4 Industry Clusters as Active Demanders

For the modeling of the industrial hydrogen demand, we draw inspiration from Wietschel (2023) and Bataille (2005) [14, 15]. Both emphasize the importance of disaggregation amongst industries, particularly when one is interested in energy price dynamics [15]. This is different from existing models, as they assume static demand (see Section B-1).

There are five key industry clusters, indicated in the core model as Groningen (1), Amsterdam (2), Rotterdam (3), Zeeland (4), and Limburg (5). The industry clusters are modeled as the market agent¹⁴ shown in Figure 4-9. The hydrogen flows within these clusters are listed in Table 4-5. Each market agent represents the aggregated demand characteristics of the demanders within the corresponding industry clusters.

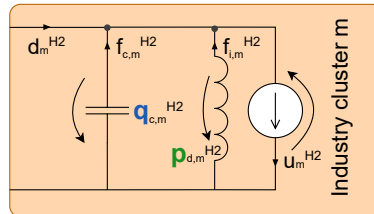


Figure 4-9: Industry clusters as active demanders

The industry clusters are modeled as active demanders with an inductor and a current source in parallel interconnection. The behavioral law of the components together represents the downward-sloping demand schedule as presented in Figure 4-10.

¹³The process of slowly gasifying imported LH₂ into hydrogen achieves almost 100% efficiency by gradually allowing the fluid to warm up.

¹⁴Although each industry cluster is built with the same components, their parameters differ such that each market agent represents the demand characteristics of that cluster. The parameter identification process is detailed in Section E-2-2.

Industry cluster m	
$d_m^{\text{H}_2}$	Total H ₂ demand of cluster
$f_{c,m}^{\text{H}_2}$	H ₂ extracted from local storage
$f_{i,m}^{\text{H}_2}$	Elastic H ₂ demand
$u_m^{\text{H}_2}$	Inelastic H ₂ demand

Table 4-5: Overview of industry-cluster-related parameters. For $m \in \{1, \dots, 5\}$.

Following Thevenin's theorem, the two components together form an equivalent voltage source [5, 16]. Hence, each industry cluster exerts an economic motive force, or motive, that drives up the hydrogen spot price. This representation reflects the demand-driven characteristic of the hydrogen spot market.

Each industry cluster $m \in \{1, \dots, 5\}$ has a small local hydrogen storage capacity to buffer small fluctuations in their supply and demand (see Section A-4). This storage is modeled as a capacitor (see Section 4-2-2). As local storage has a small storage capacity used for short-term storage, it has a low¹⁵ storage inelasticity $b_m^{\text{H}_2}$. The forces these local storage facilities exert on the market are therefore small.

The quantity demanded $d_m^{\text{H}_2}$ by each industry cluster, $m \in \{1, \dots, 5\}$, is given by

$$d_m^{\text{H}_2}(t) = u_m^{\text{H}_2} - f_{i,m}^{\text{H}_2} - f_{c,m}^{\text{H}_2} = u_m^{\text{H}_2} - \varepsilon_{d,m}^{\text{H}_2} p_{d,m}^{\text{H}_2} - f_{c,m}^{\text{H}_2}, \quad (4-21)$$

with $p_{d,m}^{\text{H}_2} = p^{\text{H}_2}$ the hydrogen spot price (see Section 4-2-4).

The hydrogen flow that is extracted from local storage $f_{c,m}^{\text{H}_2}$ cannot be written in terms of the state variables¹⁶. Instead, the network topology prescribes that the local storage is anticausal. A bond graph representation of the network easily shows that the causality is forced into the opposite direction of the storage law. Which means it goes with a differentiator instead of an integrator.

Price-Elastic Demand

Most energy systems models assume static demand, which would be represented by a vertical demand curve [17], and thus a single current source in economic circuit theory. However, there exists a certain amount of hydrogen demand flexibility in the industry clusters (see Section A-2).

In economic engineering, we use the price elasticity of demand to quantify how responsive the quantity demanded is to changes in its price, see [4]. The first derivative of the slope of the demand schedule¹⁷ represents the price elasticity of demand $\varepsilon_{d,m}^{\text{H}_2}$, see Figure 4-10.

¹⁵Compared to the storage inelasticity of the salt caverns.

¹⁶This has a consequence on the state-space representation of the network. See Section 4-5-3.

¹⁷We model the demand schedule in line with the representation [5].

Each industry cluster represents various hydrogen consumers with distinct applications for hydrogen. These applications are linked to different processes, each with its own price elasticity of demand. The price elasticities of the industry clusters are determined in Section E-2-2.

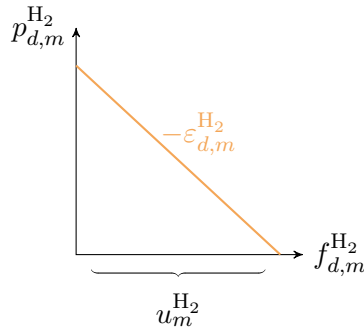


Figure 4-10: Demand schedule of an industry cluster where $u_m^{H_2}$ is the offset of the demand schedule, representing the inelastic demand, $-\epsilon_{d,m}^{H_2}$ the slope of the demand schedule, representing the price elasticity of demand, and $p_{d,m}^{H_2} = p^{H_2}$ the hydrogen spot price.

Price-Inelastic Demand

The price inelastic part of demand is captured by the current source. This inelastic-flow component provides a constant hydrogen flow $u_m^{H_2}$. This inelastic flow represents the offset of the demand schedule $f_{d,m}^{H_2} = u_m^{H_2} - \epsilon_{d,m}^{H_2} p_{d,m}^{H_2}$, as shown in Figure 4-10.

4-5 The Core Network as a Dynamical System

4-5-1 The Dynamics of Storage Levels

In line with the physical clearing conditions derived in Section 4-2-4, and detailed in Appendix C, we analytically derive the dynamics of the storage levels. From this derivation follows that the rate of change in storage levels is determined by the excess flow according to:

$$\frac{dq(t)}{dt} = f_e(t). \quad (4-22)$$

The direction of the excess flow is chosen in the direction of the quantity demanded (see Section 4-2-2). When $f_e > 0$, hydrogen is extracted from the storage, and when $f_e < 0$, hydrogen is injected into the storage. Thus when $q > 0$, the storage is understocked, and when $q < 0$, the storage is overstocked.

Hydrogen

The total hydrogen flow supplied through the four different supply chains $n \in \{1, \dots, 4\}$ is given by:

$$f_s^{\text{H}_2}(t) = \sum_{n=1}^4 s_n^{\text{H}_2}(t). \quad (4-23)$$

Where $s_n^{\text{H}_2}(t)$ is given by the following equations.

$$s_1^{\text{H}_2}(t) = \varepsilon_{11}^{\text{LH}_2} p^{\text{H}_2}(t) + (\varepsilon_{12}^{\text{LH}_2} + \varepsilon_{13}^{\text{LH}_2}) p^{\text{LH}_2}(t) \quad (4-24)$$

$$s_2^{\text{H}_2}(t) = \varepsilon_{s,2}^{\text{H}_2} p^{\text{H}_2}(t) \quad (4-25)$$

$$s_3^{\text{H}_2}(t) = c^{\text{OWE}} (u_1^{\text{OWE}} - (\varepsilon_{11}^{\text{OWE}} + \varepsilon_{12}^{\text{OWE}}) p^{\text{OWE}}(t)) \quad (4-26)$$

$$s_4^{\text{H}_2}(t) = \varepsilon_{11}^{\text{NG}} p^{\text{H}_2}(t) + (\varepsilon_{12}^{\text{NG}} + \varepsilon_{13}^{\text{NG}}) p^{\text{NG}}(t) \quad (4-27)$$

For the five industry clusters $m \in \{1, \dots, 5\}$, the total flow of hydrogen demanded is given by:

$$f_d^{\text{H}_2}(t) = \sum_{m=1}^5 d_m^{\text{H}_2}(t), \quad (4-28)$$

As the local storage is anticausal and has minimal influence on the network dynamics (see Section 4-4), it is neglected in the derivation for the state-space representation. This leaves us with the following description of the demand per industry cluster.

$$d_m^{\text{H}_2}(t) = u_m^{\text{H}_2} - \varepsilon_{d,m}^{\text{H}_2} p^{\text{H}_2}(t). \quad (4-29)$$

The total industrial hydrogen demand is therefore given by:

$$f_d^{\text{H}_2}(t) = \sum_{m=1}^5 d_m^{\text{H}_2}(t) = \sum_{m=1}^5 u_m^{\text{H}_2} - \left(\sum_{m=1}^5 \varepsilon_{d,m}^{\text{H}_2} \right) p^{\text{H}_2}(t). \quad (4-30)$$

The storage level dynamics of the salt caverns are expressed in terms of the excess flow $f_e^{\text{H}_2}(t)$ and are given by:

$$\begin{aligned}
\frac{dq_{cs}^{\text{H}_2}(t)}{dt} &= f_e^{\text{H}_2}(t) = f_d^{\text{H}_2}(t) - f_s^{\text{H}_2}(t) \\
&= \sum_{m=1}^5 d_m^{\text{H}_2}(t) - \sum_{n=1}^4 s_n^{\text{H}_2}(t) \\
&= \sum_{m=1}^5 u_m^{\text{H}_2} - \left(\sum_{m=1}^5 \varepsilon_{d,m}^{\text{H}_2} \right) p^{\text{H}_2}(t) - \left(\varepsilon_{11}^{\text{LH}_2} p^{\text{H}_2}(t) + (\varepsilon_{12}^{\text{LH}_2} + \varepsilon_{13}^{\text{LH}_2}) p^{\text{LH}_2}(t) \right) - \varepsilon_{s,2}^{\text{H}_2} p^{\text{H}_2}(t) \\
&\quad - c^{\text{OWE}} \left(u_1^{\text{OWE}} - (\varepsilon_{11}^{\text{OWE}} + \varepsilon_{12}^{\text{OWE}}) p^{\text{OWE}}(t) \right) - \left(\varepsilon_{11}^{\text{NG}} p^{\text{H}_2}(t) + (\varepsilon_{12}^{\text{NG}} + \varepsilon_{13}^{\text{NG}}) p^{\text{NG}}(t) \right) \\
&= \sum_{m=1}^5 u_m^{\text{H}_2} - (\varepsilon_{12}^{\text{LH}_2} + \varepsilon_{13}^{\text{LH}_2}) p^{\text{LH}_2}(t) - c^{\text{OWE}} u_1^{\text{OWE}} + c^{\text{OWE}} (\varepsilon_{11}^{\text{OWE}} + \varepsilon_{12}^{\text{OWE}}) p^{\text{OWE}}(t) \\
&\quad - (\varepsilon_{12}^{\text{NG}} + \varepsilon_{13}^{\text{NG}}) p^{\text{NG}}(t) - \left(\sum_{m=1}^5 \varepsilon_{d,m}^{\text{H}_2} + \varepsilon_{11}^{\text{LH}_2} + \varepsilon_{s,2}^{\text{H}_2} + \varepsilon_{11}^{\text{NG}} \right) p^{\text{H}_2}(t).
\end{aligned} \tag{4-31}$$

LH₂

The dynamics of the LH₂ storage level are given by:

$$\begin{aligned}
\frac{dq^{\text{LH}_2}(t)}{dt} &= f_e^{\text{LH}_2}(t) = f_d^{\text{LH}_2}(t) - f_s^{\text{LH}_2}(t) \\
&= \sum_{m=1}^2 d_m^{\text{LH}_2}(t) - s^{\text{LH}_2}(t) \\
&= u_2^{\text{LH}_2} + u_3^{\text{LH}_2} - w^{\text{LH}_2} - (\varepsilon_{22}^{\text{LH}_2} + 2\varepsilon_{23}^{\text{LH}_2} + \varepsilon_{33}^{\text{LH}_2}) p^{\text{LH}_2}(t) - (\varepsilon_{12}^{\text{LH}_2} + \varepsilon_{13}^{\text{LH}_2}) p^{\text{H}_2}(t).
\end{aligned} \tag{4-32}$$

OWE

The OWE market does not incorporate storage. The rate of change in stock and thus the excess flow is equal to zero, given by the following equation.

$$\begin{aligned}
\frac{dq^{\text{OWE}}(t)}{dt} &= f_e^{\text{OWE}}(t) = f_d^{\text{OWE}}(t) - f_s^{\text{OWE}}(t) \\
&= \sum_{m=1}^2 d_m^{\text{OWE}}(t) - s^{\text{OWE}}(t) \\
&= u_1^{\text{OWE}} + u_2^{\text{OWE}} - w^{\text{OWE}}(t) - (\varepsilon_1^{\text{OWE}} + 2\varepsilon_{12}^{\text{OWE}} + \varepsilon_2^{\text{OWE}}) p^{\text{OWE}}(t) = 0
\end{aligned} \tag{4-33}$$

This expression is needed to derive the OWE price dynamics.

Natural Gas

The dynamics of the natural gas storage level is given by:

$$\begin{aligned}
\frac{dq^{\text{NG}}(t)}{dt} &= f_e^{\text{NG}}(t) = f_d^{\text{NG}}(t) - f_s^{\text{NG}}(t) \\
&= \sum_{m=1}^2 d_m^{\text{NG}}(t) - (w^{\text{NG}} + \varepsilon_s^{\text{NG}} p^{\text{NG}}(t)) \\
&= u_2^{\text{NG}} + u_3^{\text{NG}}(t) - w^{\text{NG}} - (\varepsilon_{22}^{\text{NG}} + 2\varepsilon_{23}^{\text{NG}} + \varepsilon_{33}^{\text{NG}} + \varepsilon_s^{\text{NG}}) p^{\text{NG}}(t) - (\varepsilon_{12}^{\text{NG}} + \varepsilon_{13}^{\text{NG}}) p^{\text{H}_2}(t).
\end{aligned} \tag{4-34}$$

4-5-2 The Dynamics of Spot Prices

Following the price clearing conditions derived in Section 4-2-4, and detailed in Appendix C, we analytically derive the spot price dynamics in the different energy markets.

The rate of change in spot prices is determined by the price-driving market incentives:

$$\frac{dp(t)}{dt} = v(t). \tag{4-35}$$

Hydrogen

As derived in Section 4-2-4, the hydrogen market incentive equals the sum of the incentive exerted by the market operator and the incentive exerted by the storage operator: $v^{\text{H}_2}(t) = v_r^{\text{H}_2}(t) + v_c^{\text{H}_2}(t)$.

The hydrogen spot price dynamics are therefore given by:

$$\begin{aligned}
\frac{dp^{\text{H}_2}(t)}{dt} &= v^{\text{H}_2}(t) \\
&= k_{sc}^{\text{H}_2} q_{cs}^{\text{H}_2}(t) + b^{\text{H}_2} f_e^{\text{H}_2}(t) \\
&= k_{sc}^{\text{H}_2} q_{cs}^{\text{H}_2}(t) + b^{\text{H}_2} \left[\sum_{m=1}^5 u_m^{\text{H}_2} - (\varepsilon_{12}^{\text{LH}_2} + \varepsilon_{13}^{\text{LH}_2}) p^{\text{LH}_2}(t) - c^{\text{OWE}} u_1^{\text{OWE}} \right. \\
&\quad \left. + c^{\text{OWE}} (\varepsilon_{11}^{\text{OWE}} + \varepsilon_{12}^{\text{OWE}}) p^{\text{OWE}}(t) - (\varepsilon_{12}^{\text{NG}} + \varepsilon_{13}^{\text{NG}}) p^{\text{NG}}(t) - \left(\sum_{m=1}^5 \varepsilon_{d,m}^{\text{H}_2} + \varepsilon_{11}^{\text{LH}_2} + \varepsilon_{s,2}^{\text{H}_2} + \varepsilon_{11}^{\text{NG}} \right) p^{\text{H}_2}(t) \right].
\end{aligned} \tag{4-36}$$

LH₂

For the LH₂ spot price dynamics we obtain:

$$\begin{aligned}
\frac{dp^{\text{LH}_2}(t)}{dt} &= v^{\text{LH}_2}(t) \\
&= k^{\text{LH}_2} q^{\text{LH}_2}(t) + b^{\text{LH}_2} f_e^{\text{LH}_2}(t) \\
&= k^{\text{LH}_2} q^{\text{LH}_2}(t) + b^{\text{LH}_2} \left[u_2^{\text{LH}_2} + u_3^{\text{LH}_2} - w^{\text{LH}_2} \right. \\
&\quad \left. - (\varepsilon_{22}^{\text{LH}_2} + 2\varepsilon_{23}^{\text{LH}_2} + \varepsilon_{33}^{\text{LH}_2}) p^{\text{LH}_2}(t) - (\varepsilon_{12}^{\text{LH}_2} + \varepsilon_{13}^{\text{LH}_2}) p^{\text{H}_2}(t) \right].
\end{aligned} \tag{4-37}$$

OWE

In the OWE market, the price dynamics are determined differently because the conjugate storage does not exist. As a result, the price dynamics in the OWE market are fully determined by the rate of change in OWE generation $w^{\text{OWE}}(t)$.

From Equation (4-33) we know that:

$$w^{\text{OWE}}(t) = u_1^{\text{OWE}} + u_2^{\text{OWE}} - (\varepsilon_1^{\text{OWE}} + 2\varepsilon_{12}^{\text{OWE}} + \varepsilon_2^{\text{OWE}}) p^{\text{OWE}}(t). \tag{4-38}$$

By taking its derivative, we obtain:

$$\frac{dw^{\text{OWE}}(t)}{dt} = -(\varepsilon_1^{\text{OWE}} + 2\varepsilon_{12}^{\text{OWE}} + \varepsilon_2^{\text{OWE}}) \frac{dp^{\text{OWE}}(t)}{dt}. \tag{4-39}$$

The price dynamics of OWE are then given by:

$$\frac{dp^{\text{OWE}}(t)}{dt} = v^{\text{OWE}}(t) = - \left(\frac{1}{\varepsilon_1^{\text{OWE}} + 2\varepsilon_{12}^{\text{OWE}} + \varepsilon_2^{\text{OWE}}} \right) \frac{dw^{\text{OWE}}(t)}{dt}. \tag{4-40}$$

We thus need to incorporate the time derivative of the OWE generation $\dot{w}^{\text{OWE}}(t)$ in the input vector of our state-space representation.

Natural Gas

The natural gas price dynamics are given by:

$$\begin{aligned}
\frac{dp^{\text{NG}}(t)}{dt} &= v^{\text{NG}}(t) \\
&= k^{\text{NG}} q^{\text{NG}}(t) + b^{\text{NG}} f_e^{\text{NG}}(t) \\
&= k^{\text{NG}} q^{\text{NG}}(t) + b^{\text{NG}} \left[u_2^{\text{NG}} + u_3^{\text{NG}}(t) - w^{\text{NG}} - (\varepsilon_{22}^{\text{NG}} + 2\varepsilon_{23}^{\text{NG}} + \varepsilon_{33}^{\text{NG}} + \varepsilon_s^{\text{NG}}) p^{\text{NG}}(t) \right. \\
&\quad \left. - (\varepsilon_{12}^{\text{NG}} + \varepsilon_{13}^{\text{NG}}) p^{\text{H}_2}(t) \right]
\end{aligned} \tag{4-41}$$

4-5-3 State-Space Representation

As the core network is a dynamical LTI system, we can construct a state-space representation to express its dynamics. The construction of the state-space representation follows the same procedure as taken by Hutter and Mendel (2024) [5].

A state-space representation is written in the form

$$\dot{\mathbf{x}} = A\mathbf{x} + B\mathbf{u}, \quad (4-42)$$

where $A\mathbf{x}$ captures the endogenous influences and $B\mathbf{u}$ the exogenous influences in the network. The block diagram of the state-space representation is shown in Figure 4-11.

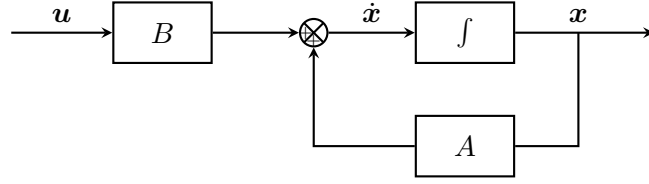


Figure 4-11: Block diagram of the state-space representation of (4-42)

The core network consists of three second-order systems and one first-order (the OWE market) system, which one can directly recognize in the state-space representation in Equation (4-46). The state vector \mathbf{x} collects the storage levels and the spot prices of the energy markets, given by:

$$\mathbf{x} = (q^{\text{LH}_2} \quad p^{\text{LH}_2} \quad p^{\text{OWE}} \quad q^{\text{NG}} \quad p^{\text{NG}} \quad q^{\text{H}_2} \quad p^{\text{H}_2})^T. \quad (4-43)$$

The derivative of the state vector $\dot{\mathbf{x}}$ contains the stock-up rates of the storage levels \dot{q} and the rates with which the spot prices \dot{p} are changed.

$$\dot{\mathbf{x}} = (\dot{q}^{\text{LH}_2} \quad \dot{p}^{\text{LH}_2} \quad \dot{p}^{\text{OWE}} \quad \dot{q}^{\text{NG}} \quad \dot{p}^{\text{NG}} \quad \dot{q}^{\text{H}_2} \quad \dot{p}^{\text{H}_2})^T, \quad (4-44)$$

The input vector \mathbf{u} is given by

$$\mathbf{u} = (w^{\text{LH}_2} \quad u_2^{\text{LH}_2} \quad u_3^{\text{LH}_2} \quad w^{\text{OWE}} \quad \dot{w}^{\text{OWE}} \quad u_1^{\text{OWE}} \quad u_2^{\text{OWE}} \quad w^{\text{NG}} \quad u_2^{\text{NG}} \quad u_3^{\text{NG}} \quad u^{\text{H}_2})^T. \quad (4-45)$$

This vector includes the inelastic supply w and demand u , as well as the rate of change in OWE generation \dot{w}^{OWE} . The inputs $w^{\text{OWE}}(t)$, \dot{w}^{OWE} and u_3^{NG} vary on time. For the industry clusters, the inelastic demands are aggregated into $\sum_{m=1}^5 u_m^{\text{H}_2} = u^{\text{H}_2}$ and their price elasticities of demand into $\sum_{m=1}^5 \varepsilon_{d,m}^{\text{H}_2} = \varepsilon_d^{\text{H}_2}$.

State Equations

Master of Science Thesis

$$\begin{pmatrix} \dot{q}^{\text{LH}_2} \\ \dot{p}^{\text{LH}_2} \\ \dot{p}^{\text{OWE}} \\ \dot{q}^{\text{NG}} \\ \dot{p}^{\text{NG}} \\ \dot{q}^{\text{H}_2} \\ \dot{p}^{\text{H}_2} \end{pmatrix} = \begin{pmatrix} 0 & -(\varepsilon_{22}^{\text{LH}_2} + 2\varepsilon_{23}^{\text{LH}_2} + \varepsilon_{33}^{\text{LH}_2}) & \vdots & 0 & \vdots & 0 & \vdots & 0 & \vdots & 0 & -(\varepsilon_{12}^{\text{LH}_2} + \varepsilon_{13}^{\text{LH}_2}) \\ k^{\text{LH}_2} & -b^{\text{LH}_2}(\varepsilon_{22}^{\text{LH}_2} + 2\varepsilon_{23}^{\text{LH}_2} + \varepsilon_{33}^{\text{LH}_2}) & \vdots & 0 & \vdots & 0 & \vdots & 0 & \vdots & 0 & -b^{\text{LH}_2}(\varepsilon_{12}^{\text{LH}_2} + \varepsilon_{13}^{\text{LH}_2}) \\ \vdots & \vdots & \vdots & \vdots & \vdots & \vdots & \vdots & \vdots & \vdots & \vdots & \vdots \\ 0 & 0 & \vdots & 0 & \vdots & 0 & \vdots & 0 & \vdots & 0 & 0 \\ 0 & 0 & \vdots & 0 & \vdots & -(\varepsilon_{22}^{\text{NG}} + 2\varepsilon_{23}^{\text{NG}} + \varepsilon_{33}^{\text{NG}} + \varepsilon_s^{\text{NG}}) & \vdots & 0 & \vdots & -(\varepsilon_{12}^{\text{NG}} + \varepsilon_{13}^{\text{NG}}) & -(\varepsilon_{12}^{\text{NG}} + \varepsilon_{13}^{\text{NG}}) \\ 0 & 0 & \vdots & 0 & \vdots & k^{\text{NG}} & -b^{\text{NG}}(\varepsilon_{22}^{\text{NG}} + 2\varepsilon_{23}^{\text{NG}} + \varepsilon_{33}^{\text{NG}} + \varepsilon_s^{\text{NG}}) & \vdots & 0 & -b^{\text{NG}}(\varepsilon_{12}^{\text{NG}} + \varepsilon_{13}^{\text{NG}}) & -b^{\text{NG}}(\varepsilon_{12}^{\text{NG}} + \varepsilon_{13}^{\text{NG}}) \\ \vdots & \vdots & \vdots & \vdots & \vdots & \vdots & \vdots & \vdots & \vdots & \vdots & \vdots \\ 0 & -(\varepsilon_{12}^{\text{H}_2} + \varepsilon_{13}^{\text{H}_2}) & \vdots & c^{\text{OWE}}(\varepsilon_{11}^{\text{OWE}} + \varepsilon_{12}^{\text{OWE}}) & \vdots & 0 & \vdots & -(\varepsilon_{12}^{\text{NG}} + \varepsilon_{13}^{\text{NG}}) & \vdots & 0 & -(\varepsilon_d^{\text{H}_2} + \varepsilon_{11}^{\text{LH}_2} + \varepsilon_{s,2}^{\text{H}_2} + \varepsilon_{11}^{\text{NG}}) \\ 0 & -b^{\text{H}_2}(\varepsilon_{12}^{\text{LH}_2} + \varepsilon_{13}^{\text{LH}_2}) & \vdots & b^{\text{H}_2}c^{\text{OWE}}(\varepsilon_{11}^{\text{OWE}} + \varepsilon_{12}^{\text{OWE}}) & \vdots & 0 & \vdots & -b^{\text{H}_2}(\varepsilon_{12}^{\text{NG}} + \varepsilon_{13}^{\text{NG}}) & \vdots & k^{\text{H}_2} & -b^{\text{H}_2}(\varepsilon_d^{\text{H}_2} + \varepsilon_{11}^{\text{LH}_2} + \varepsilon_{s,2}^{\text{H}_2} + \varepsilon_{11}^{\text{NG}}) \end{pmatrix} \begin{pmatrix} q^{\text{LH}_2} \\ p^{\text{LH}_2} \\ p^{\text{OWE}} \\ q^{\text{NG}} \\ p^{\text{NG}} \\ q^{\text{H}_2} \\ p^{\text{H}_2} \end{pmatrix} + \begin{pmatrix} -1 & 1 & 1 & \vdots & 0 & 0 & 0 & 0 & \vdots & 0 & 0 & 0 & \vdots & 0 \\ -b^{\text{LH}_2} & b^{\text{LH}_2} & b^{\text{LH}_2} & \vdots & 0 & 0 & 0 & 0 & \vdots & 0 & 0 & 0 & \vdots & 0 \\ \vdots & \vdots & \vdots & \vdots & \vdots & \vdots & \vdots & \vdots & \vdots & \vdots & \vdots & \vdots & \vdots & \vdots \\ 0 & 0 & 0 & \vdots & -\left(\frac{1}{\varepsilon_1^{\text{OWE}} + 2\varepsilon_{12}^{\text{OWE}} + \varepsilon_2^{\text{OWE}}}\right) & 0 & 0 & 0 & \vdots & 0 & 0 & 0 & \vdots & 0 \\ 0 & 0 & 0 & \vdots & 0 & 0 & 0 & 0 & \vdots & -1 & 1 & 1 & \vdots & 0 \\ 0 & 0 & 0 & \vdots & 0 & 0 & 0 & 0 & \vdots & -b^{\text{NG}} & b^{\text{NG}} & b^{\text{NG}} & \vdots & 0 \\ 0 & 0 & 0 & \vdots & 0 & -c^{\text{OWE}} & 0 & 0 & \vdots & 0 & 0 & 0 & \vdots & 1 \\ 0 & 0 & 0 & \vdots & 0 & -b^{\text{H}_2}c^{\text{OWE}} & 0 & 0 & \vdots & 0 & 0 & 0 & \vdots & b^{\text{H}_2} \end{pmatrix} \begin{pmatrix} w^{\text{LH}_2} \\ u_2^{\text{LH}_2} \\ u_3^{\text{LH}_2} \\ \vdots \\ w^{\text{OWE}} \\ w^{\text{OWE}} \\ u_1^{\text{OWE}} \\ u_2^{\text{OWE}} \\ w^{\text{NG}} \\ u_2^{\text{NG}} \\ u_3^{\text{NG}} \\ \vdots \\ u^{\text{H}_2} \end{pmatrix}$$

(4-46)

P.E. van den Berkmortel

4-6 Design of Core Network Extensions

4-6-1 Renewable and Low-Carbon Hydrogen as Separate Commodities

Instead of treating hydrogen as a homogeneous commodity, as assumed in the core network, renewable and low-carbon hydrogen can be treated as separate commodities. We model this as an extension of the core network where we split the hydrogen market into two segments: the renewable hydrogen market (**green**) on the right side in Figure 4-12, and the low-carbon hydrogen market (**blue**) on the left. We refer to this network extension as the RLCH2 network.

Renewable hydrogen includes only domestically produced hydrogen, while low-carbon hydrogen includes both domestically produced hydrogen and imported hydrogen. This differentiation is in line with sustainable hydrogen policies; however, it would necessitate the use of green certificates to trace the origin of hydrogen in real-world applications.

The transportation and storage of both renewable and low-carbon hydrogen are facilitated via the same hydrogen backbone. However, in our network, we need to design two distinct closed electrical circuits to represent each market segment.

We incorporate the price coupling between the two different hydrogen markets via the demand of the industry clusters. The clusters treat renewable and low-carbon hydrogen as substitutes, which we model with the mutual inductor in the industry clusters (**orange**).

4-6-2 Integration of the Ammonia Market

Another network extension involves the integration of the ammonia market. Ammonia serves as a substitute for hydrogen in various industrial processes, particularly in fertilizer production. We refer to this network extension as the H2A network.

For the integration of ammonia, we have selected three industry clusters - Rotterdam, Zeeland, and Limburg - that use ammonia as a substitute for hydrogen. These clusters are chosen due to their higher prevalence in industrial processes where ammonia can effectively replace hydrogen. More detailed analysis of the industry clusters and their main hydrogen applications can be found in Section E-2-2.

The integration of the ammonia market is visualized in Figure 4-13, with the ammonia market (**blue**) represented on the right side of the network. As ammonia import shares similarities with liquid hydrogen (LH₂) import, their markets are modeled similarly. However, the ammonia market is modeled with additional flexibility, incorporating price-elastic supply modeled with an inductor.

The price coupling between the hydrogen and ammonia markets is modeled with a mutual inductor within these industry clusters.

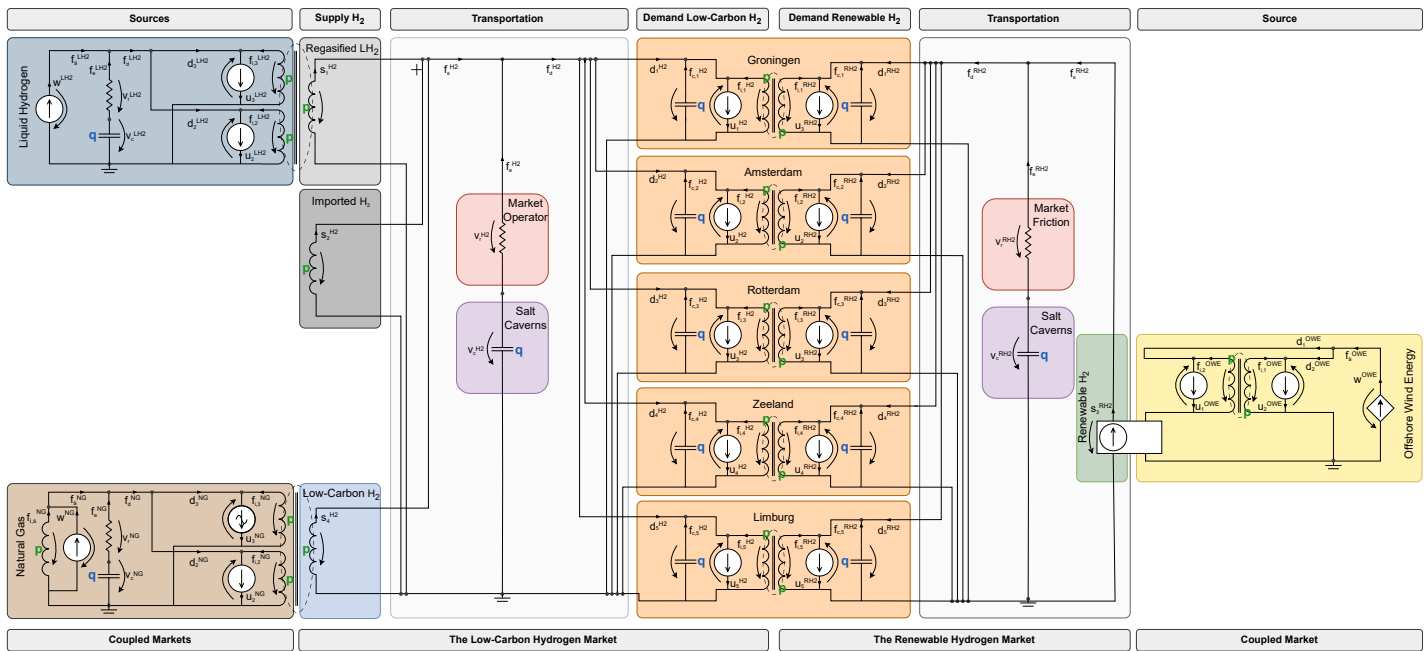


Figure 4-12: Network topology of the RLCH2 network that differentiates between renewable hydrogen and low-carbon hydrogen

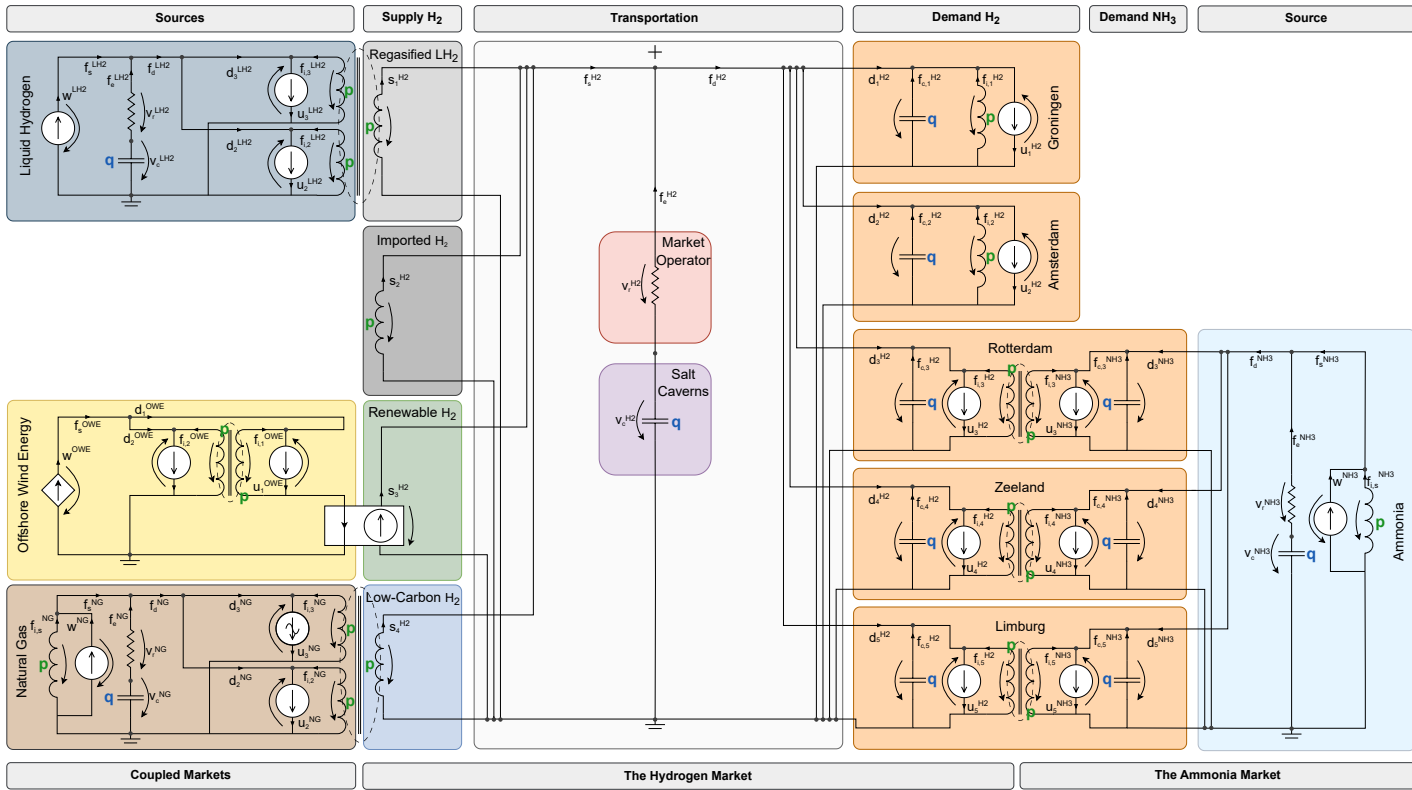


Figure 4-13: Network topology of the H2A network which integrates ammonia as a substitute for hydrogen

4-7 System Identification

We determine the network parameters through system identification. However, the lack of data on a spot market for hydrogen makes it difficult to perform system identification with additional data-intensive methods like gray-box identification.

Instead, we rely on available literature and expert knowledge to identify network parameters. These parameters are then manually tuned to ensure that the core network aligns with the anticipated behavior of a spot market, hydrogen project developments, and expert expectations. A detailed explanation of the identification process can be found in Appendix E.

Throughout the identification process, we utilize the average wind distribution method described in Section D-1 as a reference for parameter tuning. This approach allows us to refine our model iteratively and progressively improve it representing the hydrogen spot market dynamics.

Dynamic Scenario Analyses and Control of the Networks

5-1 Introduction

In this chapter, we address the price dynamics within our designed economic network models through dynamic scenario analyses and the implementation of regulatory intervention as a control application. To conduct these analyses, we model and simulate our networks using MATLAB Simscape.

In Section 5-2, we analyze the dynamics of the networks through various dynamic scenarios. We compare the three economic network models by examining their market stabilization capabilities, dynamic resilience, and response to wind variability.

In Section 5-3, we design and tune a Proportional-Integral-Derivative (PID) controller to emulate a subsidized price-settlement system in the core network. We then demonstrate and analyze the impact of this control mechanism on price dynamics and hydrogen supply.

5-2 Dynamic Scenario Analyses

5-2-1 Market Stabilization

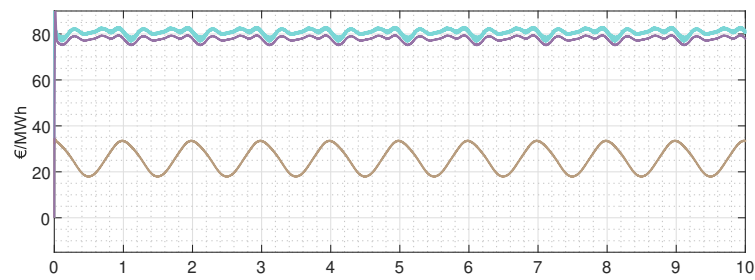
We have tuned the model parameters of the networks to ensure that the markets stabilize in the long term (see Appendix E for the identification of the parameters). Figure 5-1 shows the stabilization of energy price¹ and energy supply of the three networks over a ten-year period. We use both a seasonal input for the wind and for the natural gas demand. By comparing the stabilization of the three economic networks, we can draw the following conclusions.

The core network stabilizes the fastest, serving as a reference for the two extensions. While the two extensions stabilize over a longer but comparable period, the Renewable and Low-Carbon Hydrogen (RLCH2) network shows a larger initial deviation in total hydrogen supply. This deviation is primarily due to price coupling at the demand side, as opposed to the supply-side coupling observed with hydrogen, natural gas, and liquid hydrogen. Additionally, the RLCH2 network exhibits greater supply volatility compared to the core network and the Hydrogen and Ammonia (H2A) network.

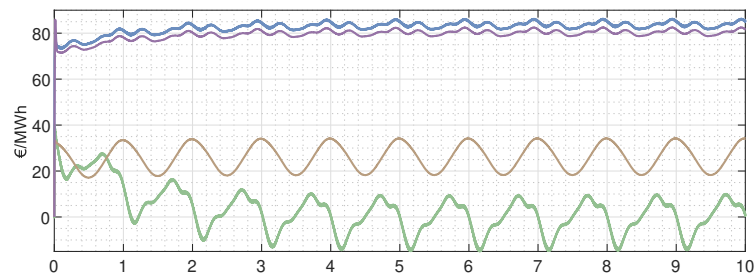
For the RLCH2 network, renewable hydrogen prices take the longest to stabilize. There is also a significant difference in price level and volatility compared to low-carbon hydrogen. This is due to two main factors: the inherent volatility of intermittent offshore wind energy (OWE) generation required for renewable hydrogen production, and the industrial preference for low-carbon hydrogen due to its more stable and less volatile supply.

In the H2A network, integrating the ammonia market results in a longer stabilization period for ammonia prices, whereas hydrogen, natural gas, and liquid hydrogen prices stabilize similarly to those in the core network. This is due to the demand-side price coupling of ammonia. We also observe that the hydrogen price in the H2A network is significantly lower compared to the core network.

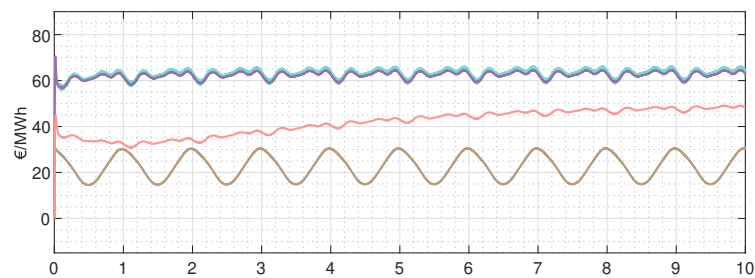
¹See Appendix E for the calibration of energy prices



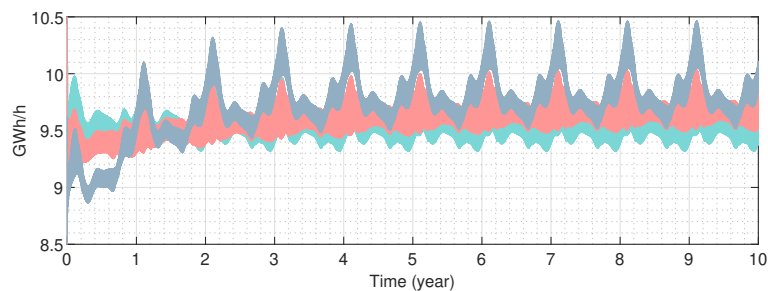
(a) Price stabilization in the core network. With hydrogen (cyan), liquid hydrogen (purple), and natural gas (brown).



(b) Price stabilization in the RLCH2 network. With renewable hydrogen (green), low-carbon hydrogen (blue), liquid hydrogen (purple), and natural gas (brown).



(c) Price stabilization in the H2A network. With hydrogen (cyan), liquid hydrogen (purple), natural gas (brown), and ammonia (pink).



(d) Supply stabilization in the core (cyan), RLCH2 (gray-blue), and H2A (pink) network

Figure 5-1: Network stabilization over a ten-year period.

5-2-2 Dynamic Resilience

An important aspect of energy systems is their resilience. Historical events such as the 1970s energy crisis, the 2014 crude oil supply shock, and the recent war in Ukraine highlight the necessity of resilience. As the frequency of potential disturbances increases due to climate change, variable renewable energy supply, and geopolitical disruptions, resilience becomes even more crucial for modern energy systems [18, 19]. Resilience theory distinguishes between static and dynamic resilience [20].

Static resilience refers to the structural integrity of a system, often evaluated through topological metrics such as network connectedness. Network theory aids in assessing static resilience by analyzing the connectedness of edges [21], which indicates the system's ability to avoid disruption. We refer to this as the network's robustness, which can be evaluated with the market-mesh matrix introduced by Hutter and Mendel as a topological metric for evaluating network robustness [5].

In this thesis, we focus on the dynamic resilience of energy systems, which deals with the operational behavior of systems in response to disturbances. Specifically, dynamic resilience refers to the system's ability to recover from disturbances and shocks [18, 19, 21, 22, 23].

To determine the dynamic resilience of the developed networks, we use constant inputs², and let the networks stabilize before subjecting them to disturbances. This allows us to analyze how well the energy prices, storage levels, and energy flows recover, and to what extent the networks maintain their functions under various conditions.

To assess dynamic resilience, we use metrics from the transient response, a well-known concept in control systems. These metrics allow us to quantify the system's ability to adapt in response to shocks by examining volatility, recovery speed, and redundancy - the ability of the markets to substitute for lost production through inventories.

In Figure 5-2, we demonstrate our metrics based on a time graph of the transient response of an energy price. However, these metrics also apply to storage levels and energy flows. We use these metrics to analyze the dynamic resilience of the three networks after an OWE disturbance, natural gas disturbance, and a demand extension.

We interpret the rise time (t_r) as a price adjustment delay representing the period it takes for the price to start significantly moving from its initial equilibrium (p_i^*) towards the new equilibrium (p_f^*). We use it as a metric for the short-term rigidity or "stickiness" of energy prices.

The peak time (t_p) is the time at which the price reaches its maximum deviation (overshoot) from the new equilibrium price after a disturbance. Representing, the time at which prices start to "unstick" and shift to the new equilibrium

The settling time (t_s) represents the time needed for the price to settle within a certain range around the new equilibrium price. We use it as a metric for the recovery speed.

The price overshoot (M_p) indicates the maximum extent to which the price exceeds the new equilibrium price during the adjustment process. We use it as a metric for the volatility of energy prices. This overshoot can be both positive and negative, depending on the nature of the exerted disturbance.

²We use the average wind speed of 9.5637 km/h. This gives an average power output of 4.47h/h MW per turbine and thus a total of 5.7 GWh/h generated OWE. Converted into our electrical circuit, this is a constant current of 0.0803 A. For the seasonal inelastic natural gas demand u_3^{NG} , we only use the offset of the sinusoidal input.

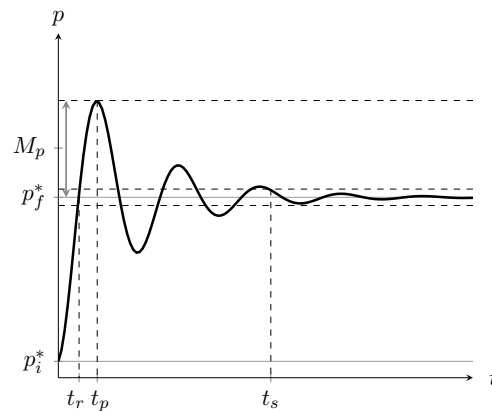


Figure 5-2: Time graph of the transient response between an initial price equilibrium p_i^* to a final one p_f^* . Also included are the rise time t_r , peak time t_p , settling time t_s , and price overshoot M_p .

Demand Extension

We first analyze a demand extension, where we subject the industry cluster in Groningen to a positive demand extension of 0.312 GWh/h. We calibrated the initial values of the energy flows, storage levels, and energy prices at zero to compare the final values with each other. The analysis focuses on the change in energy prices and energy supply.

You can think of a demand extension as the demand curve shifting to the right. Consequently, we obtain a movement along the supply curve to the new equilibrium. This leads to higher prices (Figure 5-3d) and a higher quantity supplied (Figure 5-3b).

We observe that the quantities supplied in the H2A network increase the most, which is accompanied by the largest increase in energy prices. In contrast, the quantities supplied in the RLCH2 network increase the least, and the price increase is also the smallest. From Figure 5-3a, we conclude that the low-carbon hydrogen supply chain is the most price-elastic, followed by gaseous hydrogen import.

This behavior is determined by the shift in the demand curves. For the RLCH2 network, the demand extension is split between renewable and low-carbon hydrogen according to the ratio of the industry cluster. This leads to a relatively smaller shift of the low-carbon hydrogen curve compared to the core network. In the H2A network, the demand extension affects only hydrogen demand, as the Groningen industry cluster solely demands hydrogen. Consequently, the shift of the demand curve is relatively larger compared to the core network because the initial hydrogen demand is lower. This makes the resilience of the networks difficult to compare without first determining which is more important: the recovery of supply or the lower increase in price.

From Figure 5-4a we see that the LH₂ supply chain functions as a short-term flexibility mechanism where regasification significantly scales up in the days after the disturbance. However, after a few days, this peak dies out and regasification will decrease. This is because the LH₂ market can handle only minor flexibility as LH₂ supply is inelastic as it is imported by ship. The increased gasification leads to an imbalance in the LH₂ market that drives up the price. In Figure 5-4d, we see that the LH₂ price has a long rise time and a long settling time, making it much stickier compared to other energy prices; only the ammonia price is stickier. Moreover, the LH₂ price requires more time to recover from the disruption.

OWE Disturbance

A negative OWE disturbance leads to a disturbance in renewable hydrogen production, which leads to a decrease in total hydrogen supply. As a result, the imbalance between hydrogen supply and demand increases, leading to price-increasing incentives imposed by the broker and due to the scarcity of hydrogen. In turn, hydrogen prices increase, and quantities supply and demand adjust such that we retain an equilibrium.

From Figure 5-4c, we see that each market directly starts extracting energy from storage. With the OWE disturbance holding on, the renewable hydrogen storage remains understocked in the long term. As a result, the renewable hydrogen market goes short, with the renewable hydrogen price continually increasing (Figure 5-4d).

When looking at the hydrogen prices in the RLCH2 network, the renewable hydrogen price has a much shorter rise time compared to the low-carbon hydrogen price. This is because the coupling of the two markets on the demand side leads to a time lag.

When looking at the total hydrogen supply comparison (Figure 5-4b), we see that the H2A network best recovers from the disturbance. From the supply chain comparison in Figure 5-4a, we see that this flexibility comes from the low-carbon hydrogen supply and gaseous hydrogen import, rather than ammonia. This aligns with the low flexibility in the ammonia market.

From Figure 5-4a, we see that in the RLCH2 network low-carbon hydrogen production and gaseous hydrogen import have a longer rise time, requiring more time to scale up production, compared to the other supply chains. In Figure 5-4b, we observe that this RLCH2 can cover half of the supply decrease resulting from the OWE disturbance, while the core network can cover up to two-thirds. This makes the hydrogen supply in the core network more resilient to an OWE disturbance.

Natural Gas Disturbance

We subject a negative natural gas disturbance to the natural gas market, reflecting a period of lower natural gas supply due to for example a geopolitical situation.

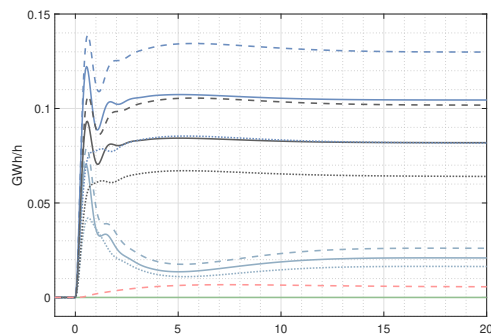
We compare the network responses to those to the OWE disturbance. We find that the RLCH2 network is highly resilient against a natural gas shock while being less resilient against an OWE shock. We conclude this from the responses of the energy prices and the total hydrogen supply.

Where after the OWE disturbance, the renewable hydrogen price had a lower rise time. After the natural gas disturbance, the low-carbon hydrogen has a lower rise time. This aligns with the market design where renewable and low-carbon hydrogen are coupled at the demand side.

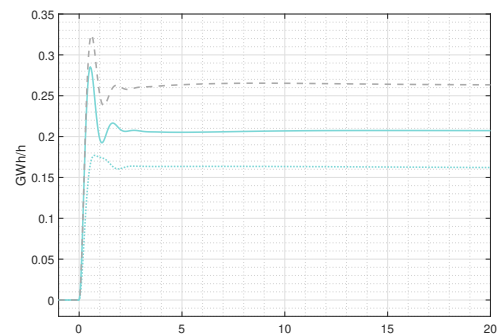
From Figure 5-5b, we obtain that the RLCH2 network can cover half of the supply decrease resulting from the OWE disturbance, while the core network can cover up to two-thirds of this. Making the hydrogen supply in the core network more resilient to a OWE disturbance.

In real life, the OWE is more volatile than the natural gas. This means that treating renewable and low-carbon hydrogen as separate commodities has implications for the dynamic resilience of the hydrogen market. Regulatory intervention is needed either to minimize OWE shocks or to enhance resilience after OWE shocks.

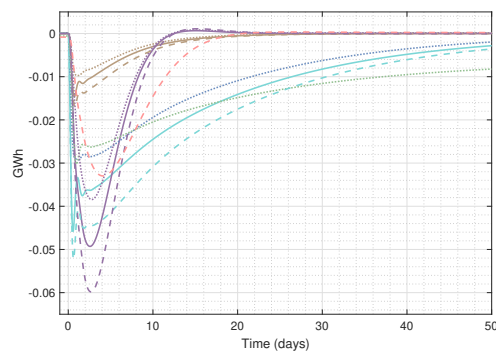
Demand Extension



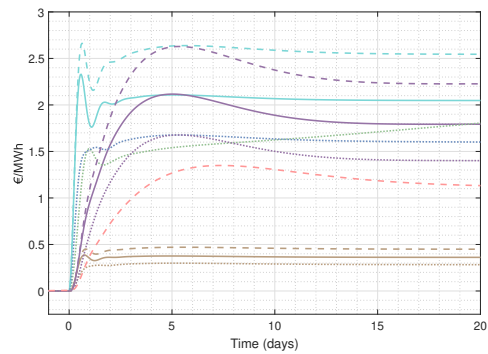
(a) Supply chain response. With the supply chains delivering renewable hydrogen (green), low-carbon hydrogen (blue), regasified LH₂ (gray-blue), imported H₂ (dark-gray), and ammonia (pink).



(b) Total hydrogen response. With hydrogen (cyan), and the hydrogen and ammonia together (light-gray).



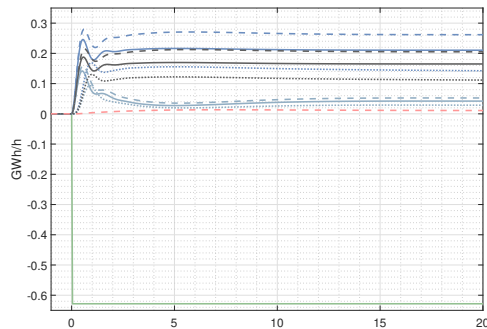
(c) Stock response. With hydrogen (cyan) (or renewable hydrogen (green) and low-carbon hydrogen (blue) separately (RLCH2)), liquid hydrogen (purple), natural gas (brown), and ammonia (H2A) (pink).



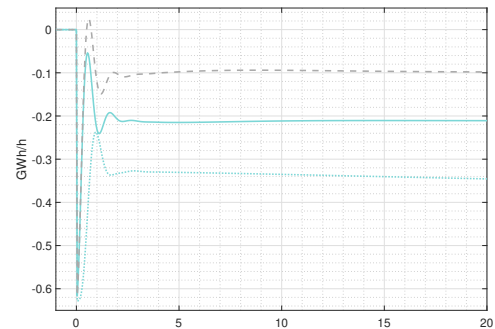
(d) Price response. Color indications are the same as for the stock comparison in (c).

Figure 5-3: Time graphs of transient responses after a demand extension in the core network (solid), the RLCH2 network (dotted), and the H2A network (dashed).

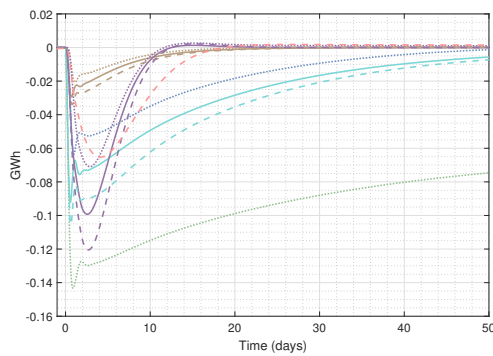
OWE Disturbance



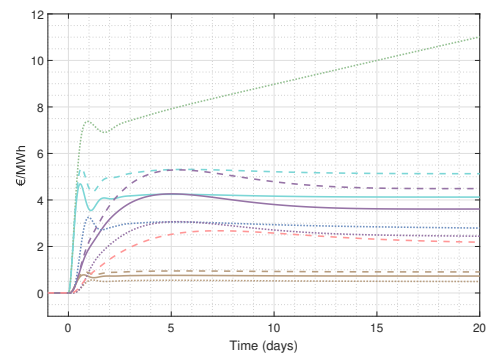
(a) Supply chain response. With the supply chains delivering renewable hydrogen (green), low-carbon hydrogen (blue), regasified LH₂ (gray-blue), imported H₂ (dark-gray), and ammonia (pink).



(b) Total hydrogen response. With hydrogen (cyan), and the hydrogen and ammonia together (light-gray).



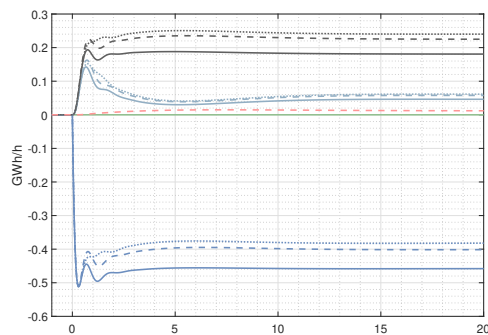
(c) Stock response. With hydrogen (cyan) (or renewable hydrogen (green) and low-carbon hydrogen (blue) separately (RLCH₂)), liquid hydrogen (purple), natural gas (brown), and ammonia (H₂A) (pink).



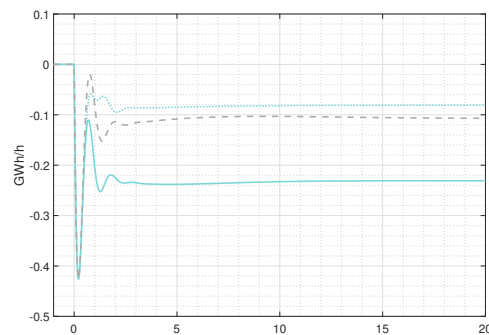
(d) Price response. Color indications are the same as for the stock comparison in (c).

Figure 5-4: Time graphs of transient responses after an OWE disturbance in the core network (solid), the RLCH₂ network (dotted), and the H₂A network (dashed).

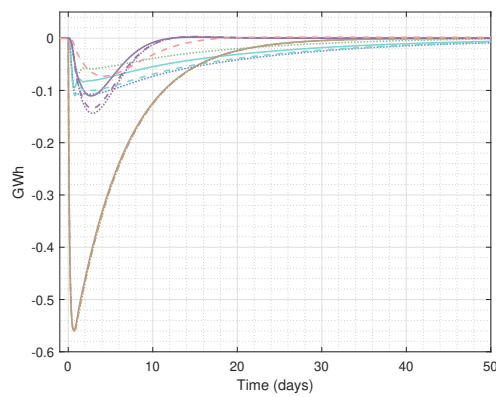
Natural Gas Disturbance



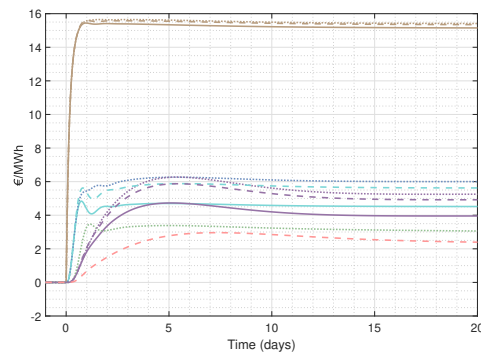
(a) Supply chain response. With the supply chains delivering renewable hydrogen (green), low-carbon hydrogen (blue), regasified LH₂ (gray-blue), imported H₂ (dark-gray), and ammonia (pink).



(b) Total hydrogen response. With hydrogen (cyan), and the hydrogen and ammonia together (light-gray).



(c) Stock response. With hydrogen (cyan) (or renewable hydrogen (green) and low-carbon hydrogen (blue) separately (RLCH₂)), liquid hydrogen (purple), natural gas (brown), and ammonia (H₂A) (pink).



(d) Price response. Color indications are the same as for the stock comparison in (c).

Figure 5-5: Time graphs of transient responses after a natural gas disturbance in the core network (solid), the RLCH₂ network (dotted), and the H₂A network (dashed).

5-2-3 Wind Variability

This section shows the influence of wind variability on energy prices, storage levels, and supply chains in the different economic networks. With this analysis, we also demonstrate the dynamic resilience of the three networks in different weather scenarios. We only discuss a few observations that were not obvious from the dynamic resilience analysis.

Real-World Wind Data as Input

To perform the simulations, we use real-world data to determine the generated OWE. This data is retrieved from the KNMI. Appendix D treats the incorporation of the wind data in more detail.

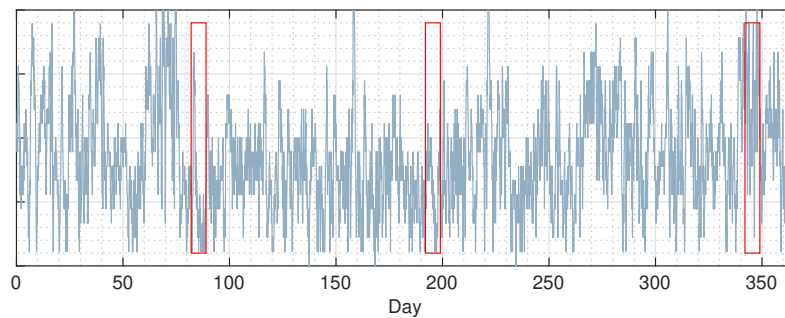


Figure 5-6: Scenario indication: the three red rectangular boxes indicate the three 7-day periods we analyze in this subsection. The first is a low-wind spring period with one extremely windy day, the second is a low-wind summer period with low wind variability, and the third is a winter period with high wind variability.

A Seasonal Comparison

We analyze the three periods indicated in Figure 5-6. These periods are selected to capture the varying characteristics of offshore wind energy, which directly impact renewable hydrogen production. The resulting supply fluctuations create a causal chain of dynamic responses, leading to ripple effects throughout the coupled energy markets. The time evolution of energy prices, storage levels, and energy flows during the spring, summer, and winter periods are shown respectively in Figures 5-7, 5-8, and 5-9.

The winter period particularly highlights the volatility in hydrogen supply, with supply ranging from 6.5 to 12.5 GWh/h within one week. In contrast, the summer period shows a more stable supply, ranging from 8.5 to 10.5 GWh/h. During spring, a stormy day causes the hydrogen supply to spike from 9 to 12 GWh/h over half a day.

In the winter period, we see that the total hydrogen supply across the core, H2A, and RLCH2 networks follow a similar trend (Figure 5-9b). However, the RLCH2 network shows a small peak time difference of around 2 hours, indicating a lag in supply chain adjustment to renewable hydrogen fluctuations. This lag is a consequence of the stickiness of the low-carbon hydrogen price (Figure 5-9d).

In the spring and summer periods, the total hydrogen supply in the RLCH2 network is notably lower than in the core and H2A networks (see figures 5-7b and 5-8b). This is due to the slightly lower low-carbon hydrogen price during these periods.

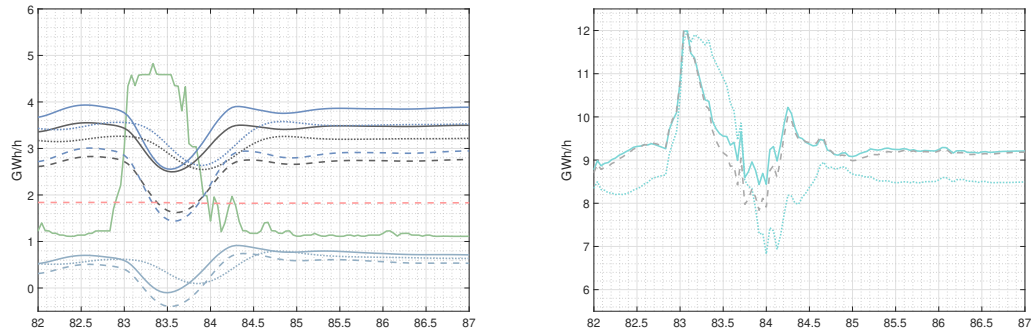
The simulations reveal seasonal influences on different hydrogen supply chains. In summer, lower natural gas prices combined with higher hydrogen prices lead to increased low-carbon hydrogen production. Conversely, in winter, higher natural gas prices and lower hydrogen prices result in decreased low-carbon hydrogen supply. During summer, we also observe a slight increase in gaseous hydrogen imports as a result of the higher hydrogen price. Across all seasons, the liquid hydrogen supply chain functions mainly as a short-term flexibility mechanism: while the base supply through this supply chain is low, it can peak for short periods.

Figures 5-7d and 5-9d show that renewable hydrogen prices exhibit significant fluctuations, even becoming negative during periods of high renewable hydrogen supply. These prices are not realistic; similar to how solar fields are unplugged when prices drop too low, this could lead wind-hydrogen operators to stop producing renewable hydrogen and sell electricity instead. This highlights the need for regulatory intervention to stabilize prices and ensure continued renewable hydrogen production. The price difference between renewable and low-carbon hydrogen could serve as an indication for determining a Feed-In Tariff (FIT) or a contract for difference (CfD) price to compensate producers for low renewable hydrogen prices and estimate the associated government costs for these subsidy schemes [24].

As wind energy can vary greatly within a short period, some supply chains are not fast enough to adjust, occasionally amplifying a supply overshoot. This shows the importance of forecasting hydrogen supply across different supply chains and ensuring effective communication between them. By anticipating renewable hydrogen supply, other supply chains can adjust their production strategies in response to forecasts of stormy days or other significant events.

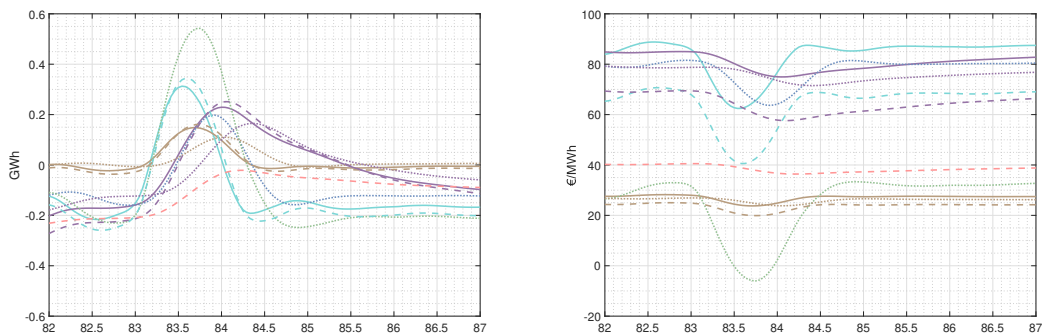
A Stormy Spring Day

In this spring period, we are looking at a period with low wind with one extremely windy day. This is a real-world example of a positive OWE disturbance.



(a) Supply comparison. With the supply chains delivering renewable hydrogen (green), low-carbon hydrogen (blue), regasified LH₂ (gray-blue), imported H₂ (dark-gray), and ammonia (pink).

(b) Total hydrogen supply. With hydrogen (cyan), and the hydrogen and ammonia together (light-gray).



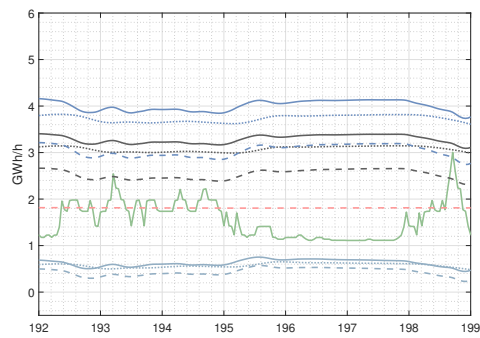
(c) Stock comparison. With hydrogen (cyan) (or renewable hydrogen (green) and low-carbon hydrogen (blue) separately (RLCH₂)), liquid hydrogen (purple), natural gas (brown), and ammonia (H₂A) (pink).

(d) Price comparison. Color indications are the same as for the stock comparison in (c).

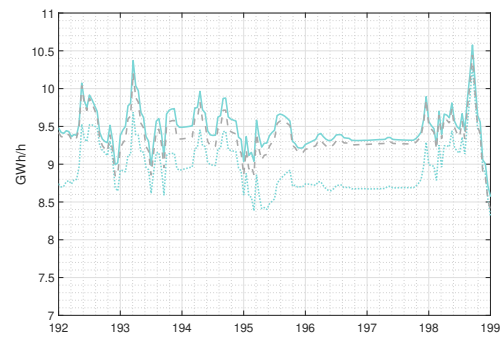
Figure 5-7: The effects of a stormy spring day on the core network (solid), the RLCH₂ network (dotted), and the H₂A network (dashed).

A Low-Wind Summer Period

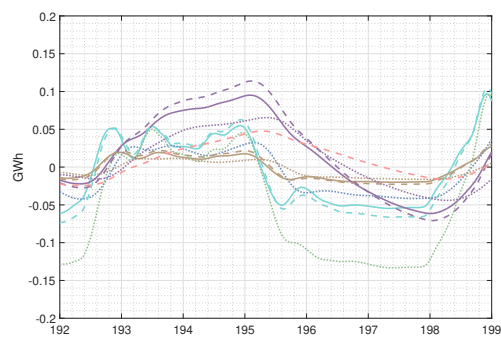
This summer period has a period with little wind and low fluctuations.



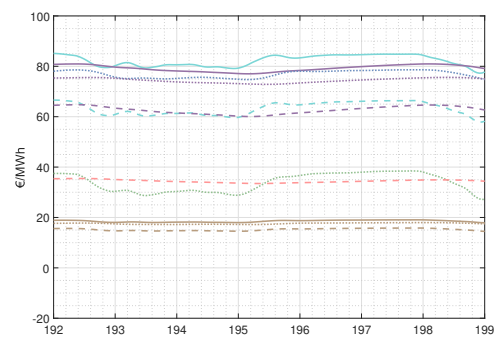
(a) Supply comparison. With the supply chains delivering renewable hydrogen (green), low-carbon hydrogen (blue), regasified LH₂ (gray-blue), imported H₂ (dark-gray), and ammonia (pink).



(b) Total hydrogen supply. With hydrogen (cyan), and the hydrogen and ammonia together (light-gray).



(c) Stock comparison. With hydrogen (cyan) (or renewable hydrogen (green) and low-carbon hydrogen (blue) separately (RLCH₂)), liquid hydrogen (purple), natural gas (brown), and ammonia (H₂A) (pink).



(d) Price comparison. Color indications are the same as for the stock comparison in (c).

Figure 5-8: The effects of a low-wind summer period with low wind variability on the core network (solid), the RLCH₂ network (dotted), and the H₂A network (dashed).

A Winter Period with High Wind Variability

This winter period contains large fluctuations in wind

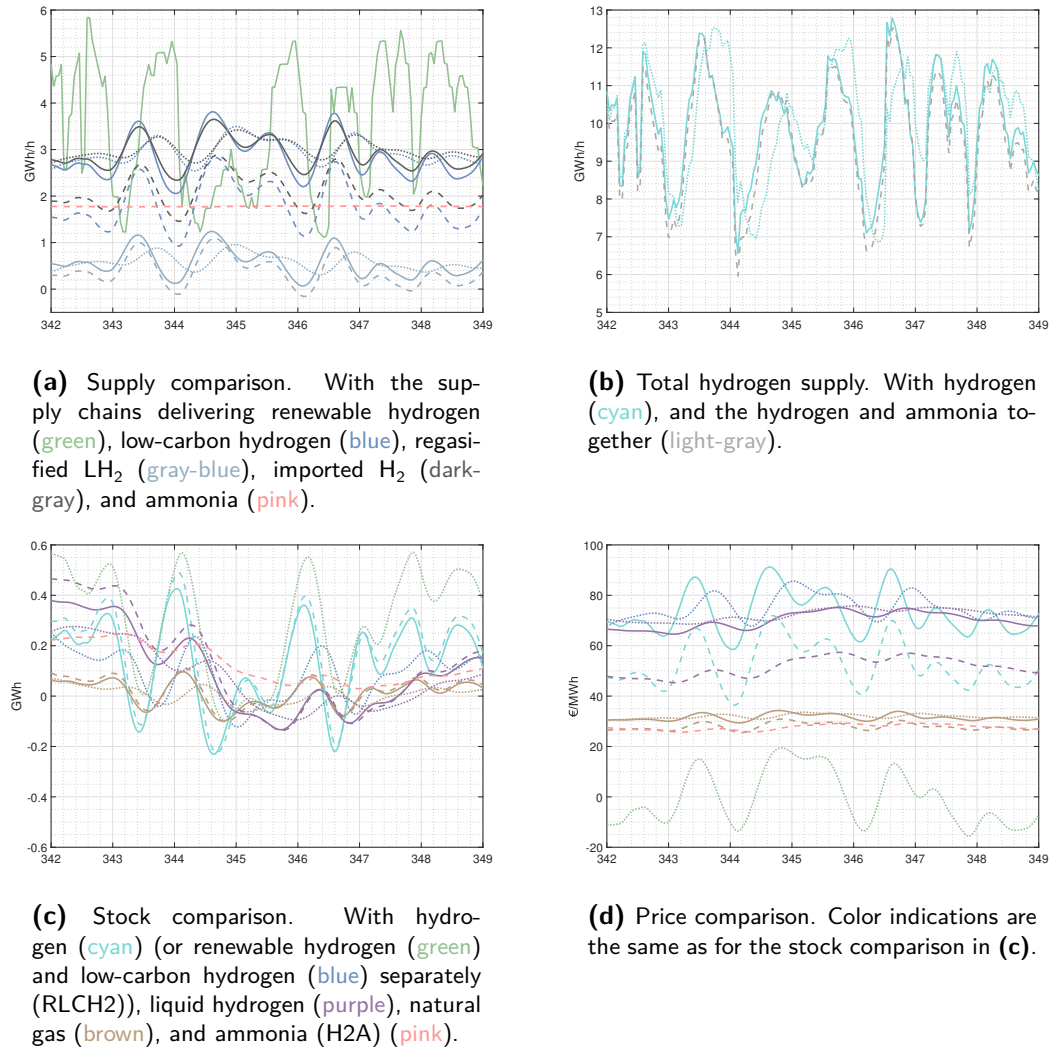


Figure 5-9: The effects of a winter period with high wind variability on the core network (solid), the RLCH₂ network (dotted), and the H₂A network (dashed).

5-3 Control

5-3-1 Closed-Loop Imbalance Settlement Design

An important advantage of our network models is that their behavior can be tuned using methods from control theory [4]. We demonstrate the design of a feedback loop in the core network and its impact on the price dynamics.

We use a PID controller for its simplicity and intuitive control actions. This controller matches our objective to build a realistic controller rather than an optimal one. We think of this controller as a regulator that intervenes in the hydrogen market, with its control actions reacting to the market incentives v^{H_2} .

We design this PID controller such that it emulates a subsidized price-settlement system, drawing inspiration from research on imbalance settlement design and government intervention. Our control objective is to enhance the dynamic resilience of the hydrogen spot market by mitigating excessive spot price levels and minimizing price volatility while ensuring supply security. We interpret this objective as a PID controller performing disturbance rejection on the price-driving market incentives as these are exactly the change in hydrogen price ($v^{\text{H}_2} = \dot{p}^{\text{H}_2}$)

Our settlement system is designed to subsidize low-carbon hydrogen production. With this production, we absorb the decrease in hydrogen supply as a result of the lower hydrogen prices. In this way, domestic low-carbon hydrogen production is leveraged as a flexibility mechanism that stabilizes the hydrogen market, financed by government subsidies.

To determine the subsidized low-carbon hydrogen production, we measure the market incentives in real-time and compare them to the reference incentive ($v^{\text{H}_2} = 0$) to generate a real-time error signal ($v_e^{\text{H}_2}(t)$). This error signal quantifies the deviation from the control objective. Based on this error signal, the regulator influences low-carbon hydrogen production (g^{H_2}).

To implement this controller, we add two controlled current sources managed by the PID controller: one to regulate the supply of low-carbon hydrogen and the other to account for the needed natural gas by deducing the natural gas supply. We show the design and implementation of the subsidized price-settlement system in the core network in Figure 5-10.

A Flow of Low-Carbon Hydrogen as a Control Action

The control action of the PID controller represents the amount of subsidized low-carbon hydrogen production as a function of time $g^{\text{H}_2}(t)$, given by the compensator formula:

$$g^{\text{H}_2}(t) = K_p v_e^{\text{H}_2}(t) + K_i \int_0^t v_e^{\text{H}_2}(\tau) d\tau + K_d \frac{dv_e^{\text{H}_2}(t)}{dt}. \quad (5-1)$$

With K_p , K_i , and K_d the control gains and $v_e^{\text{H}_2}$, $\int_0^t v_e^{\text{H}_2}(\tau) d\tau$, and $\frac{dv_e^{\text{H}_2}(t)}{dt}$ the proportional, integral, and derivative error terms. We determine the units of the control gains by filling in the units of the error terms:

$$\left[\frac{\text{MWh}}{\text{h}} \right] = [K_p] \left[\frac{\text{€}}{\text{MWh} \cdot \text{h}} \right] + [K_i] \left[\frac{\text{€}}{\text{MWh}} \right] + [K_d] \left[\frac{\text{€}}{\text{MWh} \cdot \text{h}^2} \right]. \quad (5-2)$$

This gives us the following units for the control gains:

$$[K_p] = \left[\frac{\text{MWh}^2}{\text{€}} \right], \quad [K_i] = \left[\frac{\text{MWh}^2}{\text{€} \cdot \text{h}} \right], \quad \text{and} \quad [K_d] = \left[\frac{\text{MWh}^2 \cdot \text{h}}{\text{€}} \right]. \quad (5-3)$$

Given these units, we can give them an economic interpretation, which supports their tuning. K_p can be seen as the inverse of the market friction parameter b , and K_i can be seen as a price-elasticity of supply ε (see Section 3-3). For tuning K_p and K_i , we use our identified network parameters as a base indication. For K_d we do not have a direct economic interpretation, however, it can be thought of as a rate of incentive development.

PID Controller Tuning

We manually tune the PID controller based on the hydrogen spot price response and the control action's influence on low-carbon hydrogen production.

First, we start with only the proportional control (P) by setting integral (I) and derivative (D) controls to zero. The proportional control action relates the error term $v_e^{\text{H}_2}$ directly to a flow of hydrogen. This control action minimizes the price volatility by acting as extra market friction. However, as a consequence, the control action increases the volatility in low-carbon hydrogen production. We gradually increase the proportional gain K_p until we reach a desired price response while the production volatility remains realistic.

Then, we add an integral control action. This control action lowers the hydrogen spot price by increasing subsidized low-carbon hydrogen production. This control action integrates the error term over time, accounting for the past values of the error term. As the integral over the error term is interpreted as a price ($\int v_e^{\text{H}_2} = p_e^{\text{H}_2}$), we relate a price to a flow of hydrogen, similar to an elementary demander (or supplier). We increase the integral gain K_i until we find a realizable production level where the total government costs stay below 10 million Euro³.

Last, we add a derivative term to anticipate future hydrogen spot price dynamics by looking at the acceleration of the error term $v_e^{\text{H}_2}$. We obtain that a high derivative term leads to larger fluctuations in the control action. We gradually increase the derivative gain K_d until it predicts a few hours ahead without causing excessive volatility in low-carbon hydrogen production.

To mitigate the high-frequency noise, we set the filter coefficient N to $\frac{K_d}{10}$.

The tuned control gains are listed in Table 5-1.

	Value
Proportional gain K_p	15
Integral gain K_i	4
Derivative gain K_d	2
Filter coefficient N	0.2

Table 5-1: Tuned PID controller gains

³This budget is chosen as government support is mainly put into renewable hydrogen projects.

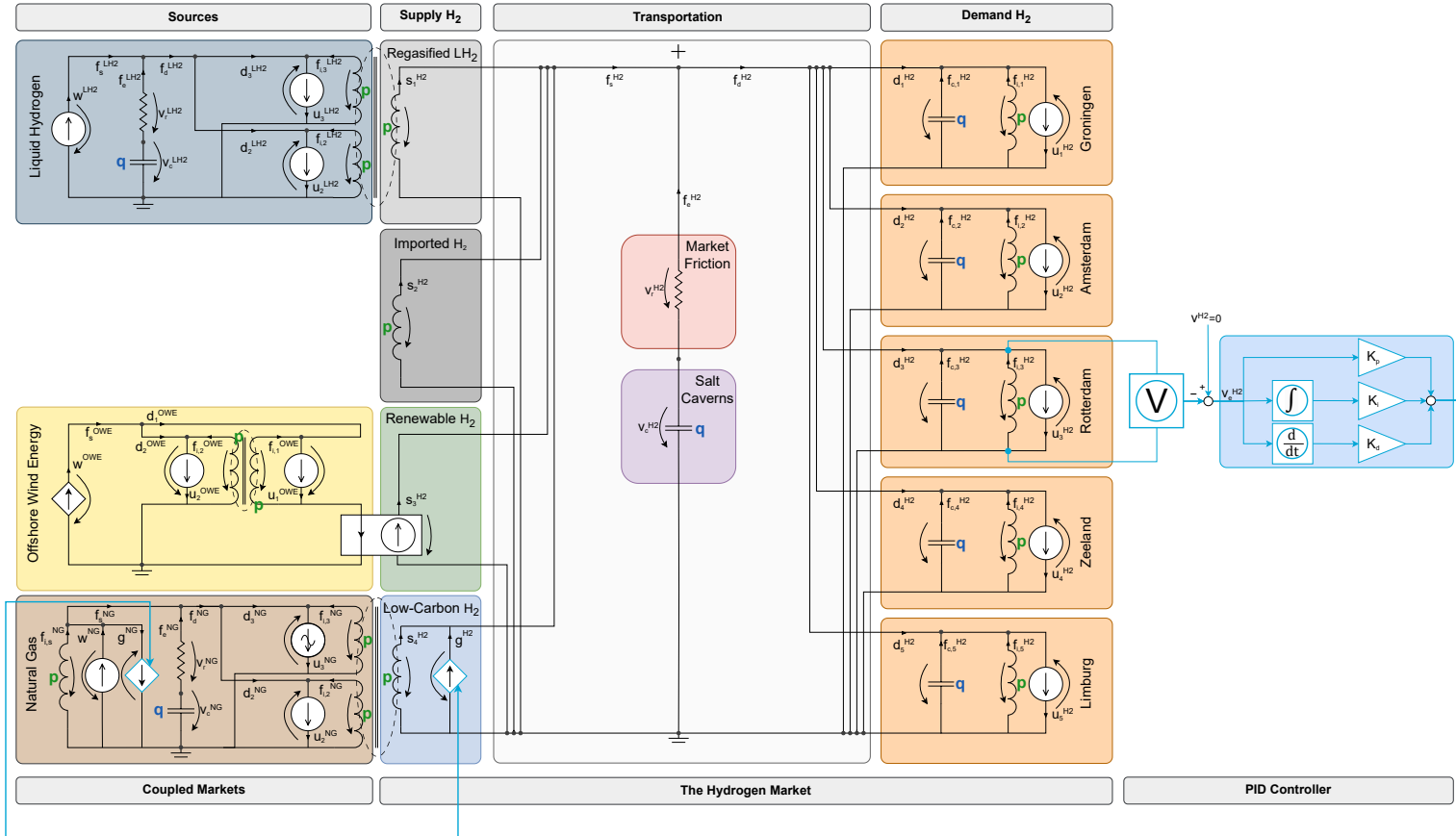


Figure 5-10: Network topology of the controlled core network. The controller is indicated in blue. We measure the incentives over the inductor of a demander with a voltage sensor. We compare this value with the reference incentive v^{H_2} , which we set to zero. Then we use proportional (P), integral (I), and derivative (D) control actions to determine the subsidized production of low-carbon hydrogen g^{H_2} . This also affects the natural gas market as more natural gas is needed for hydrogen production.

The Impact of the Controller on the Network Dynamics

We demonstrate the impact of the controller on the network dynamics by simulating the networks using the same wind data shown in Figure 5-6. Figure 5-11 shows the controlled and uncontrolled network dynamics during a winter period with large fluctuations in wind and renewable hydrogen supply.

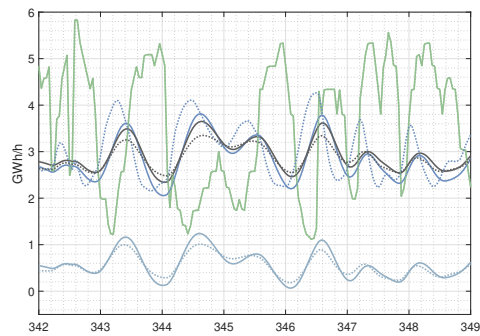
Figure 5-11 demonstrates that the controller effectively regulates the spot hydrogen price in line with the objective of minimizing price volatility while maintaining the security of supply.

Figure 5-11a shows increased volatility in low-carbon hydrogen production, with better anticipation of hydrogen spot price dynamics due to the derivative control action. However, this leads to higher volatility levels in the natural gas price (Figure 5-11d). Due to the slightly lower hydrogen prices, we see that the hydrogen supply through gaseous hydrogen import and regasified LH₂ become less volatile. As a result, the total hydrogen supply becomes slightly less volatile (see Figure 5-11b).

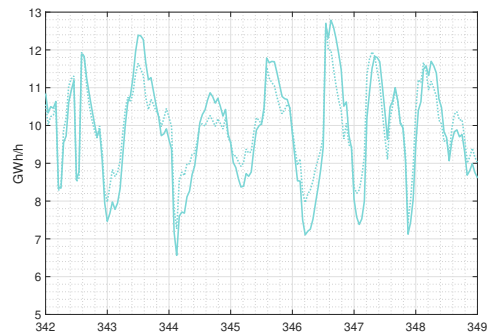
The impact of the controller is quantified in Table 5-2. This table details the percentage decrease in hydrogen price, increase in hydrogen supply, and increase in natural gas price over the full year compared to the uncontrolled core network. It also shows the cost of the subsidized price-settlement system, both in total and as a percentage of total hydrogen trade value (277M€/y).

	Value
H ₂ price decrease [%]	2.1477
H ₂ supply increase [%]	0.9257
NG price increase [%]	3.2647
Cost [M€/y]	9.2582
Cost [% of total hydrogen trade]	3.3434

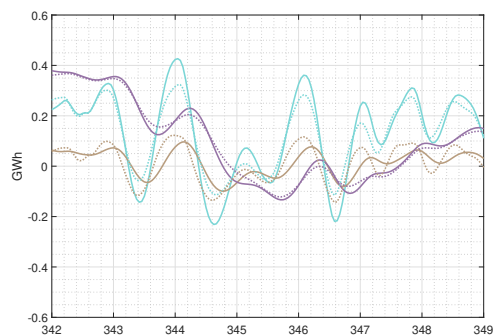
Table 5-2: The impact of the controller on the network dynamics determined over the year simulation with wind data as an input.



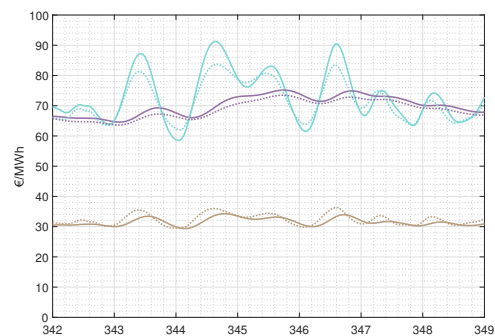
(a) Supply comparison. With the supply chains delivering renewable hydrogen (green), low-carbon hydrogen (blue), regasified LH₂ (gray-blue), imported H₂ (dark-gray), and ammonia (pink).



(b) Total hydrogen supply. With hydrogen (cyan), and the hydrogen and ammonia together (light-gray).



(c) Stock comparison. With hydrogen (cyan) (or renewable hydrogen (green) and low-carbon hydrogen (blue) separately (RLCH₂)), liquid hydrogen (purple), natural gas (brown), and ammonia (H₂A) (pink).



(d) Price comparison. Color indications are the same as for the stock comparison in (c).

Figure 5-11: The effects of PID control on the core network in a winter period with high wind variability: a comparison between the core network (solid) and the controlled core network (dotted).

Chapter 6

Conclusions

This thesis serves as a proof of concept for the application of economic circuit theory in effectively addressing supply-and-demand-driven pricing in a hypothetical spot market for hydrogen.

By designing a spot market for hydrogen as an economic network of market agents, we conceptualize it in the same way engineers do. This allows us to identify a mesh structure that determines the hydrogen price dynamics, a structure not previously recognized. While our network models reflect expected hydrogen spot market behavior, they are still simplified. The network models can be further enhanced by exploiting a port-based approach to design more complex market agents as circuit modules [25].

To design a more accurate hydrogen spot market network, we suggest a few improvements and extensions. This includes a refined representation of hydrogen storage, as our current simulations demonstrate that energy storage cannot be simply represented by a single capacitor. Another important extension would be incorporating a representative electricity market to model a renewable hydrogen production strategy that is influenced by both the electricity market and hydrogen prices; potentially with the inclusion of real-time wind forecasting models. Additionally, one could consider including minimum production prices by implementing switches, where producers only produce if the hydrogen price exceeds their costs. Other extensions could include accounting for energy losses and transportation costs by modeling industry clusters as local markets. Beyond network extensions, parameter identification is a critical factor that significantly influences spot market dynamics and necessitates further refinement.

Transient analysis techniques prevalent in engineering systems have proven to be very effective for analyzing the evolution of energy prices, storage levels, and flows. These analyses can be extended with Laplace domain analyses, such as Bode plots and pole-zero maps, to analyze behaviors not apparent in the time domain, like trade and storage cycles. Laplace domain techniques can also be used for net present value analysis for capital valuation.

We demonstrated the implementation of a simple Proportional-Integral-Derivative (PID) controller that emulates a subsidized price-settlement mechanism, which shows the potential of control mechanisms to influence spot market behavior. While this form of regulatory intervention positively influences market behavior, it incurs significant costs without a substantial effect.

Future research should look into methods to optimize the renewable hydrogen production strategy in response to both electricity and hydrogen prices to minimize hydrogen price volatility. For such control applications, optimal control methods, such as model predictive control (MPC), could be employed to achieve desirable spot market behavior.

In conclusion, economic circuit theory addresses the need for modeling price dynamics while functioning as an effective tool for hydrogen market design, as emphasized by International Renewable Energy Agency (IRENA). Our application demonstrates that our design methods are relevant to regulators, investors, and other stakeholders with an economic interest in a future spot market for hydrogen. Not only can stakeholders understand price dynamics and address hydrogen price uncertainty, they can also use our methods to design resilient market structures or regulatory interventions to stabilize market prices. Developing a user-friendly toolbox could broaden the accessibility of economic circuit theory, particularly for those without an engineering background.

Appendix A

Analysis of the Hydrogen Market

A-1 Hydrogen Supply Chains

A-1-1 Domestic Hydrogen Production

The Colors of Hydrogen

Hydrogen, represented by the molecular formula H_2 , is the simplest and most abundant element in the universe. However, on Earth, hydrogen rarely exists freely¹ in its pure form due to its lightness and the planet's gravitational field [26]. Instead, it is commonly found in combination with other elements, such as in water and hydrocarbons. As hydrogen is produced from other sources of energy, it is known as an energy carrier.

The production of hydrogen involves various processes and energy sources. Hydrogen is associated with different colors, depending on its production process [27, 28]. The three main colors of hydrogen are gray, blue, and green.

Gray hydrogen is derived from fossil fuels and is therefore accompanied with greenhouse gas (GHG) emissions. Gray hydrogen is mainly produced through steam methane reforming (SMR) with natural gas and coal gasification. SMR is currently the only production method that produces hydrogen in large quantities [7, 29]. The efficiency of SMR reaches up to 90% (assuming the Higher Heating Value (HHV) of hydrogen)² [29, 30, 31].

Blue hydrogen is a variant of gray hydrogen that incorporates carbon capture and storage (CCS) technologies. It is predominantly produced through SMR, but the integration of CCS reduces its GHG emissions compared to gray hydrogen.

Green hydrogen is produced through electrolysis using renewable energy sources (RES). Off-shore wind is the most suitable RES in North-Western Europe for directly coupling large-scale

¹Natural hydrogen, or white hydrogen, is rarely found in reserves below the ground.

²In line with HYCLICX, HyXchange, and others. As most efficiencies are provided in Lower Heating Value (LHV), the conversion factor of 1.182 is used to convert LHV to HHV

electricity generation with industrial-scale hydrogen production. The efficiency of hydrogen production through electrolysis highly depends upon the feedstock, but is approximately around 80% (assuming the HHV of hydrogen) [29, 30, 31].

Other renewable-based solutions to produce hydrogen exist as well; however, these are beyond the scope of this thesis and therefore not addressed here.

Renewable and Low-Carbon Hydrogen Production

Domestic hydrogen production includes both renewable and low-carbon hydrogen³. The majority of hydrogen supply in the Netherlands comes from its five industrial clusters located in Eemshaven, Amsterdam/IJmuiden, Rotterdam-Moerdijk, Westerscheldemond, and Chemelot in Geleen⁴ [29]. The total amount of hydrogen that is currently produced in these industry clusters is estimated at 180 petajoules (PJ) per year⁵ [33].

Current hydrogen production predominantly involves SMR using natural gas. However, there is a notable shift towards adopting electrolysis for hydrogen production, driven by its growing maturity and the transition to cleaner energy sources.

It is expected that electrolysis plants will operate in close connection to wind parks [7], as there will be a mandatory requirement⁶ to construct additional renewable electricity generation capacity to accommodate the realization of electrolyzers, starting in 2028. The close connection between an electrolysis plant and a wind park implies that the utilization rate of the electrolysis plant is weather-dependent and, hence, volatile [7].

The Dutch hydrogen strategy includes the ambition to install 3 to 4 GW of electrolyzer capacity for the production of renewable hydrogen by 2030 and then expand significantly in the subsequent years [6]. This installed capacity can produce 60-80 PJ/y of renewable hydrogen [34, 35]. And according to findings by Netherlands Environmental Assessment Agency (PBL), a total of 96 PJ/y of additional low-carbon hydrogen production capacity can be realized towards 2030 [34].

A-1-2 Hydrogen Import

To meet rising hydrogen demand and to cope with the variability in domestic renewable hydrogen production, the hydrogen strategy incorporates plans for hydrogen import. Another goal of the hydrogen strategy is to play a prominent role as an importer and transit hub for hydrogen within Europe, with ambitious plans⁷ to import up to 120 PJ/y by 2030 [34, 35, 12, 36].

³The future scenarios are explained with the new European hydrogen terminology, as the EU's current energy regulatory framework fails to define renewable (formerly named "green") and low-carbon (formerly named "blue") hydrogen. Renewable hydrogen derives its energy content from RES other than biomass and achieves a 70% GHG emission reduction compared to fossil fuels. The hydrogen referred to as low-carbon hydrogen is derived from non-renewable sources while meeting the GHG emission reduction threshold of 70% compared to fossil-based hydrogen (formerly named "gray" hydrogen) [32].

⁴Henceforth, these five industry clusters will be referred to as Groningen, Amsterdam, Rotterdam, Zeeland, and Limburg.

⁵Or 50.000 GWh/y.

⁶See European legislation for hydrogen (Delegated Acts on Renewable Hydrogen): https://energy.ec.europa.eu/topics/energy-systems-integration/hydrogen/hydrogen-delegated-acts_en.

⁷These estimates are aligned with the European Union's aspirations and industry obligations and are further informed by supply and demand projections provided by various port authorities.

Hydrogen can be imported in various forms through international pipelines or via ships. The import's cost-effectiveness depends on production and transportation costs [37].

The production costs of renewable hydrogen depend on several factors, including the cost of renewable electricity (influenced by factors such as the distribution of solar radiation and wind, land prices, and labor costs), the cost of clean water, land availability for renewable energy installations, and subsidies. Depending on transportation costs, it may be economically advantageous to import renewable hydrogen from regions with lower production costs [2, 27, 37].

The transportation costs of gaseous hydrogen by pipelines have shown to be significantly lower compared to import by ship, even for longer distances⁸. For transportation distances far above 1.000 km, import by ship may become more cost-effective, especially for large volumes and intercontinental connections⁹ [27, 34, 12].

The Dutch port facilities all have ambitions and concrete plans for hydrogen import. These imports can take various forms, such as liquid hydrogen (LH₂)¹⁰, or in the form of a carrier such as ammonia or methanol¹¹, or using liquid organic hydrogen carriers (LOHCs)¹². Each form requires a conversion process before the imported hydrogen can be fed into the hydrogen backbone.

The most potential lies in the import of liquid hydrogen and ammonia. Liquid hydrogen offers advantages as no additional expensive energy is needed to release the hydrogen (unlike LOHCs). On the other hand, ammonia is more cost-effective as it does not require the extreme cooling that liquid hydrogen does¹³. Moreover, ammonia is demanded and used as a raw material for the production of artificial fertilizer.

The import of hydrogen via ships is likely to be realized sooner due to existing and well-established port facilities. The Netherlands has already made official announcements regarding overseas collaborations with Australia and the potential for partnerships with African countries¹⁴. However, in the long run, hydrogen will predominantly be imported via international pipelines, while the role of import via ships will mainly be to enhance supply security, similar to the current function of LNG imports [2, 10].

A-2 Industrial Demand for Hydrogen

The demand for hydrogen primarily comes from the five industry clusters in the Netherlands. The distribution of current hydrogen demand over these clusters is illustrated in Figure A-1.

Within the different industry clusters, hydrogen is used in various types of industrial processes [33]. Hydrogen is mainly used as a feedstock for the production of other commodities (including ammonia and methanol), or as an energy carrier to produce high-temperature heat in refineries (including desulfurization, hydrogenation, and cracking of oil) [33, 29, 38].

⁸As is evident from existing natural gas pipeline connections from Russia, Algeria, and Norway.

⁹The selection of a transportation mode also depends on the intended end-use, to minimize unnecessary hydrogen conversion during transit to mitigate extra costs and energy losses.

¹⁰The transportation of liquefied hydrogen via ships has been successfully demonstrated for long-distance transport, albeit in limited quantities.

¹¹The importation of ammonia and methanol are established forms of transportation.

¹²LOHCs are organic compounds that chemically absorb and release hydrogen.

¹³Liquid hydrogen must be cooled, transported, and stored at -253°C [33].

¹⁴Given that the transportation of hydrogen can span several weeks, these long-term contracts will encompass pre-established delivery schedules.

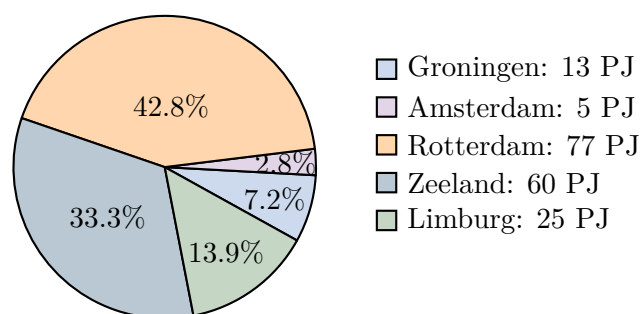


Figure A-1: Current distribution of domestic hydrogen demand per industry cluster of the total yearly demand (180 PJ)¹⁵. Source: data retrieved from TNO (2020) [33].

Forecasts indicate that industrial demand for hydrogen could reach up to 250 PJ/y by 2030 [29]. Looking further ahead to 2050, hydrogen demand in the Netherlands is expected to increase greatly [33, 38].

It is important to note that not all industrial demand can be fulfilled with renewable hydrogen. Currently, only 50 PJ/y of the demand can be replaced without major modifications to processing facilities [33, 34]. Hence, the proportion of renewable hydrogen within the overall hydrogen demand varies among industry clusters, depending on the industrial processes within the cluster.

The prospect of future hydrogen demand also extends beyond industry, including sectors such as mobility and transportation, agriculture, power production, and low-temperature heating in the built environment [29, 38]. The demand from these sectors in 2030 remains relatively small compared to the industry sector. However, in the longer term, toward 2050, the demand from these sectors will increase [33, 38].

Hydrogen Demand Flexibility

Although often assumed, hydrogen demand is not completely inelastic [14]. Demanders can adapt to the hydrogen availability and hydrogen prices, a concept known as demand response (DR).

In some cases, demanders might opt for alternative commodities. For instance, in clean steel production, instead of utilizing hydrogen for pelletizing iron ore domestically, one can choose to import pre-pelleted iron ore. Similarly, for the production of fertilizers, one can directly import ammonia instead of producing it with hydrogen. This is already a common practice.

A-3 The Hydrogen Backbone Connecting Supply and Demand

The hydrogen backbone¹⁶ is the most important prerequisite of a spot market for hydrogen [2, 10, 8, 7, 9, 3, 12, 43]. This infrastructure connects suppliers and demanders, as well as provides access to storage facilities.

¹⁶The Netherlands possesses an extensive network of gas pipelines that can be repurposed for hydrogen transportation with the phase-out of natural gas [12, 39, 40, 41]. The existing gas infrastructure includes multiple parallel pipelines. These steel pipeline grades are suitable for hydrogen transportation with minor modifications. With the expected decrease in demand for natural gas in the coming years, there is an opportunity to convert the existing L-gas grid infrastructure to transport pure hydrogen [40, 41].

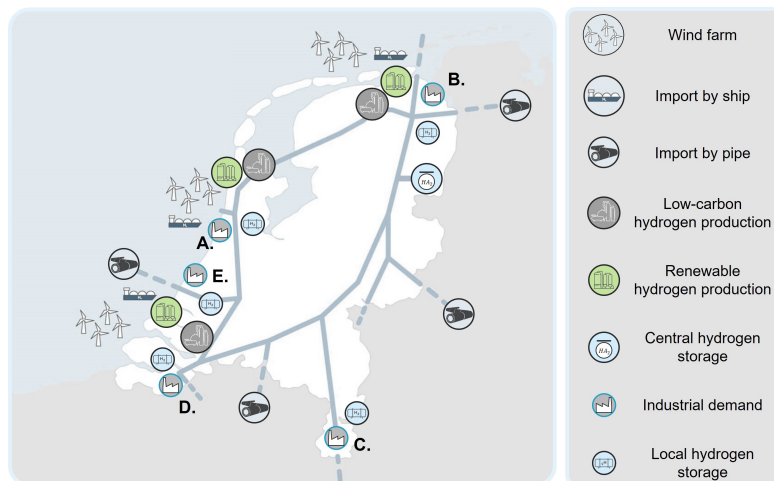


Figure A-2: The hydrogen backbone. The letters A. to E. respectively correspond to the industrial clusters of Amsterdam, Groningen, Limburg, Zeeland, and Rotterdam. Domestic production consists of renewable and low-carbon (see subsection A-1-1) and storage consists of small storage facilities at the industry clusters and a large storage facility in the Northern Netherlands (see section A-4).

The backbone will connect the five industry clusters located in Groningen, Amsterdam, Rotterdam, Zeeland, and Limburg, as well as storage facilities, as illustrated in Figure A-2. Hydrogen can be transported bi-directional on this network.

The European Hydrogen Backbone Connecting Countries

There also exist plans for an extensive European Hydrogen Backbone (EHB) to connect countries across the continent. It is anticipated that between 2030 and 2040, this infrastructure will enable the transportation and trading of hydrogen across European borders ¹⁷.

A-4 Storage of Hydrogen

A second important prerequisite of a spot market is sufficient storage capacity to cope with production and seasonal fluctuations, and to balance supply and demand [27, 12, 36]. Particularly with the increasing integration of renewable hydrogen production.

As hydrogen has a relatively low volumetric energy density compared to its energy density by weight, it requires larger spaces for storage [44]. The hydrogen backbone can accommodate

Gasunie has developed a national hydrogen backbone plan that envisions a 1400 km pipeline network to transport gaseous compressed hydrogen by 2030 [42, 35]. Repurposed natural gas pipelines are expected to comprise around 85% of this network [40].

¹⁷As of 2030, the EHB initiative envisions an initial 11,600 km pipeline network, setting the stage for the gradual development of a pan-European hydrogen infrastructure. For detailed information about the EHB initiative, see the EHB website: <https://ehb.eu/>.

minor pressure differences, providing flexibility within a day. This form of storage is known as linepack. The management of larger surpluses and shortages of hydrogen requires extensive storage facilities.

Different hydrogen storage possibilities exist, depending on the different transportation methods, time scales, and storage capacities. Generally, hydrogen storage is categorized in above-ground hydrogen storage (AHS) and underground hydrogen storage (UHS). UHS is designed to accommodate mid- to long-term fluctuations in supply and demand, whereas AHS is typically employed for short-term or daily fluctuations [35, 44].

Plans exist for UHS within salt caverns¹⁸ in the Northern Netherlands, due to its proven maturity [27]. According to Gasunie, a salt cavern can store around 140-280 GWh or $\sim 0,5-1$ PJ of hydrogen [47, 12]. By 2030, a minimum of 3 to 4 salt caverns with a total storage capacity of 750 to 1000 GWh will be required (3 to 4 PJ) [35]. The losses caused by the leaks in these underground caverns are relatively small, accounting for 13% of total annual volumes [44].

To fulfill the need for short-term storage, a currently proven method is AHS in high-pressure tanks. These tanks have a capacity of approximately 45 MWh, equivalent to the annual gas consumption of three Dutch households [7].

Hydrogen can also be stored in liquid form, which is advantageous when space is a determining factor [48]. However, due to high conversion costs, this approach is economically viable primarily when the hydrogen is supplied in liquid form or through a liquid carrier (ammonia, and LOHCs). This form of storage will mainly be used by port facilities that import liquid hydrogen¹⁹.

A-5 A Supply-and-Demand-Driven Spot Market for Hydrogen

Currently, the Dutch hydrogen market operates through specialized contracts between suppliers and demanders, so-called Hydrogen Purchase Agreements (HPAs), with hydrogen mainly produced on-site in industry or supplied through privately owned pipelines. The hydrogen prices are determined by marginal-cost-plus pricing.

However, the establishment of the hydrogen backbone²⁰ and the growth and diversification of the hydrogen supply, will accelerate the need for spot market trade [2, 10, 8].

A-5-1 Spot Price Volatility

In the current marginal-cost-plus-pricing market, the hydrogen price volatility is low as trade predominantly exists through HPAs. However, the establishment of a spot market will significantly

¹⁸Other options for geological hydrogen storage include storage in depleted natural gas fields. Depleted natural gas fields in the North Sea have a potential of over 200 TWh of hydrogen storage capacity [36, 45, 46]. and offshore located salt caverns [7, 27, 47]. However, there is no experience with these methods yet.

¹⁹For example, a large oil tank with a capacity of 114,000 m³ could theoretically store 220 GWh of hydrogen in the form of LOHCs (50 kg H₂/m³) or 530 GWh of hydrogen in the form of ammonia (120 kg H₂/m³) [12, 35, 49].

²⁰According to the latest update from HyXchange, trading on the common hydrogen backbone is expected to begin by 2026, with initial regional trading taking place in the four port-areas and industrial clusters [3].

influence market behavior and price volatility²¹.

On a spot market for hydrogen, the price volatility is primarily determined by changes in supply and demand [2]. The integration of weather-dependent RES for hydrogen production will lead to fluctuations in supply, and consequently increased price volatility. Other influential factors impacting volatility encompass economic conditions, economic growth, and storage levels.

Particularly the emerging phase of a spot market will be characterized by increased price volatility. When there are a limited number of suppliers and demanders, their actions have a relatively large impact on market prices. Consequently, unanticipated shifts in demand can amplify price volatility. However, as the market matures and adapts to supply and demand, price volatility is expected to stabilize [3].

A hydrogen spot market is expected to demonstrate behavior that lies between the behaviors of the electricity²² and natural gas²³ spot markets [2]. While expected to be less volatile than the electricity market due to storage, the hydrogen market remains responsive to the availability of wind and solar power, resulting in price variations throughout the day and year.

A-5-2 Market Design and Regulatory Intervention

Emerging spot markets, as evidenced by the natural gas market, do not naturally evolve into mature wholesale markets due to market failures²⁴. Therefore, market design and regulatory intervention play an important role in the development of a spot market for hydrogen [7, 24].

Valuable insights in market design can be obtained from experiences of existing energy markets [50]. The production side of the hydrogen market can be compared with the electricity market, while transportation and spot trade will be more comparable to the natural gas market [7].

To enhance liquidity and foster a competitive market, regulatory intervention is needed to boost domestic hydrogen production, stimulate consumption, and maintain reasonable prices, particularly during market ramp-up [8]. Various forms of regulatory intervention by agencies such as the government exist. These include serving as a market maker and issuing subsidies like a Feed-In Tariff (FIT) or contract for difference (CfD)²⁵ [24].

²¹Energy prices, including those of basic energy sources such as natural gas, electricity, and heating oil, tend to exhibit higher volatility compared to other commodities. This heightened price variability is particularly noticeable for industrial users, as wholesale prices closely mirror the daily price fluctuations in the market [2].

²²The electricity market experiences high price variability on an hourly basis due to the need for real-time balancing of demand and production, especially with the integration of intermittent RES.

²³The natural gas market benefits from extensive storage infrastructure. Therefore it exhibits less short-term price differences compared to the electricity market.

²⁴Including negative (network) externalities, a possible hold-up, and economies of scale [7].

²⁵Such as the **SDE⁺⁺**! (**SDE⁺⁺**!) subsidy.

A-6 Model Assumptions

Hydrogen Supply:

Supply Distribution

- The hydrogen supply in the Netherlands between 2030 and 2040 is in line with the distribution^a as depicted in Figure A-3.

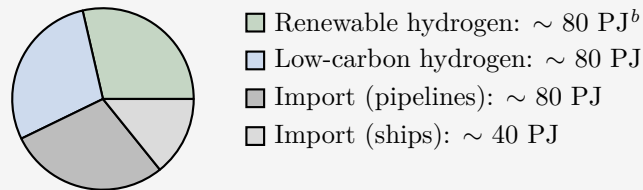


Figure A-3: Distribution of hydrogen supply (total 280 PJ/y)^c

Domestic Hydrogen Production

- Low-carbon hydrogen, produced via SMR with natural gas, achieves an efficiency of 90%, and renewable hydrogen, produced through electrolysis using offshore wind energy, operates at an efficiency of 80% efficiency.
- The wind distribution is modeled using data.
- Low-carbon hydrogen production is adjusted in response to renewable hydrogen production, making it a price-elastic supplier in the model.

Hydrogen Import

- Hydrogen import is split into via ships and import via the European hydrogen backbone.
- Liquid hydrogen import via ships is assumed constant over time.
- Ammonia import, which is considered as a model extension, is assumed to be slightly elastic.
- Import via pipelines is modeled as an aggregated price-elastic supplier.

^aThe total amount of 280 PJ is roughly in line with the hydrogen demand assumed in the Integrated Electricity, Hydrogen and Gas (I-ELGAS) model. Which is 288 PJ (or 80 TWh).

^bSanity check: supply of 80 PJ/y, or 2.5 GWh/h, of renewable hydrogen requires around 6.25 GW of installed capacity of electrolyzers assuming a capacity factor of 40%.

^cOr approximately 2.5, 2.5, 2.5, and 1.25 GWh/h for the respective supply chains.

Coupled Commodity Markets

- The hydrogen market is coupled with the natural gas market and the liquid hydrogen market through price coupling.
- In the natural gas and liquid hydrogen markets, it is assumed that both suppliers and demanders exhibit price-elastic behavior. Demanders are further categorized into general demanders and those who use the commodity as a resource for hydrogen production.
- The electricity market is out of scope but a fictitious offshore wind energy market is incorporated to include price effects.
- Offshore wind energy production depends on weather conditions. Demand is assumed to be price elastic and is again split into two groups.
- When ammonia import is integrated into the model, its respective market is integrated in line with the natural gas and liquid hydrogen markets.
- The markets for GHG emissions and green certificates are out of scope.

Hydrogen Demand:**Demand Distribution**

- The distribution of domestic demand among industry clusters in 2030 will closely resemble the current distribution, as illustrated in Figure A-1^a.

Domestic Hydrogen Demand

- The model focuses on industrial demand only.
- Each industry cluster is modeled as a flexible (price-elastic) market agent, having its own aggregate demand and storage capabilities.
- The hydrogen demand per industry cluster can be split into demand for renewable hydrogen and demand for low-carbon hydrogen.
- Although a full substitution of gray hydrogen with renewable hydrogen is not possible due to changes in production processes, this aspect is not considered in the model.
- Industrial hydrogen demand is assumed to be price-elastic, depending on the industrial processes within those clusters.

^aFor modeling purposes and in line with planned hydrogen developments, it is chosen to slightly increase the demand in Groningen and Amsterdam.

A Supply-and-Demand-Driven Spot Market for Hydrogen:

Hydrogen Pricing

- A hydrogen spot market is competitive.
- Hydrogen can be treated as a homogeneous product or split in renewable and low-carbon hydrogen.
- Supply and demand are closely matched by the market operator.
- The uniform trading unit for hydrogen is MWh.
- Hydrogen is priced through a uniform pricing scheme with one market clearing price per hour.
- Price volatility is caused by changes in supply, demand, and storage levels.

The Hydrogen Backbone

- Hydrogen is transported between industry clusters through the national hydrogen backbone, as depicted in Figure A-2.
- The losses attributed to pipeline transportation are considered negligible.

Storage of Hydrogen

- Linepack is considered negligible.
- Hydrogen is stored in large amounts^a in a central storage facility (salt caverns) and in small amounts in local tanks at industry clusters^b.
- The losses attributed to hydrogen storage are considered negligible.
- Maximum injection and distraction rates are out of scope, as well as the pressure-dependent filling rate of hydrogen storage systems.

Government Regulation

- The government can perform a regulatory intervention to influence spot prices through subsidies^c.

^aWith a maximum capacity of 1000 GWh.

^bWith a maximum capacity of 45 MWh.

^cSuch as a CfD scheme (e.g. SDE⁺⁺ (Subsultion scheme for Stimulating Renewable Energy Production and Energy Transition) or a FIT.

Appendix B

Modeling a Marginal-Cost-Plus-Pricing Market for Hydrogen

B-1 Existing Hydrogen Market Models

The Integrated Electricity, Hydrogen and Gas Model

The Integrated Electricity, Hydrogen and Gas (I-ELGAS) model is an optimization model for energy dispatch and prices for hydrogen, electricity, and methane, developed by TNO in collaboration with Berenschot. HyXchange, the hydrogen exchange initiative, employs this model to conduct spot market simulations on the hydrogen backbone

The model determines the marginal production costs for hydrogen, electricity, and methane, based on the merit order¹ of the various production methods. The energy prices are then established based on the marginal costs of the highest-cost production unit that is required to meet the energy demand. The model heavily relies on data from future expectations² and incorporates over a hundred equations to determine a cost-optimal under the assumption of market equilibrium [11, 51].

The EYE Model

The EYE model is another model developed by TNO that functions as a simulation tool by combining agent-based modeling and Monte Carlo simulations [52]. This model is used by HyXchange to assess the impact of bid behavior and uncertainty in a hydrogen spot market.

¹The merit order ranks the various production methods (e.g., different types of power plants or production facilities) based on their marginal production costs, from the lowest to the highest.

²Including II2050 and IP2024.

In the EYE model, supply and demand are treated as exogenous parameters with predefined distributions, and hydrogen prices are determined using a clearing mechanism based on marginal pricing.

The HyWay 27 Model

The Hyway 27 model simulates the future allocation of hydrogen through the hydrogen backbone in the Netherlands. This model is part of a study on the hydrogen backbone conducted by Strategy& in collaboration with TNO.

The model simulates various supply-driven scenarios that track hydrogen flows through the backbone and into central storage in salt caverns. It features a network of hydrogen supply and demand hubs and a storage location connected by pipelines. Hydrogen transmission flows are driven by regional imbalances between supply and demand, and the need for hydrogen storage. However, supply, demand, and storage capacities are treated as exogenous variables, leading to a static view of hydrogen flows.

The Energy Transition Model

The Energy Transition Model (ETM) is an open-source³, interactive tool for energy system modeling. The ETM functions as both a design and scenario tool, allowing users to build and explore scenarios for the entire energy system, including hydrogen.

The ETM employs an input-output modeling approach, using input data and assumptions to calculate energy outcomes. It adopts a demand-driven framework, enabling users to manipulate demand inputs and observe how supply adjusts to meet these demands. The primary focus of the ETM is on scenario exploration and understanding the consequences of policy interventions, rather than explicitly determining energy prices for individual commodities like hydrogen.

B-2 Overview of General Energy Systems Modeling Approaches

B-2-1 An Overarching Classification Based on Discipline

Besides existing hydrogen market models, a broad field of energy systems modeling approaches can be used for modeling a marginal-cost-plus-pricing market for hydrogen.

The continuous evolution of energy systems makes energy systems modeling (ESM) an active area of research for a variety of modelers. Given the different academic backgrounds, objectives, and perspectives on energy systems, there is a diversity of established modeling approaches, each designed to analyze and simulate specific aspects of energy systems [53].

Numerous classifications have been introduced to categorize existing modeling approaches. The most prevalent classifications are based on analytical approach, time horizon, underlying methodology, modeling approach, and modeling field⁴.

³The ETM is developed by Quintel Intelligence in collaboration with Netherlands Environmental Assessment Agency (PBL). It can be accessed at <https://www.energytransitionmodel.com/>.

⁴See the classifications made by Grubb et al. (1993), Van Beeck (1999), Hourcade et al. (2006), and Subramanian et al. (2018) [54, 55, 56, 57].

While certain existing classifications of energy systems models acknowledge the distinction between economics and engineering, no classification explicitly differentiates these two disciplines. To provide a comprehensive overview of the ESM spectrum, we introduce an overarching classification that explicitly distinguishes between these two disciplines⁵, as presented in Table B-1.

The rest of this section walks through the different classifications and energy systems modeling approaches, reviewing their strengths and limitations in detail.

		Overarching Classification Based on Discipline	
		Economics	Engineering
Existing Classifications	Analytical approach	Top-down	Bottom-up
	Underlying methodology	Econometric, macroeconomic, and economic equilibrium	Simulation and optimization
	Modeling approach	Mathematical (statistical)	Computational, physical, and mathematical (mechanistic)
	Modeling field	Energy Economics	Process Systems Engineering

Table B-1: Classification of ESM approaches by overarching discipline and existing classifications

Analytical Approach

Both top-down and bottom-up models are commonly used in ESM and are extensively reviewed in the literature (e.g., [58, 53, 59, 56]). Top-down models, typically employed by economists, leverage macroeconomic theory and large-scale economic data, while bottom-up models, preferred by engineers, focus on detailed technological descriptions and specific energy technologies.

Top-down models provide an aggregate view of energy systems, emphasizing economic theory and historical data correlations. These models operate on the assumption that historical relationships among key variables remain constant, which can be restrictive in dynamic environments [58]. Their strength lies in the ability to incorporate macroeconomic feedback loops and broader economic impacts, including welfare and economic growth [58]. However, they often lack detailed technological specificity [58, 60].

Bottom-up models are grounded in detailed technical descriptions of energy system components and their interconnections, as highlighted in several reviews (e.g., [53, 59, 56]). These models excel in providing insights into energy supply and demand technologies. However, they face significant challenges related to data availability and computational intensity, particularly when modeling new or integrated energy systems [57, 58]. Furthermore, bottom-up models often neglect the interactions between market participants and do not account for how supply and demand dynamics drive energy prices.

⁵The classification based on time horizon is omitted in this distinction.

To overcome the limitations of both top-down and bottom-up approaches, hybrid models have been developed. These models aim to combine the macroeconomic scope of top-down models with the technological detail of bottom-up models, leveraging the strengths of both perspectives [58].

Underlying Methodology

Energy systems models can be constructed using various underlying methodologies, depending on the specific modeling objectives⁶ [55, 54, 59, 60]. These methodologies can be broadly categorized into econometric, macroeconomic, and equilibrium models on the economic side, and simulation and optimization models on the engineering side.

Econometric models rely on historical correlations between economic variables to forecast future trends in energy prices [53, 61, 56]. As a result, these models struggle in data-scarce scenarios or when historical correlations no longer hold, making them less suitable for rapidly changing or emerging markets like a hydrogen spot market.

Macroeconomic models employ macroeconomic theory to perform an aggregate analysis of energy systems. Similar to econometric models, these models determine prices based on trends while relying on extensive data, posing challenges in interpretation and application in data-scarce scenarios [53, 61, 56].

Economic equilibrium models, such as general equilibrium models, are employed to study energy system behavior in the long term, assuming they reach an equilibrium state. These models are limited in their ability to explicitly address out-of-equilibrium behavior and the dynamics leading to equilibrium [55, 62], making them inapplicable for modeling a volatile short-term spot market.

Simulation models, including differential equation models and agent-based models (ABMs), are commonly used by engineering using bottom-up approaches. ABMs, developed in response to the limitations of traditional bottom-up models, treat energy systems as multi-agent systems where individual agents' interactions are explicitly modeled [58, 63]. ABMs are particularly useful for modeling complex interactions within energy systems and are well-suited for modeling distributed systems that rely on decentralized decision-making [64].

Optimization models are also a prevalent engineering approach. These models seek to find the best allocation of resources under given constraints, making them valuable for planning and operational decision-making in energy systems. However, they can be computationally intensive and require detailed data on system components and constraints.

Modeling Approach

Energy systems models can be categorized into three primary classes based on their underlying methodologies: computational, mathematical, and physical modeling. Mathematical modeling is further divided into statistical (empirical or black-box) and mechanistic (first-principles or white-box) approaches [57, 61].

Computational modeling includes knowledge-based modeling, network-based modeling, and ABMs, all of which align with an engineering perspective [61]. These models are adept at handling complex systems and interactions by simulating the behavior of individual components and their interactions. However, their high computational intensity often limits the model's scope and

⁶For a detailed description of the different underlying methodologies see Van Beeck (1999) [55].

scalability, posing significant challenges when attempting to model large or highly detailed systems.

Statistical mathematical models, often linked with an economic approach, utilize methods such as regression and optimization to analyze input-output data [57]. These models heavily depend on data for both the model structure and the parameter identification. The primary challenge with statistical models is their lack of interpretability; they do not provide insights into the underlying processes of the system being modeled, making it difficult to understand the causal relationships within the energy system.

Mechanistic mathematical models are based on fundamental theories and principles to construct equations that real-world system behavior from an engineering perspective [57]. These models offer directly interpretable parameters and insights as the system phenomena are typically modeled using differential equations. While mechanistic models are ideal for their accuracy and interpretability, they require a comprehensive mathematical understanding of the system, which can be complex and sometimes infeasible. Furthermore, energy prices in these mechanistic models often follow from static look-up tables, see e.g. [65].

Physical modeling, though less prevalent in ESM, adopts an engineering approach by developing physical prototypes to describe the behavior of various energy system components. These models are typically used to model specific system components rather than entire systems due to their practical and complexity constraints.

Modeling Field

Energy systems are studied by researchers from different modeling fields, primarily within Process Systems Engineering (PSE) and Energy Economics (EE). This classification is introduced by Subramanian et. al. in [57]. Due to the theoretical underpinnings of the modeling fields, PSE models take an engineering approach, while EE models take an economic approach.

PSE models predominantly follow a mechanistic modeling approach, focusing primarily on the technological and physical aspects of energy systems. Often drawing inspiration from theories in chemical engineering, they provide detailed descriptions of individual technological components and processes. Economic variables, on the other hand, are usually treated as external inputs to the model.

EE models focus on the economic aspects of energy systems and are based on economic theories and principles. These models are based on fundamental economic laws, including supply, demand, and market equilibrium. Unlike PSE models, EE models incorporate economic variables endogenously, including equilibrium prices that are determined where the quantity of goods supplied equals the quantity demanded, i.e., the market clears [57]. However, this results in a static view of market equilibrium, lacking insights into the forces driving energy price fluctuations over time.

Time Horizon

Different energy systems models exist for various time horizons, often categorized by short- (day-to-day), medium- (months), and long-term (years). The modeling objective is often tied to the specific time horizon: long-term models assume economic equilibrium and short-term models focus on transitional or disequilibrium effects [55]. Integrating these timescales into a single framework remains a challenge [50, 59, 66, 67].

Spot Market Clearing Conditions

C-1 Core Network Simplification

Following the procedure from Hutter and Mendel in [5]. For a detailed explanation of the steps taken in the derivation, we refer to this paper.

Figure C-1 presents a graphical representation of the core model where the industry clusters are aggregated into one representative industrial demander. Here, we use generic agents as the focus lies on the topology. Also, active demanders and suppliers, consisting of a current source and an inductor, are reduced to a single agent. However, in this figure, we cannot visually indicate the meshes. Therefore, we translate the model into a vertical horizontal representation in Figure C-2.

In the figure, we indicate the agents (edges), exchange loci (nodes), and meshes respectively by \mathcal{E} (S,D,R, and C), \mathcal{N} , and \mathcal{M} . Using the topological structure, we construct the incidence matrix \mathbf{N} , the agent-mesh matrix \mathbf{M} , and the markets-mesh matrix \mathbf{T} in section C-2.

The storages receive their stock from exchange loci $\mathcal{N}_0^{\text{LH}_2}$, $\mathcal{N}_0^{\text{NG}}$, and $\mathcal{N}_0^{\text{H}_2}$.

$$\mathbf{v} = \mathbf{N}^t \boldsymbol{\phi} \tag{C-1}$$

C-1-1 Graphical Network Representation

Figure C-2 indicates the nodes \mathcal{N} , edges \mathcal{E} , and meshes \mathcal{M} we use these for the derivation of the market clearing conditions. Per market holds that $\mathcal{M} = \mathcal{E} - \mathcal{N} + 1$. With the physical clearing given by

$$\mathbf{N} \mathbf{f} = 0, \tag{C-2}$$

and the price clearing given by

$$\mathbf{M} \mathbf{v} = 0. \tag{C-3}$$

Where \mathbf{N} is the incidence matrix, \mathbf{M} the agent-mesh matrix, \mathbf{f} the vector containing all flows, and \mathbf{v} the vector containing all incentives.

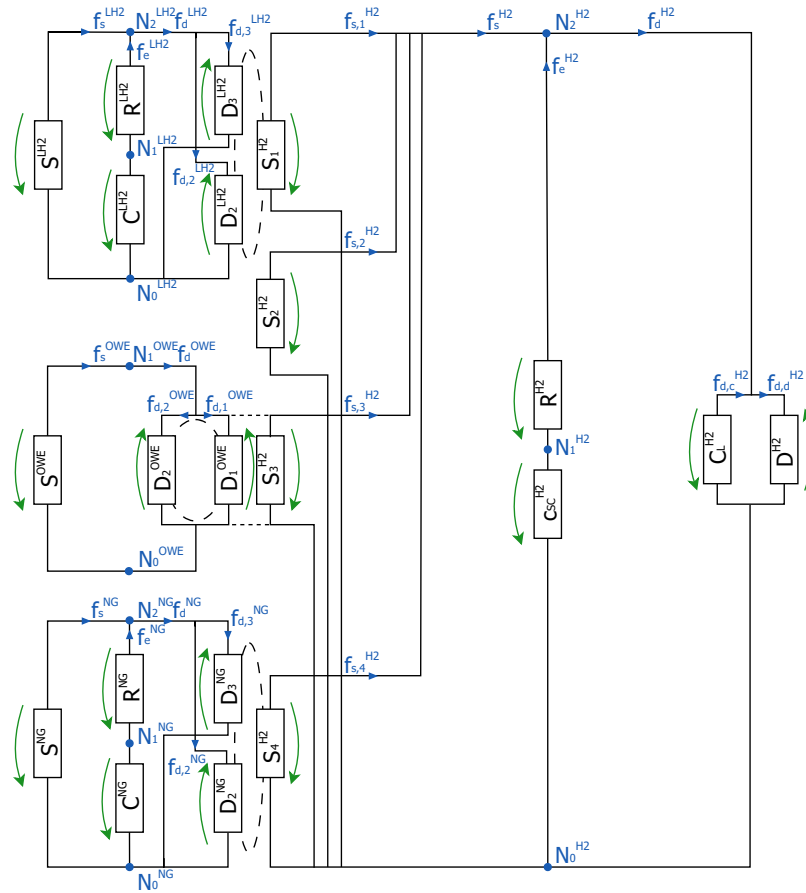


Figure C-1: Simplified representation of the core model

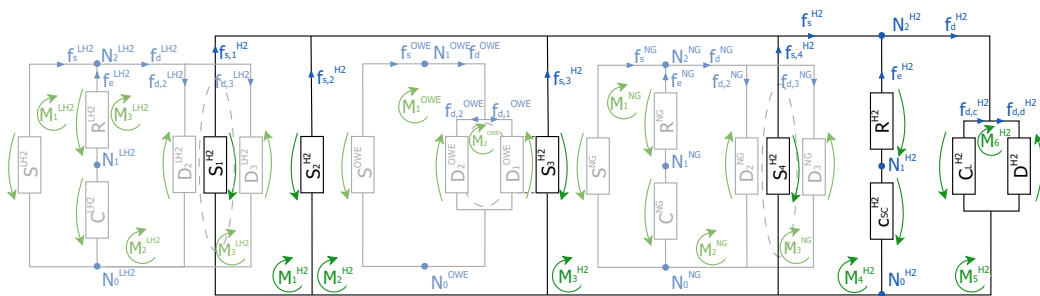


Figure C-2: Graphical network representation of the core model (horizontal) with the hydrogen market in black and the coupled markets in light gray.

C-2 Node, Mesh, and Market Matrices

We have 11 nodes \mathcal{N} , 21 edges \mathcal{E} , and 14 meshes \mathcal{M} that are given by

$$\begin{aligned} \mathcal{N} &\in \{\mathcal{N}_0^{\text{LH}_2}, \mathcal{N}_1^{\text{LH}_2}, \mathcal{N}_2^{\text{LH}_2}, \mathcal{N}_0^{\text{OWE}}, \mathcal{N}_1^{\text{OWE}}, \mathcal{N}_0^{\text{NG}}, \mathcal{N}_1^{\text{NG}}, \mathcal{N}_2^{\text{NG}}, \mathcal{N}_0^{\text{H}_2}, \mathcal{N}_1^{\text{H}_2}, \mathcal{N}_2^{\text{H}_2}\}, \\ \mathcal{E} &\in \{\mathcal{S}^{\text{LH}_2}, \mathcal{C}^{\text{LH}_2}, \mathcal{R}^{\text{LH}_2}, \mathcal{D}_2^{\text{LH}_2}, \mathcal{D}_3^{\text{LH}_2}, \mathcal{S}^{\text{OWE}}, \mathcal{D}_1^{\text{OWE}}, \mathcal{D}_2^{\text{OWE}}, \mathcal{S}^{\text{NG}}, \mathcal{C}^{\text{NG}}, \mathcal{R}^{\text{NG}}, \mathcal{D}_2^{\text{NG}}, \mathcal{D}_3^{\text{NG}}, \mathcal{S}_1^{\text{H}_2}, \mathcal{S}_2^{\text{H}_2}, \mathcal{S}_3^{\text{H}_2}, \mathcal{S}_4^{\text{H}_2}, \mathcal{C}_{CS}^{\text{H}_2}, \mathcal{R}^{\text{H}_2}, \mathcal{C}_L^{\text{H}_2}, \mathcal{D}^{\text{H}_2}\}, \text{ and} \\ \mathcal{M} &\in \{\mathcal{M}_1^{\text{LH}_2}, \mathcal{M}_2^{\text{LH}_2}, \mathcal{M}_3^{\text{LH}_2}, \mathcal{M}_1^{\text{OWE}}, \mathcal{M}_2^{\text{OWE}}, \mathcal{M}_1^{\text{NG}}, \mathcal{M}_2^{\text{NG}}, \mathcal{M}_3^{\text{NG}}, \mathcal{M}_1^{\text{H}_2}, \mathcal{M}_2^{\text{H}_2}, \mathcal{M}_3^{\text{H}_2}, \mathcal{M}_4^{\text{H}_2}, \mathcal{M}_5^{\text{H}_2}, \mathcal{M}_6^{\text{H}_2}\}. \end{aligned} \quad (\text{C-4})$$

The incidence matrix \mathbf{N} and the agent-mesh matrix \mathbf{M} are given on the next page. These two matrices keep track of the flows and incentives within the network. With the agent-mesh matrix, we can derive the market-mesh matrix \mathbf{T} . With this matrix, we can check the number of markets through the number of submatrices, the number of agents in each mesh through the diagonal entries in each submatrix, and the shared agents between two corresponding meshes through the off-diagonal entries.

The entries in the incidence matrix \mathbf{N} are

$$\mathbf{N}_{ij} = \begin{cases} 1 & \text{if } \mathcal{E}_j \text{ provides commodities to } \mathcal{N}_i \\ -1 & \text{if } \mathcal{E}_j \text{ receives commodities from } \mathcal{N}_i \\ 0 & \text{if } \mathcal{E}_j \text{ is not incident to } \mathcal{N}_i, \end{cases} \quad (\text{C-5})$$

where $i \in \{1, \dots, \mathcal{N}\}$ for \mathcal{N} exchange loci and $j \in \{1, \dots, \mathcal{E}\}$ for \mathcal{E} agents.

And the entries in the agent-mesh matrix \mathbf{M} are

$$\mathbf{M}_{kj} = \begin{cases} 1 & \text{if } \mathcal{E}_j \text{ is in } \mathcal{M}_k \text{ and directions agree} \\ -1 & \text{if } \mathcal{E}_j \text{ is in } \mathcal{M}_k \text{ and directions disagree} \\ 0 & \text{if } \mathcal{E}_j \text{ is not part of } \mathcal{M}_k, \end{cases} \quad (\text{C-6})$$

where $k \in \{1, \dots, \mathcal{M}\}$ for \mathcal{M} meshes.

The market-mesh matrix is determined by $\mathbf{T} = \mathbf{M}\mathbf{M}^T$ and is presented by the following matrix.

$$\mathbf{T} = \begin{matrix} & \mathcal{M}_1^{\text{LH}_2} & \mathcal{M}_2^{\text{LH}_2} & \mathcal{M}_3^{\text{LH}_2} & \mathcal{M}_1^{\text{OWE}} & \mathcal{M}_2^{\text{OWE}} & \mathcal{M}_1^{\text{NG}} & \mathcal{M}_2^{\text{NG}} & \mathcal{M}_3^{\text{NG}} & \mathcal{M}_1^{\text{H}_2} & \mathcal{M}_2^{\text{H}_2} & \mathcal{M}_3^{\text{H}_2} & \mathcal{M}_4^{\text{H}_2} & \mathcal{M}_5^{\text{H}_2} & \mathcal{M}_6^{\text{H}_2} \\ \mathcal{M}_1^{\text{LH}_2} & \left(\begin{array}{cccccccccccccccc} 3 & -2 & -2 & \vdots & 0 & 0 & \vdots & 0 & 0 & \vdots & 0 & 0 & 0 & 0 & 0 \\ -2 & 3 & -1 & \vdots & 0 & 0 & \vdots & 0 & 0 & \vdots & 0 & 0 & 0 & 0 & 0 \\ -2 & -1 & 2 & \vdots & 0 & 0 & \vdots & 0 & 0 & \vdots & 0 & 0 & 0 & 0 & 0 \\ \hdashline 0 & 0 & 0 & \vdots & 2 & -1 & \vdots & 0 & 0 & \vdots & 0 & 0 & 0 & 0 & 0 \\ 0 & 0 & 0 & \vdots & -1 & 2 & \vdots & 0 & 0 & \vdots & 0 & 0 & 0 & 0 & 0 \\ \hdashline 0 & 0 & 0 & \vdots & 0 & 0 & \vdots & 3 & -2 & \vdots & 0 & 0 & 0 & 0 & 0 \\ 0 & 0 & 0 & \vdots & 0 & 0 & \vdots & -2 & 3 & \vdots & 0 & 0 & 0 & 0 & 0 \\ 0 & 0 & 0 & \vdots & 0 & 0 & \vdots & -2 & -1 & \vdots & 0 & 0 & 0 & 0 & 0 \\ \hdashline 0 & 0 & 0 & \vdots & 0 & 0 & \vdots & 0 & 0 & \vdots & 2 & -1 & 0 & 0 & 0 \\ 0 & 0 & 0 & \vdots & 0 & 0 & \vdots & 0 & 0 & \vdots & -1 & 2 & -1 & 0 & 0 \\ 0 & 0 & 0 & \vdots & 0 & 0 & \vdots & 0 & 0 & \vdots & 0 & -1 & 2 & -1 & 0 \\ 0 & 0 & 0 & \vdots & 0 & 0 & \vdots & 0 & 0 & \vdots & 0 & 0 & -1 & 3 & -2 \\ 0 & 0 & 0 & \vdots & 0 & 0 & \vdots & 0 & 0 & \vdots & 0 & 0 & 0 & -2 & 3 \\ 0 & 0 & 0 & \vdots & 0 & 0 & \vdots & 0 & 0 & \vdots & 0 & 0 & 0 & -1 & 2 \end{array} \right) \end{matrix}$$

We observe that there are four submatrices, indicating four markets. This indeed aligns with the model shown in Figure C-2.

C-3 Clearing Conditions for Spot Prices and Energy Flows

To obtain the physical clearing conditions, we multiply the incidence matrix with the flow vector ($\mathbf{N}\mathbf{f} = 0$). Where the flows are measured through each edge.

$$\begin{aligned}\mathbf{f} &= (f_1, \dots, f_{\mathcal{E}})^T, \\ &= (f_{S^{\text{LH}_2}}, f_{C^{\text{LH}_2}}, f_{\mathcal{R}^{\text{LH}_2}}, f_{D_2^{\text{LH}_2}}, f_{D_3^{\text{LH}_2}}, f_{S^{\text{OWE}}}, f_{D_1^{\text{OWE}}}, f_{D_2^{\text{OWE}}}, f_{S^{\text{NG}}}, f_{C^{\text{NG}}}, f_{\mathcal{R}^{\text{NG}}}, f_{D_2^{\text{NG}}}, f_{D_3^{\text{NG}}}, f_{S_1^{\text{H}_2}}, f_{S_2^{\text{H}_2}}, f_{S_3^{\text{H}_2}}, f_{S_4^{\text{H}_2}}, f_{C_{CS}^{\text{H}_2}}, f_{\mathcal{R}^{\text{H}_2}}, f_{C_L^{\text{H}_2}}, f_{D^{\text{H}_2}})^T \\ &= (f_s^{\text{LH}_2}, f_e^{\text{LH}_2}, f_e^{\text{LH}_2}, f_{d,2}^{\text{LH}_2}, f_{d,3}^{\text{LH}_2}, f_s^{\text{OWE}}, f_{d,1}^{\text{OWE}}, f_{d,2}^{\text{OWE}}, f_s^{\text{NG}}, f_e^{\text{NG}}, f_e^{\text{NG}}, f_{d,2}^{\text{NG}}, f_{d,3}^{\text{NG}}, f_{s,1}^{\text{H}_2}, f_{s,2}^{\text{H}_2}, f_{s,3}^{\text{H}_2}, f_{s,4}^{\text{H}_2}, f_e^{\text{H}_2}, f_e^{\text{H}_2}, f_{d,c}^{\text{H}_2}, f_{d,d}^{\text{H}_2})^T\end{aligned}\quad (\text{C-7})$$

To obtain the price clearing condition $\mathbf{M}\mathbf{v} = 0$, we first need to determine the incentives vector \mathbf{v} . This vector is obtained through

$$\mathbf{v} = \mathbf{N}^T \boldsymbol{\phi}.\quad (\text{C-8})$$

Where $\boldsymbol{\phi}$ is the desirability vector. The desirability levels ϕ are measured at the nodes \mathcal{N} while the incentives v are measured over the edges \mathcal{E} . This is shown in Figure C-3.

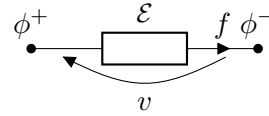


Figure C-3: Sign convention: an incentive v measures the desirability drop ($\phi^+ - \phi^-$) across a passive agent \mathcal{E} .

We obtain the following vectors for the desirabilities $\boldsymbol{\phi}$ and incentives \mathbf{v} .

$$\begin{aligned}\boldsymbol{\phi} &= (\phi_1, \dots, \phi_{\mathcal{N}})^T \\ &= (\phi_{\mathcal{N}_0}^{\text{LH}_2}, \phi_{\mathcal{N}_1}^{\text{LH}_2}, \phi_{\mathcal{N}_2}^{\text{LH}_2}, \phi_{\mathcal{N}_0}^{\text{OWE}}, \phi_{\mathcal{N}_1}^{\text{OWE}}, \phi_{\mathcal{N}_0}^{\text{NG}}, \phi_{\mathcal{N}_1}^{\text{NG}}, \phi_{\mathcal{N}_2}^{\text{NG}}, \phi_{\mathcal{N}_0}^{\text{H}_2}, \phi_{\mathcal{N}_1}^{\text{H}_2}, \phi_{\mathcal{N}_2}^{\text{H}_2})^T\end{aligned}\quad (\text{C-9})$$

$$\begin{aligned}\mathbf{v} &= (v_1, \dots, v_{\mathcal{E}})^T \\ &= (v_{S^{\text{LH}_2}}, v_{C^{\text{LH}_2}}, v_{\mathcal{R}^{\text{LH}_2}}, v_{D_2^{\text{LH}_2}}, v_{D_3^{\text{LH}_2}}, v_{S^{\text{OWE}}}, v_{D_1^{\text{OWE}}}, v_{D_2^{\text{OWE}}}, v_{S^{\text{NG}}}, v_{C^{\text{NG}}}, v_{\mathcal{R}^{\text{NG}}}, v_{D_2^{\text{NG}}}, v_{D_3^{\text{NG}}}, v_{S_1^{\text{H}_2}}, v_{S_2^{\text{H}_2}}, v_{S_3^{\text{H}_2}}, v_{S_4^{\text{H}_2}}, v_{C_{CS}^{\text{H}_2}}, v_{\mathcal{R}^{\text{H}_2}}, v_{C_L^{\text{H}_2}}, v_{D^{\text{H}_2}})^T\end{aligned}\quad (\text{C-10})$$

From the physical clearing and the price-clearing laws, we obtain the following sets of equations.

$$\mathbf{Nf} = \begin{pmatrix} f_{d,2}^{\text{LH}_2} - f_e^{\text{LH}_2} - f_s^{\text{LH}_2} + f_{d,3}^{\text{LH}_2} \\ f_e^{\text{LH}_2} - f_e^{\text{LH}_2} \\ f_s^{\text{LH}_2} + f_e^{\text{LH}_2} - f_{d,2}^{\text{LH}_2} - f_{d,3}^{\text{LH}_2} \\ \dots \\ f_{d,1}^{\text{OWE}} - f_s^{\text{OWE}} - f_{d,2}^{\text{OWE}} \\ f_s^{\text{OWE}} - f_{d,1}^{\text{OWE}} - f_{d,2}^{\text{OWE}} \\ \dots \\ f_{d,2}^{\text{NG}} - f_e^{\text{NG}} - f_s^{\text{NG}} + f_{d,3}^{\text{NG}} \\ f_e^{\text{NG}} - f_e^{\text{NG}} \\ f_s^{\text{NG}} + f_e^{\text{NG}} - f_{d,2}^{\text{NG}} - f_{d,3}^{\text{NG}} \\ \dots \\ f_{d,d}^{\text{H}_2} - f_{d,c}^{\text{H}_2} - f_{s,1}^{\text{H}_2} - f_{s,2}^{\text{H}_2} - f_{s,3}^{\text{H}_2} - f_{s,4}^{\text{H}_2} - f_e^{\text{H}_2} \\ f_e^{\text{H}_2} - f_e^{\text{H}_2} \\ f_{s,1}^{\text{H}_2} + f_{s,2}^{\text{H}_2} + f_{s,3}^{\text{H}_2} + f_{s,4}^{\text{H}_2} + f_e^{\text{H}_2} + f_{d,c}^{\text{H}_2} - f_{d,d}^{\text{H}_2} \end{pmatrix} = \begin{pmatrix} 0 \\ 0 \\ 0 \\ \dots \\ 0 \\ 0 \\ 0 \\ \dots \\ 0 \\ 0 \\ 0 \\ \dots \\ 0 \\ 0 \end{pmatrix}, \quad \text{and} \quad \mathbf{Mv} = \begin{pmatrix} -v_{\mathcal{S}^{\text{LH}_2}} + v_{\mathcal{C}^{\text{LH}_2}} + v_{\mathcal{R}^{\text{LH}_2}} \\ -v_{\mathcal{C}^{\text{LH}_2}} - v_{\mathcal{R}^{\text{LH}_2}} - v_{\mathcal{D}_2^{\text{LH}_2}} \\ v_{\mathcal{D}_2^{\text{LH}_2}} - v_{\mathcal{D}_3^{\text{LH}_2}} \\ \dots \\ -v_{\mathcal{S}^{\text{OWE}}} - v_{\mathcal{D}_2^{\text{OWE}}} \\ -v_{\mathcal{D}_1^{\text{OWE}}} + v_{\mathcal{D}_2^{\text{OWE}}} \\ \dots \\ -v_{\mathcal{S}^{\text{NG}}} + v_{\mathcal{C}^{\text{NG}}} + v_{\mathcal{R}^{\text{NG}}} \\ -v_{\mathcal{C}^{\text{NG}}} + -v_{\mathcal{R}^{\text{NG}}} - v_{\mathcal{D}_2^{\text{NG}}} \\ v_{\mathcal{D}_2^{\text{NG}}} - v_{\mathcal{D}_3^{\text{NG}}} \\ \dots \\ -v_{\mathcal{S}_1^{\text{H}_2}} + v_{\mathcal{S}_2^{\text{H}_2}} \\ -v_{\mathcal{S}_2^{\text{H}_2}} + v_{\mathcal{S}_3^{\text{H}_2}} \\ -v_{\mathcal{S}_3^{\text{H}_2}} + v_{\mathcal{S}_4^{\text{H}_2}} \\ -v_{\mathcal{S}_4^{\text{H}_2}} + v_{\mathcal{C}_{CS}^{\text{H}_2}} + v_{\mathcal{R}^{\text{H}_2}} \\ -v_{\mathcal{C}_{CS}^{\text{H}_2}} - v_{\mathcal{R}^{\text{H}_2}} + v_{\mathcal{C}_L^{\text{H}_2}} \\ -v_{\mathcal{C}_L^{\text{H}_2}} - v_{\mathcal{D}^{\text{H}_2}} \end{pmatrix} = \begin{pmatrix} 0 \\ 0 \\ 0 \\ \dots \\ 0 \\ 0 \\ 0 \\ \dots \\ 0 \\ 0 \\ 0 \\ \dots \\ 0 \\ 0 \end{pmatrix}.$$

We can reduce the equations to one physical and one price-clearing condition per market. This leaves us with the following two sets of equations. Respectively describing the liquid hydrogen (LH₂) market, offshore wind energy (OWE) market, natural gas (NG) market, and hydrogen (H₂) market

$$\text{Physical clearing : } \begin{cases} f_e^{\text{LH}_2} = f_{d,2}^{\text{LH}_2} + f_{d,3}^{\text{LH}_2} - f_s^{\text{LH}_2} \\ f_s^{\text{OWE}} = f_{d,1}^{\text{OWE}} + f_{d,2}^{\text{OWE}} \\ f_e^{\text{NG}} = f_{d,2}^{\text{NG}} + f_{d,3}^{\text{NG}} - f_s^{\text{NG}} \\ f_e^{\text{H}_2} = f_{d,d}^{\text{H}_2} - f_{s,1}^{\text{H}_2} - f_{s,2}^{\text{H}_2} - f_{s,3}^{\text{H}_2} - f_{s,4}^{\text{H}_2} - f_{d,c}^{\text{H}_2} \end{cases} \quad (\text{C-11})$$

$$\text{Price clearing : } \begin{cases} v_{\mathcal{S}^{\text{LH}_2}} = v_{\mathcal{C}^{\text{LH}_2}} + v_{\mathcal{R}^{\text{LH}_2}} = -v_{\mathcal{D}_2^{\text{LH}_2}} = -v_{\mathcal{D}_3^{\text{LH}_2}} \\ v_{\mathcal{S}^{\text{OWE}}} = -v_{\mathcal{D}_1^{\text{OWE}}} = -v_{\mathcal{D}_2^{\text{OWE}}} \\ v_{\mathcal{S}^{\text{NG}}} = v_{\mathcal{C}^{\text{NG}}} + v_{\mathcal{R}^{\text{NG}}} = -v_{\mathcal{D}_2^{\text{NG}}} = -v_{\mathcal{D}_3^{\text{NG}}} \\ v_{\mathcal{S}_1^{\text{H}_2}} = v_{\mathcal{S}_2^{\text{H}_2}} = v_{\mathcal{S}_3^{\text{H}_2}} = v_{\mathcal{S}_4^{\text{H}_2}} = v_{\mathcal{C}_{CS}^{\text{H}_2}} + v_{\mathcal{R}^{\text{H}_2}} = v_{\mathcal{C}_L^{\text{H}_2}} = -v_{\mathcal{D}^{\text{H}_2}} \end{cases} \quad (\text{C-12})$$

For the LH₂, natural gas and hydrogen market, we have derived that in these markets hold that $v_{\mathcal{S}} = v_{\mathcal{C}} + v_{\mathcal{R}} = -v_{\mathcal{D}}$. Following the behavioral laws of the storage and the friction, as listed in Table 3-2, we know that we can express the incentives over those elements in terms of the excess flow $f_e = f_d - f_s$. We can relate the excess flows in the markets to the markets' price levels.

The offshore wind energy market does not have an excess flow, there the price dynamics are fully determined by wind variability. This is detailed in subsection 4-3-2.

Appendix D

Modeling Offshore Wind Distribution

D-1 Average Yearly and Daily Wind Distributions

Renewable hydrogen production is determined by offshore wind energy generation. As the generation is weather-dependent, it varies throughout the year and slightly throughout the day. We can approximate offshore wind energy generation using yearly averages.

In such a case, we assume perfect foresight of the wind distribution. We use average yearly and daily wind distributions to determine the amount of generated offshore wind energy. The distributions are determined with data from TNO, obtained from [68]. The distributions come from annual wind speed (m/s) monthly averages at 116 m height¹ (the yellow dots in Figure D-1), which are determined with data from 2016 to 2020.

Recognizing the sinusoidal behavior of both distributions, the yearly and daily wind distributions are fitted as fifth and third order Fourier series² respectively as shown in Figure D-1. This gives us a periodic approximation of the wind distributions. Although the generated power is also influenced by the the wind-direction, this is not taken into account here.

D-2 Measured Wind Distribution

To model a real-world scenario we use measured wind data. The offshore data of hourly wind averages is retrieved from the Dutch KNMI³.

¹Slightly above the hub height (approximately 105 m) of the Vestas V164-9.5 turbine.

²A Fourier series describes a periodic function as a sum of sine and cosine functions.

³Downloaded from 'KNMI - Uurgegevens van Noordzee stations': https://www.knmi.nl/nederland-nu/klimatologie/uurgegevens_Noordzee.

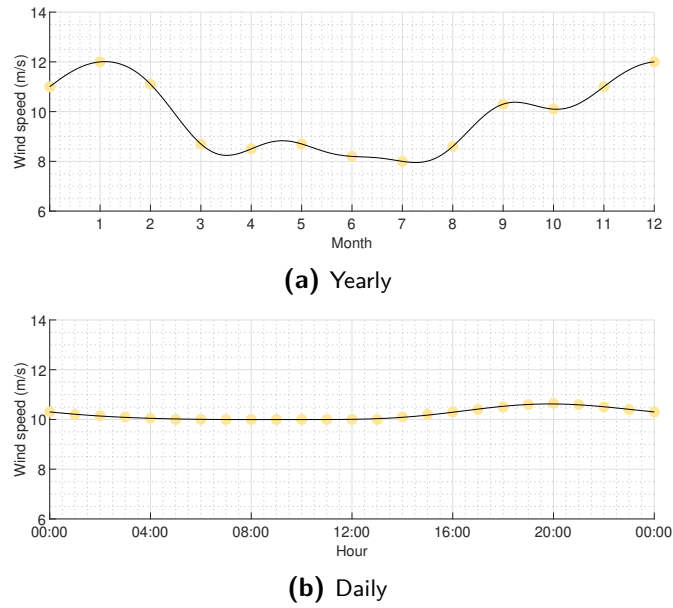


Figure D-1: Wind distribution in the Netherlands. Source: TNO (2021) [68]

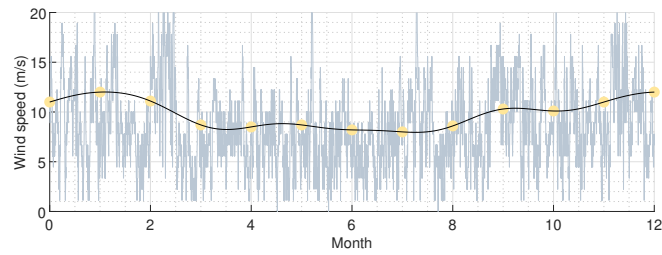


Figure D-2: Deterministic wind distribution, shown by the blue curve, compared to the average wind distribution, as shown by the black curve with yellow dots

Data is used from Station 320 - Lichteiland Goeree for the year 2019. Lichtplatform Goeree lies 30 km offshore and measures the wind speed at 30m. As wind speed is a function of height, we can determine the wind speed at the desired 116m:

$$v_2 = v_1 \frac{\ln\left(\frac{h_2}{z_0}\right)}{\ln\left(\frac{h_1}{z_0}\right)} \quad (\text{D-1})$$

where wind speed v_1 is measured at height $h_1 = 30\text{m}$, v_2 is the wind speed at height $h_2 = 116\text{m}$, and the roughness length⁴ is given by $z_0 = 0.0002\text{m}$. This gives us a scaling factor of approximately 1.1135.

⁴This parameter which represent the roughness of the landscape.

Appendix E

System Identification

E-1 Identification Method

The system identification has turned out to be a very delicate issue. For the tuning of the parameters, we build on the hydrogen market analysis in Appendix A. The parameters are tuned such that they stabilize in the long run.

The identification is an iterative process of tuning and reflecting on the system behavior. We make sure the energy flows in the network are in line with the expected energy flows via the various supply chains and to the five industry clusters. The flow of incentives is calibrated using data from TNO.

Note that the parameters are provided in line with its usage in MATLAB. The price elasticity ε is given as the inverse of the inductance parameter (or price-inelasticity) according to $\varepsilon = 1/L$. The storage inelasticity k is given as the inverse of the capacitance parameter (or storage elasticity) according to $k = 1/C$. The market friction parameter b is equal to the resistance parameter R .

E-2 Core Network

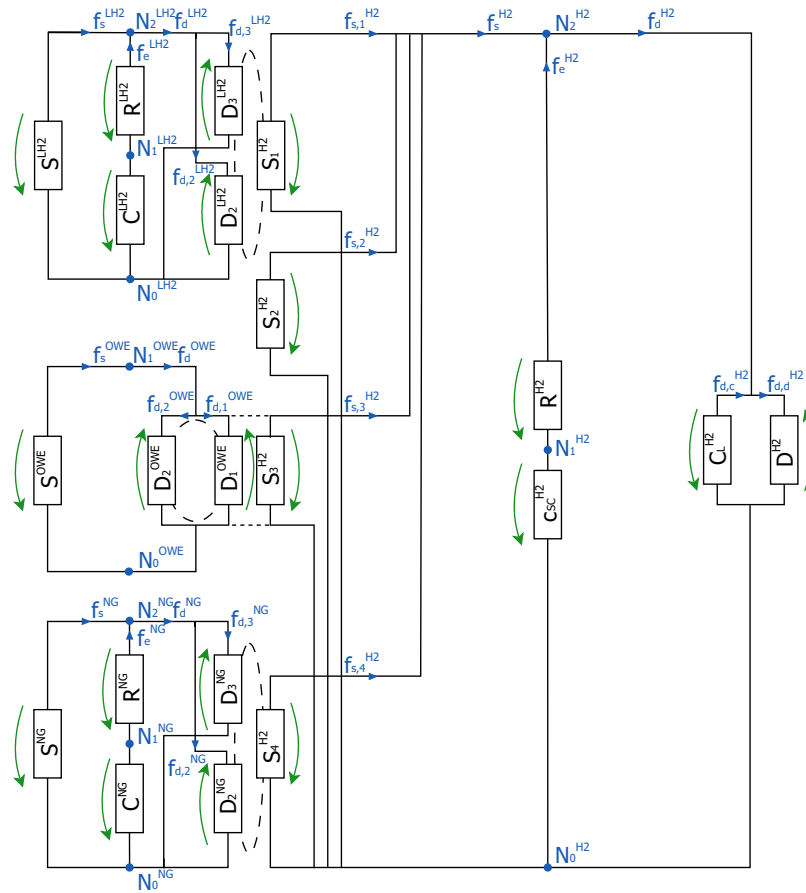


Figure E-1: Simplified representation of the core model

E-2-1 Hydrogen Supply Chains

Gaseous Hydrogen Import by Pipeline

	Agent		Parameter	Value
$\mathcal{S}_2^{\text{H}_2}$	Import agent	$L_2^{\text{H}_2}$	Price-inelasticity	0.025

Table E-1: Parameter value belonging to the gaseous hydrogen import

The Renewable Hydrogen Supply Chain

To find the right values for L_1^{OWE} , L_2^{OWE} and k^{OWE} , we look at the running utility of the operator given by

$$U(f_1^{\text{OWE}}, f_2^{\text{OWE}}) = -\frac{1}{2}L_1^{\text{OWE}}(u_1^{\text{OWE}} - f_1^{\text{OWE}})^2 - M^{\text{OWE}}(u_1^{\text{OWE}} - f_1^{\text{OWE}})(u_2^{\text{OWE}} - f_2^{\text{OWE}}) - \frac{1}{2}L_2^{\text{OWE}}(u_2^{\text{OWE}} - f_2^{\text{OWE}})^2. \quad (\text{E-1})$$

Where the terms containing L_1^{OWE} and L_2^{OWE} represent the utility obtained from selling each good separately and the term containing M^{OWE} represents the utility from selling the two goods together. The selling strategy can be translated into a concave preference of the two possibilities [13]. When the price is low, the operator prefers to sell hydrogen and when the hydrogen price is high the operator prefers to sell electricity. He can sell both at the same time, however, this is less preferable as one of the two strategies will result in more profits. For this preference, we know that $(M^{\text{OWE}})^2 < L_1^{\text{OWE}}L_2^{\text{OWE}}$.

To obtain the negative correlation between two possibilities as described above, M^{OWE} is bounded¹ by

$$\min(L_1^{\text{OWE}}, L_2^{\text{OWE}}) < M^{\text{OWE}} < \sqrt{L_1^{\text{OWE}}L_2^{\text{OWE}}}, \quad (\text{E-2})$$

and² thus $\frac{\min(L_1^{\text{OWE}}, L_2^{\text{OWE}})}{\sqrt{L_1^{\text{OWE}}L_2^{\text{OWE}}}} < k^{\text{OWE}} < 1$.

The primary goal of the operator is to produce hydrogen, therefore $u_1^{\text{OWE}} > u_2^{\text{OWE}}$. However, the production is more price-elastic compared to selling electricity, and thus $L_1^{\text{OWE}} < L_2^{\text{OWE}}$.

The elasticity matrix indeed shows the negative cross-correlation $\varepsilon_{12}^{\text{OWE}}$:

$$\begin{pmatrix} \varepsilon_{11}^{\text{OWE}} & \varepsilon_{12}^{\text{OWE}} \\ \varepsilon_{12}^{\text{OWE}} & \varepsilon_{22}^{\text{OWE}} \end{pmatrix} = \begin{pmatrix} L_1^{\text{OWE}} & k\sqrt{L_1^{\text{OWE}}L_2^{\text{OWE}}} \\ k^{\text{OWE}}\sqrt{L_1^{\text{OWE}}L_2^{\text{OWE}}} & L_2^{\text{OWE}} \end{pmatrix}^{-1} = \begin{pmatrix} 24.0240 & 15.8176 \\ 15.8176 & 14.4144 \end{pmatrix}. \quad (\text{E-3})$$

¹When $k = \frac{\min(L_1, L_2)}{\sqrt{L_1 L_2}}$, the demand d_j , with j corresponding to $L_j = \max(L_1, L_2)$, remains constant.

When $k < \frac{\min(L_1, L_2)}{\sqrt{L_1 L_2}}$, you obtain a positive correlation between d_1 and d_2 .

²This can be deduced by filling $M^{\text{OWE}} = k^{\text{OWE}}\sqrt{L_1^{\text{OWE}}L_2^{\text{OWE}}}$ into Equation (E-3) and stating that $p_1^{\text{OWE}} = p_2^{\text{OWE}} = p^{\text{OWE}}$. One can also note that when $u_1^{\text{OWE}} = u_2^{\text{OWE}} = 0$ and $L_1^{\text{OWE}} = L_2^{\text{OWE}}$, it follows that $d_1^{\text{OWE}} = d_2^{\text{OWE}}$ ($= f_1^{\text{OWE}} = f_2^{\text{OWE}}$).

	Agent		Parameter	Value
$\mathcal{S}_3^{\text{H}_2}$	Electrolysis plant	c^{OWE}	Electrolyser efficiency	0.8
$\mathcal{D}_1^{\text{OWE}}$	Demander	L_1^{OWE}	Price-inelasticity	0.15
		u_1^{OWE}	Inelastic demand	0.16
$\mathcal{D}_2^{\text{OWE}}$	Demander	L_2^{OWE}	Price-inelasticity	0.25
		u_2^{OWE}	Inelastic demand	0.05
		k^{OWE}	Coupling coefficient	-0.85

Table E-2: Parameter values belonging to the offshore wind energy (OWE) market

This is in line that the two forms of demand are substitutes of each other.

As the efficiency associated with electrolysis is assumed to reach 80%, the current gain c^{OWE} of the current controlled current source is set to 0.8.

The Low-Carbon Hydrogen Supply Chain

The identification of the three-winding mutual inductor parameters involves an iterative process that combines geometric analysis and optimization. Levenberg-Marquardt optimization is employed due to the non-square system formed by equations E-4 and E-5.

However, integrating it into an electrical circuit, particularly within Simscape, poses challenges due to built-in constraints.

In this equation, the commodity flows are positive when they align with the direction indicated by the arrows. This is the case when the flows enter into the positive node of their respective inductor terminal, indicated with the dot³ in Figure 4-7. However, the values of f_2^{NG} and f_3^{NG} can be either positive or negative, depending on the market prices.

For $s_4^{\text{H}_2}$ to be approximately equal to $0.9d_2^{\text{NG}}$, such that it reflects the production process, the flows should react exactly the same to price differences in the two markets (the steam methane reforming (SMR) production agents adjust its demand for natural gas and hydrogen production proportionally. For $s_4^{\text{H}_2}$ and d_2^{NG} to react the same on p^{NG} and p^{H_2} (for now assuming $u_2^{\text{NG}} = 0$), we find that both the Equations E-4 and E-5 should.

$$\frac{1 - (k_{23}^{\text{NG}})^2}{L_1^{\text{NG}}} = -\frac{k_{23}^{\text{NG}}k_{13}^{\text{NG}} - k_{12}^{\text{NG}}}{\sqrt{L_1^{\text{NG}}L_2^{\text{NG}}}} \quad (\text{E-4})$$

$$\frac{k_{23}^{\text{NG}}k_{13}^{\text{NG}} - k_{12}^{\text{NG}}}{\sqrt{L_1^{\text{NG}}L_2^{\text{NG}}}} + \frac{k_{12}^{\text{NG}}k_{23}^{\text{NG}} - k_{13}^{\text{NG}}}{\sqrt{L_1^{\text{NG}}L_3^{\text{NG}}}} = -\left(\frac{1 - (k_{13}^{\text{NG}})^2}{L_2^{\text{NG}}} + \frac{k_{12}^{\text{NG}}k_{13}^{\text{NG}} - k_{23}^{\text{NG}}}{\sqrt{L_2^{\text{NG}}L_3^{\text{NG}}}}\right) \quad (\text{E-5})$$

³The application of the dot convention in mutual inductance dictates the sign of the mutual inductances, denoted as M_{ij} : when all currents either enter or exit at the dot, the mutual inductances are considered positive. In contrast, if there's a mix of currents entering and leaving at the dot, the mutual inductances become negative.

To cope with the production losses, we use u_2^{NG} to move d_2^{NG} upwards such that $s_4^{\text{H}_2} \approx 0.9d_2^{\text{NG}}$. As the $d_2^{\text{NG}} \ll d_3^{\text{NG}}$ this does not affect the kinematics too much. However, note that by doing this, d_2^{NG} flows into the negative direction and thus flows into the inductor in the negative node. We can interpret this as that the natural gas demand by the SMR agent acts more like a supplier and therefore differs from the standard demander as defined by Hutter (2023) in [5].

The sinusoidal current source u_3 is described by the function listed in Table E-4 such that it mimics the natural gas demand throughout the year.

	Agent	Parameter	Value
\mathcal{S}^{NG}	Supplier	L_s^{NG}	Price-inelasticity 0.0045
		w^{NG}	Inelastic supply 0.4
\mathcal{R}^{NG}	Market operator	R^{NG}	Market friction 0.025
\mathcal{C}^{NG}	Storage	C^{NG}	Storage elasticity 250
$\mathcal{S}_4^{\text{H}_2}$	SMR plant	$L_1^{\text{H}_2}$	Price-inelasticity 0.28
$\mathcal{D}_2^{\text{NG}}$	Demander	L_2^{NG}	Price-inelasticity 0.2931
		u_2^{NG}	Inelastic demand 0.02
$\mathcal{D}_3^{\text{NG}}$	Demander	L_3^{NG}	Price-inelasticity 0.19135
		$u_3^{\text{NG}}(t)$	Seasonal demand 0.5 $+0.08e^{-(t-\frac{365}{4})} \sin(\frac{2\pi}{365}(t - \frac{365}{4}))$
		k_{12}^{NG}	Coupling coefficient 0.965
		k_{13}^{NG}	Coupling coefficient -0.3062
		k_{23}^{NG}	Coupling coefficient -0.2228

Table E-3: Parameter values belonging to the (LH2)-(H2) supply chain

Checking the resulting elasticity matrix, we indeed observe a positive correlation between natural gas demand for hydrogen production and hydrogen supply, aligning with the idea that these two commodities act as complements. The cross-correlations $\varepsilon_{23}^{\text{NG}}$ and $\varepsilon_{13}^{\text{H}_2/\text{NG}}$ are both negative. The former denotes the two types of natural gas demand as substitutes, while the latter illustrates that the relationship where the supply of hydrogen and the general demand for natural are also perceived as substitutes. This aligns with the expected relationships between the three different flows.

$$\begin{aligned}
 \begin{pmatrix} \varepsilon_1^{\text{H}_2} & \varepsilon_{12}^{\text{H}_2/\text{NG}} & \varepsilon_{13}^{\text{H}_2/\text{NG}} \\ \varepsilon_{12}^{\text{H}_2/\text{NG}} & \varepsilon_2^{\text{NG}} & \varepsilon_{23}^{\text{NG}} \\ \varepsilon_{13}^{\text{H}_2/\text{NG}} & \varepsilon_{23}^{\text{NG}} & \varepsilon_3^{\text{NG}} \end{pmatrix} &= \begin{pmatrix} L_1^{\text{NG}} & M_{12}^{\text{NG}} & M_{13}^{\text{NG}} \\ M_{12}^{\text{NG}} & L_2^{\text{NG}} & M_{23}^{\text{NG}} \\ M_{13}^{\text{NG}} & M_{23}^{\text{NG}} & L_3^{\text{NG}} \end{pmatrix}^{-1} \\
 &= \begin{pmatrix} 59.5005 & -54.8768 & 6.9069 \\ -54.8768 & 54.2024 & -5.3802 \\ 6.9069 & -5.3802 & 6.3008 \end{pmatrix}
 \end{aligned} \tag{E-6}$$

The LH₂-H₂ Supply Chain

The parameter identification follows the same reasoning as described in Section E-2-1. The identified parameters are listed in Table E-4.

Agent		Parameter		Value
$\mathcal{S}^{\text{LH}_2}$	Supplier	$L_s^{\text{LH}_2}$	Inelastic supply	0.275
$\mathcal{R}^{\text{LH}_2}$	Market operator	R^{LH_2}	Market friction	0.025
$\mathcal{C}^{\text{LH}_2}$	Storage	C^{LH_2}	Storage elasticity	150
$\mathcal{S}_1^{\text{H}_2}$	LH ₂ gasification	$L_1^{\text{H}_2}$	Price-inelasticity	0.46465
$\mathcal{D}_2^{\text{LH}_2}$	Demander	$L_2^{\text{LH}_2}$	Price-inelasticity	0.4431
		$u_2^{\text{LH}_2}$	Inelastic demand	0.009
$\mathcal{D}_3^{\text{LH}_2}$	Demander	$L_3^{\text{LH}_2}$	Price-inelasticity	0.19135
		$u_3^{\text{LH}_2}$	Inelastic demand	0.275
		$k_{12}^{\text{LH}_2}$	Coupling coefficient	0.965
		$k_{13}^{\text{LH}_2}$	Coupling coefficient	-0.3062
		$k_{23}^{\text{LH}_2}$	Coupling coefficient	-0.2228

Table E-4: Parameter values belonging to the wind-hydrogen operator

We again check the elasticity matrix, given by:

$$\begin{aligned}
 \begin{pmatrix} \varepsilon_1^{\text{H}_2} & \varepsilon_{12}^{\text{H}_2/\text{LH}_2} & \varepsilon_{13}^{\text{H}_2/\text{LH}_2} \\ \varepsilon_{12}^{\text{H}_2/\text{LH}_2} & \varepsilon_2^{\text{LH}_2} & \varepsilon_{23}^{\text{LH}_2} \\ \varepsilon_{13}^{\text{H}_2/\text{LH}_2} & \varepsilon_{23}^{\text{LH}_2} & \varepsilon_3^{\text{LH}_2} \end{pmatrix} &= \begin{pmatrix} L_1^{\text{LH}_2} & M_{12}^{\text{LH}_2} & M_{13}^{\text{LH}_2} \\ M_{12}^{\text{LH}_2} & L_2^{\text{LH}_2} & M_{23}^{\text{LH}_2} \\ M_{13}^{\text{LH}_2} & M_{23}^{\text{LH}_2} & L_3^{\text{LH}_2} \end{pmatrix}^{-1} \\
 &= \begin{pmatrix} 35.8552 & -34.6467 & 5.3617 \\ -34.6467 & 35.8536 & -4.3758 \\ 5.3617 & -4.3758 & 6.3008 \end{pmatrix}
 \end{aligned} \tag{E-7}$$

E-2-2 Industry Clusters

Inelastic Demand

The total hydrogen demand per industry cluster is determined by the inelastic demand combined with the variable demand. The demand distribution as shown in Figure 4-10, functions as a reference to determine the inelastic demand $u_m^{\text{H}_2}$ per cluster. However, I have chosen to double the amounts of Amsterdam and Groningen, as these are relatively low and there are many planned projects in these clusters⁴.

⁴Including the switch to hydrogen by Tata Steel in IJmuiden and the plans in Groningen to become a hydrogen hub

	Industry Cluster	Price-elasticity $\varepsilon_{d,m}^{\text{H}_2}$	$L_{d,m}^{\text{H}_2}$	Inelastic demand $u_m^{\text{H}_2}$	Storage convenience $C_m^{\text{H}_2}$
$\mathcal{D}_1^{\text{H}_2}$	Groningen	10	$1e^{-1}$	$6.91e^{-2}$	1
$\mathcal{D}_2^{\text{H}_2}$	Amsterdam	4	$2.5e^{-1}$	$2.69e^{-2}$	1
$\mathcal{D}_3^{\text{H}_2}$	Rotterdam	20	$5e^{-2}$	$2.05e^{-1}$	1
$\mathcal{D}_4^{\text{H}_2}$	Zeeland	12.5	$8e^{-2}$	$1.60e^{-1}$	1
$\mathcal{D}_5^{\text{H}_2}$	Limburg	5	$2e^{-1}$	$6.80e^{-2}$	1

Table E-5: Overview of industry-cluster-related parameters. Where $L_{d,m}^{\text{H}_2} = 1/\varepsilon_{d,m}^{\text{H}_2}$ and $C_m^{\text{H}_2} = 1/k_{d,m}^{\text{H}_2}$

Price-Elasticity of Demand

Each industry cluster consists of various industrial consumers utilizing hydrogen for specific applications or processes. The price-elasticity of demand $\varepsilon_{d,m}^{\text{H}_2}$ is directly influenced by the application of hydrogen, as studied by Wietschel (2023) [14]. Therefore, estimating the price-elasticity of hydrogen demand across different industry clusters requires examining the specific industrial applications within these clusters. However, data on the flexibility of industry is limited, as indicated by an inventory study conducted by Kalavasta (2023) [69].

According to above-mentioned research, the demand for hydrogen utilized as a raw material is generally inelastic. Conversely, the use of hydrogen in industrial furnaces, the demand for hydrogen demonstrates price elasticity, with steam cracking processes exhibiting the highest elasticity.

The study by Wietschel (2023) does not cover all aspects of price elasticity, such as the potential to switch to alternative substances like ammonia in fertilizer production or the importation of pelletized iron ore for steelmaking. For instance, in the industry clusters of Zeeland and Limburg, a considerable proportion of the overall hydrogen demand is used in ammonia production for fertilizers. These clusters tend to exhibit relatively higher elasticity in their hydrogen demand, primarily because there is an option to directly import ammonia instead of producing it⁵.

To determine the price elasticity per industry cluster, I consider the hydrogen applications of the largest industrial companies within each cluster, as well as the location and total demand per industry cluster. An overview of the various applications per industry cluster is presented in Table E-6, where the hydrogen usage is categorized into raw material or fuel-based.

The total demand per cluster is considered as a higher total demand often creates a larger scope for elasticity. Additionally, factors such as the geographical location of industry clusters and the presence of port facilities affect the price elasticity of the industry cluster. For instance, Limburg has limited options for hydrogen production, while clusters near seaports have greater hydrogen accessibility.

⁵Further details will be provided in the subsequent chapter, where ammonia is modeled as a substitute for hydrogen.

Industry Cluster	Large companies	industrial	Industrial applications	Hydrogen usage
Groningen	Nouryon, Teijin	Aramid	Various naphtha ⁶ and LPG ⁷ applications	Raw material & fuel
Amsterdam	Tata Steel, (future)	Schiphol	Steel- and aluminum making, aircraft fuel	Fuel
Rotterdam	Shell, Vopak, BP, Exxon-Mobil, Sasol, Uniper		Refinery	Fuel
Zeeland	Yara, ArcelorMittal, Dow , Zeeland Refinery	ICL,	Fertilizers, refinery	Raw material & fuel
Limburg	OCI Nitrogen, Sabic, DSM		Various naphtha and LPG applications	Raw material

Table E-6: Industrial applications of hydrogen per industry cluster

E-2-3 Market Operators

For tuning the parameters for the market operators, we conducted both time-domain and frequency-domain (pole) analyses. This tuning significantly influences the behavior of the network in terms of speed and damping.

The core network consists of three second-order systems (the hydrogen, liquid hydrogen, and natural gas markets) and one first-order system (the OWE market). The transfer function of a general second-order system can have two poles in one of three configurations: both poles can be real-valued and on the negative real axis, they can form a double-pole on the negative real axis, or they can form a complex conjugate pole pair. The first-order system introduces one pole.

The pole closest to the imaginary axis determines the long-term response, while the pole furthest from the imaginary axis determines the short-term response. Fast poles, indicative of fast dynamics, are poles that respond or oscillate rapidly. These poles lie far from the origin in the left-half plane and correspond to components that decay rapidly, while poles near the origin correspond to slowly decaying components. A pole at the origin defines a component that is constant in amplitude and influenced by initial conditions. A complex conjugate pole pair $\sigma \pm j\omega$ in the left-half of the s-plane combines to generate a response component that is a decaying sinusoid. The rate of decay is specified by σ , and the frequency of oscillation is determined by ω .

Considering the nature of a spot market, where energy prices, stocks, and flows must respond to hourly variations, a fast settling time is required. While both a fast settling time and appropriate damping are desirable, achieving both simultaneously is not feasible with manual tuning of these networks and without advanced control mechanisms.

Figures E-2 and E-3 show the pole-zero plots for the under-damped and over-damped configurations, respectively, as well as the resulting energy price and stock dynamics. Table E-7 lists the values of the resistance parameters of the market operators in the different commodity markets. The over-damped system, with its fast poles, ensures that the network quickly adapts to hourly fluctuations in supply and demand, thereby supporting the volatile nature of a hydrogen spot

market. Although this choice results in an over-damped system, the rapid response to market changes justifies this decision, making it suitable for modeling the dynamic behavior of hydrogen spot trading.

Parameter	Over-damped	Under-damped
R^{LH_2}	0.025	0.025
R^{NG}	0.025	0.0075
R^{H_2}	0.05	0.005

Table E-7: Under- and over-damped market operator values. We have chosen to go with the over-damped market operators as this better reflects the hydrogen spot market behavior.

E-2-4 Storage in Salt Caverns

We observe during tuning that we cannot obtain the storage functioning as we would want it to function. Although energy is stored and extracted as expected, it is not of the right magnitude. We can adjust the magnitude with parameter tuning, but this influence is minimal. The parameter is tuned such that it influences hydrogen spot prices properly.

Further research should explore storage representations where a capacitor is combined with an inductor, as storage facilities may also act as demanders.

Agent	Parameter	Value
$C_2SC^{H_2}$ Salt caverns	$C_{CS}^{H_2}$ Storage elasticity	375

Table E-8: Parameter value belonging to the salt caverns

E-3 Two-Sort Hydrogen Model

In the two-sort hydrogen market model, only the industry cluster parameters are changed. The single inductor is replaced with a mutual inductor, coupling the demand for renewable and low-carbon hydrogen. Parameters are manually tuned in a way that the elasticities are compatible with the core network.

The total inelastic demand, as given in Table E-5, is multiplied by 0.7 such that the demanded hydrogen stays roughly the same. The inelastic demand for renewable hydrogen is determined by $0.69 * u_m^{H_2} * s_m^{R,H_2}$, and the inelastic demand for low-carbon hydrogen is then determined by $0.69 * u_m^{H_2} * (1 - s_m^{R,H_2})$. See the values in Table E-9.

E-4 Integrated Ammonia Model

In the two-sort hydrogen market model, only the industry cluster parameters of Rotterdam, Zeeland, and Limburg are changed. The single inductor is replaced with a mutual inductor,

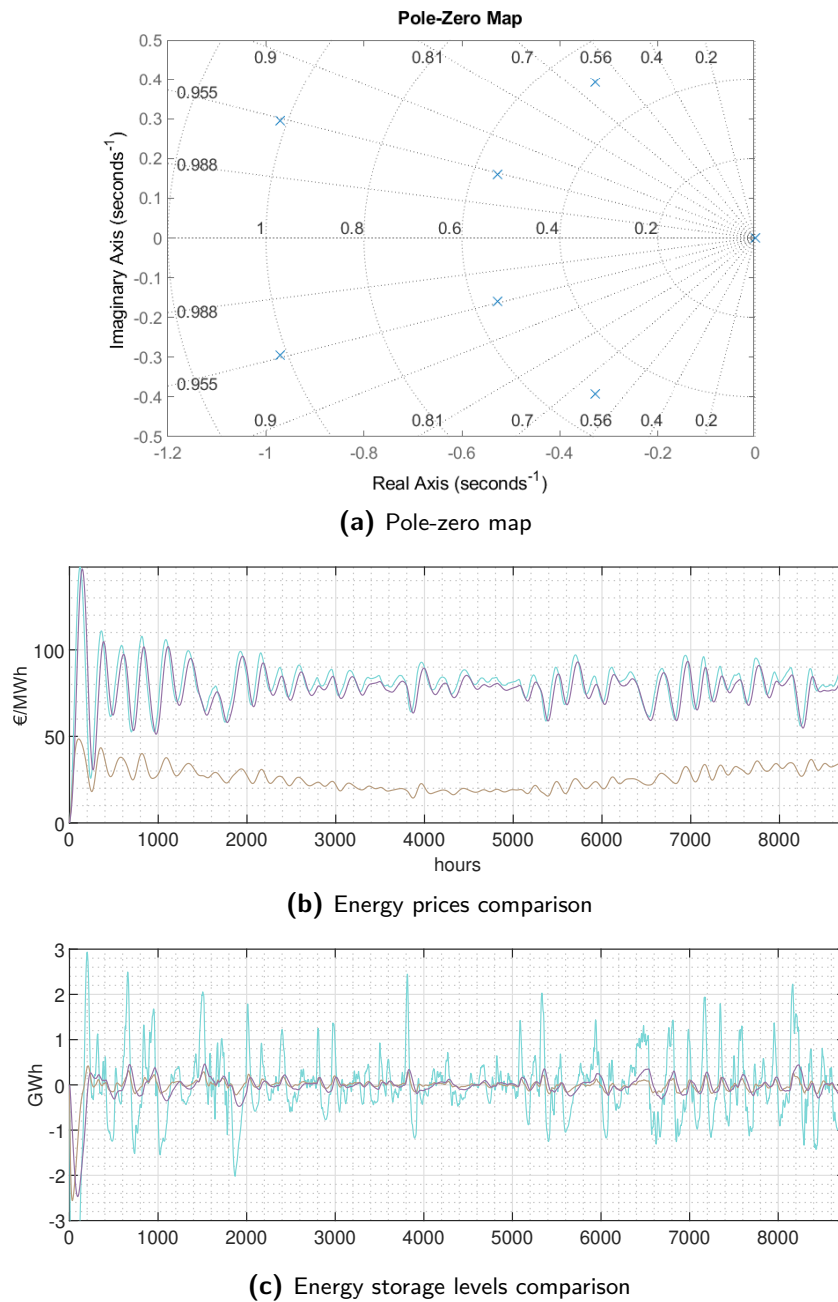


Figure E-2: Under-damped core network demonstrated with a pole-zero map and simulation with a measured wind sequence as input. With the hydrogen (cyan), liquid hydrogen (purple), natural gas (brown), and ammonia (pink).

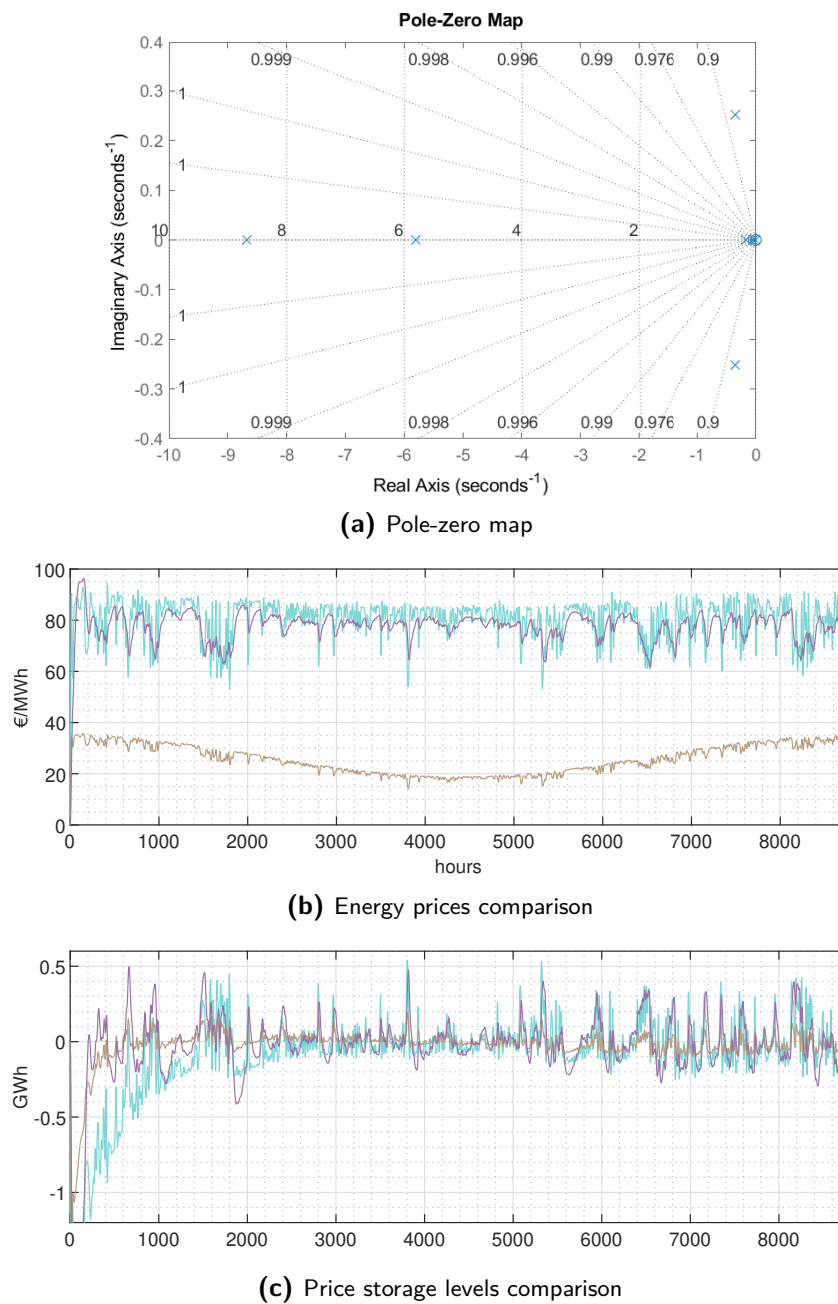


Figure E-3: Under-damped core network demonstrated with a pole-zero map and simulation with a measured wind sequence as input. With the hydrogen (cyan), liquid hydrogen (purple), natural gas (brown), and ammonia (pink).

Industry Cluster	Share green H_2 s_m^{R,H_2}	L_1^{LC,H_2}	L_2^{R,H_2}	Coupling coefficient	$\begin{pmatrix} \varepsilon_1^{R,H_2} & \varepsilon_{12}^{H_2} \\ \varepsilon_{12}^{H_2} & \varepsilon_2^{LC,H_2} \end{pmatrix}$
Groningen	0.29	0.45	0.2	0.85	$\begin{pmatrix} 8.0080 & -10.2102 \\ -10.2102 & 18.0180 \end{pmatrix}$
Amsterdam	0.3	0.4	0.3	0.6	$\begin{pmatrix} 3.9063 & -2.7063 \\ -2.7063 & 5.2083 \end{pmatrix}$
Rotterdam	0.19	0.25	0.1	0.9	$\begin{pmatrix} 21.0526 & -29.9584 \\ -29.9584 & 52.6316 \end{pmatrix}$
Zeeland	0.19	0.25	0.1	0.85	$\begin{pmatrix} 14.4144 & -19.3725 \\ -19.3725 & 36.0360 \end{pmatrix}$
Limburg	0.3	0.475	0.2	0.75	$\begin{pmatrix} 4.8120 & -5.5619 \\ -5.5619 & 11.4286 \end{pmatrix}$

Table E-9: Overview of industry-cluster-related parameters in the RLCH2 network

coupling the demand for hydrogen and ammonia. Parameters are manually tuned in a way that the elasticities are compatible with the core network.

The total inelastic demand of these three clusters, as given in Table E-5, is multiplied by 0.72 such that the demanded hydrogen stays roughly the same. The inelastic demand for ammonia is determined by $0.72 * u_m^{H_2} * s_m^{NH_3}$, and the inelastic demand for hydrogen is then determined by $0.69 * u_m^{H_2} * (1 - s_m^{NH_3})$. See the values in Table E-10.

The ammonia market is tuned such that it has limited flexibility in supply. The ammonia market parameters are listed in Table E-11.

E-5 Model Calibration

Calibration of Time

Since our commodity flow is measured in MWh/h, we adopt a one-hour time step to align with the common practice of having one clearing price per hour, as observed in HYCLIX and Integrated Electricity, Hydrogen and Gas (I-ELGAS). This configuration implies a time step of $1/24s$, where one day corresponds to one second, and a complete year of 8760 hours equal to approximately 365 days and thus 365 seconds in the model.

The model starts its time counting according to the calendar year where $t = 0$ aligns with the beginning of the year.

Industry Cluster	Share NH_3 $s_m^{\text{NH}_3}$	$L_1^{\text{H}_2}$	$L_2^{\text{NH}_3}$	Coupling coefficient	$\begin{pmatrix} \varepsilon_1^{\text{H}_2} & \varepsilon_{12}^{\text{H}_2/\text{NH}_3} \\ \varepsilon_{12}^{\text{H}_2/\text{NH}_3} & \varepsilon_2^{\text{NH}_3} \end{pmatrix}$
Rotterdam	0.2	0.45	0.35	0.75	$\begin{pmatrix} 5.0794 & -4.3196 \\ -4.3196 & 6.5306 \end{pmatrix}$
Zeeland	0.25	0.45	0.35	0.65	$\begin{pmatrix} 3.8480 & -2.8361 \\ -2.8361 & 4.9474 \end{pmatrix}$
Limburg	0.3	0.45	0.3	0.6	$\begin{pmatrix} 3.4722 & -2.5516 \\ -2.5516 & 5.2083 \end{pmatrix}$

Table E-10: Overview of industry-cluster-related parameters in the H2A network. With $id^{\text{NH}_3} = 0.72$

	Agent		Parameter	Value
$\mathcal{S}^{\text{NH}_3}$	Supplier	$L_s^{\text{NH}_3}$	Price-inelasticity	0.063
		w^{NH_3}	Inelastic NH_3 supply	0.2
$\mathcal{R}^{\text{NH}_3}$	Market operator	R^{NH_3}	Market friction	0.025
$\mathcal{C}^{\text{NH}_3}$	Storage	C^{NH_3}	Storage elasticity	250

Table E-11: Parameter values ammonia market

Calibration of Energy Flows and Spot Prices

The calibration of the energy flows and spot prices is done using a core network simulation with an average wind yearly wind distribution. We determine a scaling factor that relates the network values to real-world values. This is possible as our system is linear time-invariant (LTI).

First, the energy flows and spot prices are calibrated separately. We match the energy flows in the network to the right real-world values and we calibrate the energy prices using data from TNO.

Then, we tune our model parameters such that these scaling factors match

Energy Flows

The calibration of commodity flows in the model is established based on the assumption that the total supplied hydrogen amounts to 280 petajoules (PJ) per year, equivalent to 77.778 GWh per year (8760 hours) or 8.88 GWh/h. Although energy is traded in MWh, the common convention is to express energy volumes in terms of GWh. Consequently, the scaling process converts the flows directly into GWh.

Within the model, we can measure and accumulate the current related to the total yearly hydrogen supply, denoted by $f_s^{\text{H}_2}$. As 1 second in the model represents a day, we integrate $f_s^{\text{H}_2}$ over a full calendar year of 365 seconds in the model. The scaling factor for the commodity flows is then determined by:

$$SF_{\text{flow}} = \frac{\frac{77.778}{8760}}{\int_0^{365} \frac{f_s^{\text{H}_2}(t) dt}{365}}. \quad (\text{E-8})$$

This scaling factor is applicable uniformly across all integrated markets.

Energy Prices

Since energy is priced in €/MWh, the calibration of energy prices is done in the same units. The calibration relies on data derived from the I-ELGAS model, specifically, the hydrogen prices obtained from the IP2024 KA scenario for 2035. These hydrogen prices are consistent with those in HYCLIX and HYDEX.

The integration constant that arises by determining the energy prices is set to zero ($p(0) = 0$). The scaling factor is then determined by matching the average hydrogen price obtained from the core network to the average hydrogen price from the I-ELGAS model:

$$SF_{\text{price}} = \frac{\bar{p}_{\text{I-ELGAS}}^{\text{H}_2}}{\bar{p}_{\text{ECT}}^{\text{H}_2}}. \quad (\text{E-9})$$

This scaling factor is uniformly applied across all integrated markets as the resulting average natural gas price is obtained to be in line with the average gas price from the I-ELGAS model.

Matching of Scaling Factors

Through an iterative process, we tune our inductor parameters such that the energy flow and energy price scaling factors match.

$$SF_{\text{flow}} = SF_{\text{price}} = 2600 \quad (\text{E-10})$$

This leaves us with a scaling factor of 26000 to determine flows and prices in MWh (or 26 to determine them in GWh).

Appendix F

Matlab and Simulink

F-1 Overview of Matlab Scripts and Simulink Files

To run the network simulations, one can run `Main_Script.m`. Model adjustments can be made in the Simulink files. MATLAB version 2023a is used. An overview of the files needed to perform the simulations is given in Table F-1. The MATLAB scripts, Simulink files, and Excel files can be accessed at GitHub: https://github.com/pienvdberkmortel/Thesis_Hydrogen_Spot_Market_Network_Scripts.git.

Name	Type	Function
Main_Script.m	Matlab Code	Central script that manages simulations and plots
Model_Parameters.m	Matlab Code	Script containing model parameters
Seasonal_Wind_Series.m	Matlab Code	Script that fits an average wind distributions
KNMI_Wind_Data_2019.xlsx	Excel	Wind data retrieved from KNMI
Import_KNMI_Wind_Data_2019.m	Matlab Code	Function that imports wind data from excel file
TNO_Data_Price_Calibration.xlsx	Excel	Price data from the TNO I-ELGAS model
Import_TNO_Price_Calibration_Data.m	Matlab Code	Function that imports price data from excel file
Core_Model_Cal.slx	Simulink model	Core model used for calibration (do not change this model)
Core_Model.slx	Simulink model	Core model
Green_Blue_Model.slx	Simulink model	RLCH2 model
Ammonia_Model.slx	Simulink model	H2A model
Core_Model_Dynamics.slx	Matlab Code	State-space model of the core network

Table F-1: Overview of MATLAB, Simulink, and Excel files that can be found on GitHub

Bibliography

- [1] Ministry of Economic Affairs and Climate Policy, *National Climate Agreement - The Netherlands*. 2019.
- [2] B. den Ouden, “A Hydrogen Exchange for the Climate,” tech. rep., 2020.
- [3] HyXchange, “Workshop Hydrogen spotmarket simulation Programme,” tech. rep., 2022.
- [4] M. B. Mendel, “The Newtonian Mechanics of Demand: Foundations of Economic Engineering,” 2023.
- [5] C. Hutter and M. B. Mendel, “Economic Circuit Theory: Electrical Network Theory for Dynamical Economic Systems (Preprint),” 2024.
- [6] Ministry of Economic Affairs and Climate Policy, *Government Strategy on Hydrogen*. 2020.
- [7] M. Mulder, P. Perey, and J. L. Moraga, “Outlook for a Dutch hydrogen market: economic conditions and scenarios,” *CEER Policy Papers; No. 5*, 2019.
- [8] C. van der Linde and J. van Leeuwen, “From an invisible to a more visible hand?,” tech. rep., Clingendael International Energy Programme, 2019.
- [9] M. Mulder, B. Willems, and M. Mulder, “The Dutch retail electricity market,” *Energy Policy*, vol. 127, pp. 228–239, 2019.
- [10] A. van Wijk, “The Green Hydrogen Economy in the Northern Netherlands,” tech. rep., 2017.
- [11] B. Koirala, S. Hers, G. Morales-España, . Özdemir, J. Sijm, and M. Weeda, “Integrated electricity, hydrogen and methane system modelling framework: Application to the Dutch Infrastructure Outlook 2050,” *Applied Energy*, vol. 289, p. 116713, 2021.
- [12] Strategy&, “HyWay 27: hydrogen transmission using the existing natural gas grid?,” tech. rep., PwC, 2021.
- [13] C. Hutter and M. Mendel, “Indifference Curves as Conic Sections: Deriving a Generalized Utility Function from an Analogous Electrical Network (Preprint).” 2024.

- [14] M. Wietschel, B. Weißenburger, M. Rehfeldt, B. Lux, and L. Zheng, “Price-Elastic Demand for Hydrogen in Germany - Methodology and Results.” 2023.
- [15] C. G. F. Bataille, “Design and application of a technologically explicit hybrid energy-economy policy model with micro and macro economic dynamics,” 2005.
- [16] C. K. Alexander and M. N. Sadiku, *Fundamentals of electric circuits*. McGraw-Hill, 5 ed., 2013.
- [17] M. Chang, J. Z. Thellufsen, B. Zakeri, B. Pickering, S. Pfenninger, H. Lund, and P. A. Østergaard, “Trends in tools and approaches for modelling the energy transition,” *Applied Energy*, vol. 290, 2021.
- [18] W. Fan, W. Lv, and Z. Wang, “How to measure and enhance the resilience of energy systems?,” *Sustainable Production and Consumption*, vol. 39, pp. 191–202, 7 2023.
- [19] B. J. Jesse, H. U. Heinrichs, and W. Kuckshinrichs, “Adapting the theory of resilience to energy systems: A review and outlook,” *Energy, Sustainability and Society*, vol. 9, pp. 1–19, 7 2019.
- [20] X. Ma, H. Zhou, and Z. Li, “On the resilience of modern power systems: A complex network perspective,” *Renewable and Sustainable Energy Reviews*, vol. 152, p. 111646, 12 2021.
- [21] C. S. Bale, L. Varga, and T. J. Foxon, “Energy and complexity: New ways forward,” *Applied Energy*, vol. 138, pp. 150–159, 2015.
- [22] R. Pant, K. Barker, and C. W. Zobel, “Static and dynamic metrics of economic resilience for interdependent infrastructure and industry sectors,” *Reliability Engineering & System Safety*, vol. 125, pp. 92–102, 5 2014.
- [23] A. Gatto and C. Drago, “Measuring and modeling energy resilience,” *Ecological Economics*, vol. 172, p. 106527, 6 2020.
- [24] Roland Berger, “Making the Hydrogen Market: Requirements for the Netherlands to become a hydrogen hub,” tech. rep., 2022.
- [25] C. Hutter and M. Mendel, “A Multiport Network Framework for Dynamic Agent-Based Economic Modeling (Preprint),” 2024.
- [26] Air Liquide, “Hydrogen - At the origin of the Universe,” 2022.
- [27] IEA, “The Future of Hydrogen,” tech. rep., 2019.
- [28] International Renewable Energy Agency, “Green hydrogen: A guide to policy making,” tech. rep., 2020.
- [29] International Energy Agency, “The Netherlands 2020 - Energy Policy Review,” tech. rep., Paris, 2020.
- [30] M. Younas, S. Shafique, A. Hafeez, F. Javed, and F. Rehman, “An Overview of Hydrogen Production: Current Status, Potential, and Challenges,” *Fuel*, vol. 316, p. 123317, 2022.
- [31] S&P Global, “Methodology and Specifications Guide Global Hydrogen & Ammonia,” 2023.
- [32] R. Oyarzabal, P. Mertenskötter, and C. G. Molyneux, “New Definitions for Blue and Green Hydrogen: The European Commissions Package on Hydrogen and Decarbonized Gas Markets,” *EUROPEAN ENERGY & CLIMATE POLICY, HYDROGEN, TARIFFS*, 1 2022.

-
- [33] TNO, “The Dutch hydrogen balance, and the current and future representation of hydrogen in the energy statistics,” tech. rep., 2020.
- [34] CE Delft, “50% green hydrogen for Dutch industry ,” tech. rep., Delft, 2022.
- [35] Nationaal Waterstof Programma, “Routekaart Waterstof,” 2022.
- [36] J. Juez-Larré, S. van Gessel, R. Dalman, G. Remmelts, and R. Groenenberg, “Assessment of underground energy storage potential to support the energy transition in the Netherlands,” *First Break*, vol. 37, no. 7, pp. 57–66, 2019.
- [37] IRENA, “Global hydrogen trade to meet the 1.5°C climate goal: Part I Trade outlook for 2050 and way forward,” *International Renewable Energy Agency*, 2022.
- [38] TNO, “Hydrogen in the Netherlands: A review of recent Dutch scenario studies,” tech. rep., 2020.
- [39] International Renewable Energy Agency, “Green Hydrogen Cost Reduction: Scaling up Electrolysers to Meet the 1.5C Climate Goal,” tech. rep., IRENA, Abu Dhabi, 2020.
- [40] Netherlands Enterprise Agency (RVO), FME, and TKI New Gas (Topsector Energy), *Excelling in Hydrogen: Dutch technology for a climate-neutral world*. 2022.
- [41] A. van den Noort, W. Sloterdijk, and M. Vos, “Verkenning waterstofinfrastructuur ,” tech. rep., DNV-GL, 2017.
- [42] Gasunie, “Hydrogen network Netherlands,” 2022.
- [43] J. Chatzimarkakis, C. Levoyannis, A. van Wijk, and F. Wouters, “Hydrogen Act: Towards the Creation of the European Hydrogen Economy,” tech. rep., Hydrogen Europe, 2021.
- [44] C. Allevi and G. Collodi, “Hydrogen production in IGCC systems,” in *Integrated Gasification Combined Cycle (IGCC) Technologies*, ch. 12, pp. 419–443, Woodhead Publishing, 2017.
- [45] TNO and EBN, “Ondergrondse Energieopslag in Nederland 2030 - 2050,” tech. rep., 2021.
- [46] TNO and EBN, “Haalbaarheidsstudie offshore ondergrondse waterstofopslag,” tech. rep., EBN, 2022.
- [47] TNO, “Large-Scale Energy Storage in Salt Caverns and Depleted Fields ,” tech. rep., 2020.
- [48] IMBEMA, “Hydrogen gas as an alternative to natural gas; is it that easy?,” 7 2022.
- [49] J. Andersson and S. Grönkvist, “Large-scale storage of hydrogen,” *International Journal of Hydrogen Energy*, vol. 44, no. 23, pp. 11901–11919, 2019.
- [50] A. E. Roth, “The Economist as Engineer: Game Theory, Experimentation, and Computation as Tools for Design Economics,” *Econometrica*, vol. 70, no. 4, pp. 1341–1378, 2002.
- [51] TNO, “Energy System and Market Analysis,” *North Sea Energy 2020-2022*, 2020.
- [52] P. Verstraten and A. H. van der Weijde, “The Case for Simple Simulation: Stochastic Market Simulation to Assess Renewable Business Cases,” *Current Sustainable/Renewable Energy Reports*, vol. 10, pp. 75–81, 9 2023.
- [53] S. Pfenninger, A. Hawkes, and J. Keirstead, “Energy systems modeling for twenty-first century energy challenges,” *Renewable and Sustainable Energy Reviews*, vol. 33, pp. 74–86, 2014.

- [54] M. Grubb, J. Edmonds, P. Ten Brink, and M. Morrison, "The costs of limiting fossil-fuel CO₂ emissions: a survey and analysis," *Annual Review of Energy and the Environment*, vol. 18, no. 1, pp. 397–478, 1993.
- [55] N. Van Beeck, "Classification of Energy Models," 1999.
- [56] J. Hourcade, M. Jaccard, C. Bataille, and F. Ghersi, "Hybrid modeling: new answers to old challenges introduction to the special issue of the energy journal," *The Energy Journal*, no. 2, 2006.
- [57] A. S. R. Subramanian, T. Gundersen, and T. A. Adams, "Modeling and Simulation of Energy Systems: A Review," *Processes 2018, Vol. 6, Page 238*, vol. 6, no. 12, p. 238, 2018.
- [58] A. Herbst, F. Toro, F. Reitze, and E. Jochem, "Introduction to Energy Systems Modelling," *Statistics*, vol. 148, no. 2, pp. 111–135, 2012.
- [59] M. G. Prina, G. Manzolini, D. Moser, B. Nastasi, and W. Sparber, "Classification and challenges of bottom-up energy system models - A review," *Renewable and Sustainable Energy Reviews*, vol. 129, p. 109917, 2020.
- [60] J. Hourcade, R. Richels, J. Robinson, and L. Schrattenholzer, "Estimating the costs of mitigating greenhouse gases," *Climate Change 1995: Economic and Social Dimensions of Climate Change*, 1996.
- [61] K. O. Yoro, M. O. Daramola, P. T. Sekoai, U. N. Wilson, and O. Eterigho-Ikelegbe, "Update on current approaches, challenges, and prospects of modeling and simulation in renewable and sustainable energy systems," *Renewable and Sustainable Energy Reviews*, vol. 150, p. 111506, 2021.
- [62] R. Hanna and R. Gross, "How do energy systems model and scenario studies explicitly represent socio-economic, political and technological disruption and discontinuity? Implications for policy and practitioners," *Energy Policy*, vol. 149, 2 2021.
- [63] J. D. Farmer and D. Foley, "The economy needs agent-based modelling," *Nature 2009*, vol. 460, pp. 685–686, 8 2009.
- [64] H. Van Dyke Parunak, R. Savit, and R. L. Riolo, "Agent-Based Modeling vs. Equation-Based Modeling: A Case Study and Users' Guide," *Proceedings of Multi-agent systems and Agent-based Simulation (MABS)*, pp. 10–25, 1998.
- [65] V. Sai, G. Vunnava, and S. Singh, "Integrated mechanistic engineering models and macro-economic inputoutput approach to model physical economy for evaluating the impact of transition to a circular economy," *Energy Environ. Sci.*, vol. 14, pp. 5017–5034, 2021.
- [66] M. Fodstad, P. Crespo del Granado, L. Hellemo, B. R. Knudsen, P. Pisciella, A. Silvast, C. Bordin, S. Schmidt, and J. Straus, "Next frontiers in energy system modelling: A review on challenges and the state of the art," *Renewable and Sustainable Energy Reviews*, vol. 160, 2022.
- [67] K. C. Hoffman and D. O. Wood, "Energy System Modeling and Forecasting," *Annual Review of Energy*, vol. 1, no. 1, pp. 423–453, 1976.
- [68] TNO, "Offshore wind energy deployment in the North Sea by 2030," tech. rep., 2021.
- [69] Kalavasta, "Cluster Energie Strategieën uitvraagmethodiek: Een uniforme methode om ontwikkelingen op het gebied van energie, uitstoot en flexibiliteit bij de industrie te inventariseren," tech. rep., 2023.

Glossary

List of Acronyms

ABMs	agent-based models
AHS	above-ground hydrogen storage
CCS	carbon capture and storage
CfD	contract for difference
DR	demand response
EE	Energy Economics
EHB	European Hydrogen Backbone
ESM	energy systems modeling
ETM	Energy Transition Model
FIT	Feed-In Tariff
GHG	greenhouse gas
HHV	Higher Heating Value
HPAs	Hydrogen Purchase Agreements
I-ELGAS	Integrated Electricity, Hydrogen and Gas
IRENA	International Renewable Energy Agency
LTI	linear time-invariant
LHV	Lower Heating Value
LOHCs	liquid organic hydrogen carriers
MPC	model predictive control
OWE	offshore wind energy
PBL	Netherlands Environmental Assessment Agency
PID	Proportional-Integral-Derivative
PSE	Process Systems Engineering
PJ	petajoules
RES	renewable energy sources

SMR	steam methane reforming
TTF	Title Transfer Facility
UHS	underground hydrogen storage